Can Gravitational Microlensing Explain AGNs Variability ?

Thesis Submitted for the Degree of
Magister Philosophiae

Candidate:	Supervisor:
Yuan Zhou	Prof. M. A. Abramowicz

Academic Year 1988/89

Acknowledgements

I would like to take this opportunity to express my deepest gratitude to my supervisor M. A. Abramowicz for his many guidance in my master studies. His constant support for my studies, like providing references and discussing confusing points, is greatly acknowledged. I would also like to thank my colleagues for discussions and a lot of interesting seminars which are useful in some cases. Thank also goes to Profs. D. Sciama and M. Calvani for their kindness which is very important when my health was not so good. At last but not least I also thank Dr. Xu Cong for many very useful discussions and comments on this thesis.

Part of this thesis was typesetted by Mrs. Zhang Manlian and Mr. C.-J. Zhu. Without their works this thesis would not be appeared as it is.

CONTENTS

INTRODUCTION

Over past a few years both the data on observations of active galaxies and the models for explaining the phenomenally powerful and compact energy sources within the galaxies have grown in number at a tremendous rate. A theoretical consensus concerning the nature of the commom powerhouse seems to be forming, in this sense accretion onto a supermassive black hole is the basis of the majority of recent models, i.e. the so-called "standard model" for AGN. Accretion disk is an important model to explain the variability of AGN. In this standard model it was believed that the violent and rapid variability of light curves of AGN was caused by accretion disk instabilities: dynamical, thermal, viscous and those which are specific to transonic flows. However this model encounters many difficulties and is not satisfactory to meet the data. Therefore people are convinced that may be this model does not express the real mechanism of AGN, so are motivated to search for new ways in which the AGN variability can be better explained. The gravitational lens model is an alternative one.

Gravitational lens provides a reasonable way to explain the variability of AGN. The variability of AGN might originate "midway" instead of intrinsic variation. In this scenario the most spectacular effect of gravitational light deflection is the generation of multiple and/or strongly distorted images of distant galaxies and quasars due to the lens-like action of foreground galaxies and clusters. In fact one can expect $\sim 10^6$ QSO's in the sky, then with a lensing probability of $\sim 10^{-3}$, ~ 1000 lens system. In this model the gravitational lens can be made of galaxies, cluters, black holes and even the cosmic strings. The light bending is caused by such objects as an overall body without any internal structure. It gives rise to a reasonable description for the amplification of AGN. Naturally, one could conjecture that the next step to develop this idea is to take into account for the influence from the internal structure of the lens. Thus the effects of microlensing has begun to be discussed. As usual, there are many models about the microlensing which we will discuss in every detail later in this context.

From the above discussion it is clear that the gravitational microlensing originating from compact objects (black holes, stars, brown dwarfs, Jupiter etc.) in a foreground galaxy is of great astrophysical importance. However, no microlensing phenomenon has yet been positively identified, although there are several papers predicting its possible ap-

pearence. Microlensing is difficult to be identified, because it does not lead to an image which fine structure the prensently available techniques can offer sufficient resolution to observe. The only signal of microlensing which can be observed is the time-dependent amplification which occurs if the source, lens and the observer change their relative positions with respect to time. Microlensing may lead to a slipting up of each microimage produced by the corresponding smoothed-out galaxy, i.e. by the "macrolensing" into several microimages with separations of the order of a few micro-arcseconds.

One can immediately figure out that this new improved model is much more complicated because the inner structure and the density distribution of the matter inside the galaxy or cluster are under consideration. Generally speaking the adjacent materials around the light beam can give rise to an influence on the beam. By the commonly acceptable theory, the material inside the light beam makes the beam converge, whereas the surrounding material of the beam produces a sheer which causes distortion of the image from the original object.

Of particular interest are the large amplification which may occur as a compact source crosses a critical curve (anti-caustic). By such a high amplification event (HAE) one gets a typical asymmetric peak on the light curve. depending on the optical depth, in the model light curves shown "active phases" alternating with quiet periods, or low level "flickering". The qualitative agreement with the observed AGN light curves (e.g. 3C345) suggests that microlensing can account for the AGN variablity at a certain degree. So far there are some models on microlensing, however the predicted results still can not agree with the data on the variablity of AGN quantitatively. There is no doubt that taking the internal structure into account is a natural and necessary development. However we still lack of enough knoweledge about the structure of the galaxy etc., therefore one cann't expect a perfect agreement at this stage. On the other hand the investigation of the microlensing can provide us more information of the unknown structure inside the astrophysical objects. More accurate calculations and further improved models can lead to results that can be in much better agreement with the observable data.

In this review article we will overlook the present theories of microlensing as well as the observation on it. Part I shows observational data on variability of AGN and sevaral typical light curves. Finding out the variablities of light curves can be explained by microlensing.

Part II surveys the theory on gravitational lens and gravitational microlensing, of course we only concentrate our discussions on microlensing. We also show the details of the principles of microlensing, employed methods in the calculations and give a summary account on the microlensing. Finally, in part III we discuss the light curves of AGN based on both theory and observation. In the conclusion we draw a summary of all the possible effects of microlensing which can make the observed data on AGN variablity understandable, and indicate some confusing points and difficulties in the theory.

Part I. Variability of AGN

1. Phonomena of AGNs in general

All of quasars, radio galaxies, Seyfert galaxies and BL Lacertae objects have violent active nuclei. In general, they are named Active Galactic Nuclei (AGN). AGN are special kind of objects interested by astronomer.

Early photographic images of galaxies typically were produced by using the longest exposures possible so as to pick up the faint structure towards their edges. This had the unfortunate corollary of overexposing the bright cores, and much important information on the central regions of both spiral and elliptical galaxies was effectively ignored. Although the study of the outer parts of galaxies continues unabated, over the past twenty years or so the emphasis in extragalatic observation has shifted towards the probing of the compact bright nuclei that many galaxies exhibit. The first real discussion of galactic activity was Seyfert's (1943) examination of spiral galaxies with bright nuclei. He noted that hydrogen emission lines in many of these were much wider than in normal spirals. The study of AGN only began in earnest when lunar occultation radio measurements were able to provide both accurate positions and sturctural information on the 1″ angular scale. Although in the early 1960's quasars were considered to be unique, it began to be suspected that other types of AGN were related to them. The key sense of this relationship is that quasars are just the most spactacular examples of the dominance of ordinary stellar luminosity by nonthermal emission from the nucleus of the galaxies. For example, BL Lacertae objects, first recognized by Schmidt (1968) as extragalatic, are much like quasars in many properties, but show no strong emission features. Seyfert and N galaxies could be classified as QSOs if they were further away, for then their nuclei might dominate more completely over their stellar output, because of the differing decline of these two spectral components with distance (the K correction). On the other hand, recent observations of QSOs with better resolutions and higher signal-to-noise ratios have recently revealed the galaxies around some of those nuclei. Under the classical defintion of QSOs such objects would be removed from the roll and reclassified as Seyfert or N galaxies.

When QSOs were just found as some very bright, compact, faraway extragalactic objects, we also found some of them with the property of variability in their luminosity. In fact, galaxies with active nuclei have been kept under observation for many years (Lyutyi, 1979; Penston, et.al, 1975; Hackney, et.al, 1975) and enough datas are now available for

us to discern some general aspects of their optical variability. To a first approximation the light curve of an active nuclei will exhibit comparatively long waves (the slow variability component) whose characterstic time is a number of years; superimposed on them will be shorter flares (the fast component) lasting only a few weeks or days. Particular, violent, irregular variability has been observed for many quasars, Seyfert nuclei and BL lac objects (Strittmatter et.al, 1972) at optical (Cannon, Penston and Brett 1971; Angione, 1973), infrared (Rieke and Low, 1972) and radio wavelengths (Medd et.al, 1972). The cores of these objects have nonthermal spectra and are unresolved optically. If it is assumed that the characteristic size of these sources is less than $\sim c\Delta t$, where Δt is the characteristic time scale of their flux variations, at least some of these objects must be extremely compact. There are several typical picture of light curves, they are that Fig.1 is for 3C273, Fig. 2 is for 3C345, Fig.3 is for NGC3516, Fig.4 is for OJ287 respectively. Now, it is well known that variability is a common property of AGN which is appearant in every kind of active galatic nuclei and every radiation band (Witta, P.J. 1985). But the new optical catalog of quasi-stellar objects (Hewitt and Burbidge, 1987) contains 427 objects. Reference to variability are made for only 12 percent of quasars in this catalog. In other samples, however, a substantially larger fraction of sources was found to vary: in the Rosemary Hill Observatory sample 50 percent of the objects are variable (Pica et.al., 1980), and in the Asiago sample 43 percent of observed objects show variability (Barbieri et.al, 1983). When all of the published data is included, then 56 percent of the objects from the Asiago sample are variable. This is contrary to the commonly held opinion, that variability of AGN is rare (Abramowicz, 1988).

From the pictures, we can find two kinds of variability. The more accurate classfication was done by Mc Grimsey et.al (1975) and summarized by Abramowicz (1988). They describe the complex morphology of the light curves of AGN in terms of four basic types by using two main characteristics of the time behavior: short-term flickering occurring with time scales of days or weeks and having amplitude $0.3 - 0.5^m$. The short term produce irregular jumps (non-periodic) in the light curevs, we also called flares. Although the typical time scale is a few days, we also found some quick flares. In some case they were a few hours, even a few minutes (Xie et.al 1987). The long-term variations (secular trends) occurring with timescales of months or years ($10^6 - 10^8 sec$). The long-term varia-

tion shows the periodic variability (or quasi-periodic). But in some case, there were short periodic variability, for example, a few days or a few hours (Ozernoy et.al, 1977). The typical amplitude of perodic variability is $0.5-1$ magnitude. *The first* type contains light curves dominated by rapid short-term flickering. Long-term trends are inconspicuous and, if present, are very gradual. *The second* type is characterized by prominent long-term variations in the mean level. Flickering appears as minor excursions about this changing average. In *the third* type, the light curves are dominated by a mixture of the two components which here have comparable amplitudes. *The forth* type contains light curves having long periods of quiescence which are interrupted by relatively brief periods of activity (bursts). These four types are generic for AGN variability and are characteristic not only of optical light curves, but also (with different timescales and amplitudes) of other variability phoenomena. For the real data, they can be recognised in Fig.5, which shows the variability of 3C345 (Kidger abd Beckman 1986), and in other Figures. One can also add to this classification *the fifth* type having no variability at all. Another character, especially the optical type light curves for BL Lac objects, show not only outbursts but occasionally also deep minima. Often, after a primary maximum of brightness, there is a decline followed by a secondary maximun. The secondary maximum can be delayed after the primary one a few days, some months or even several years (Dent and Balonek, 1980; Picak et.al, 1985; Sillanpaa et.al, 1985). Such a behavior suggests that the mechanism of the outburst may be a sort of damped oscilation. Outbursts appear also at other frequencies, and events occurring at different wavelengths are often correlated, for example, 3C345 (Bregman et.al, 1986).

Abramowicz (1988) gave a perfect review in variability of AGN. He showed two important Figures: in Fig.6 he show the typical causal, dynamical, thermal and viscous timescales. Here the nature of the equilibrium and stability of these disks, which are characterized by $\dot{m} \ll 1$ and $0 < \alpha \leq 1$ is rather well understood in term of the Shakura-Sunyaev model (reviewed by Pringle, 1981). The $t_d \simeq 2m$ is the dynamical timescale, the $t_t \simeq 2m\alpha^{-1}$ is the thermal timescale, the $t_v \simeq 5\alpha^{-1}\dot{m}^{-2}m$ is the viscous timescale. Fig.6 is from theory. In Fig.7, Abramowicz present the timescale actually observed in different objects and at different frequencies.

The linear polarization of the radio sources has been observed to vary in the rapid and

complicated way (Astschuler et.al, 1976), we found that the changes in radio polarization of ON231 have clear similarities to changes in intensity in the optical range. The changes of optical polarization in ON325 are extremely well correlated with the optical light curve (see E.Szuszkiewicz Ph.D thesis 1988). From the comparison with the optical light curve we can then better derive the minima of the degree of polarization. As noticed by Kikuchi et.al (1988), two interpretations of rapid flux and polarization in blazars, i.e, relativistic beaming and simple two component model, predict that the minmum degree of polarization is always associated with the maximum rate of variation of the polarization angles. They have found consistency with their observation of OJ 287. In other case (Abramowicz, 1988) the position angle does not show large amplitude changes, remaining in the range 135-175 degree. However, two fast changes appear correlated with the polarization minima. Optical polarimetry of RS4 is extremely poor. There are four points in the V band and in the B band (Wills et.al, 1980; Sanduleak and Pesch, 1984). The four points in the V band show tendency to increase starting from 4.6% in 1980 and reach 8.4% in 1982. The position angle in this period is changing in the range of 48-58 degrees. No clear correlation with light curve can be found.

In the infrared, both flickering and secular trends have been observed (Abramowicz 1988). The shortest timescale for flickering being about 40 days in the case of 3C345. They pointed out, in general, there is a close correspondence between the brightness changes in all of the infrared bands. Outbursts are more pronounced at shorter wavelengths. For 3C345, flickering is not observed. Although the three largest infrared-optical outbursts of 3C345 preceded the three largest radio outbursts by roughly 1-2 years. the correlation between these events doubtful. Abframowicz pointed out, in general, there is no obvious correlation between variaibility in the optical- infrared and radio frequencies.

Although X-ray observation have a much shorter histoty than the other bands that have already been discussed, the observers who have had access to satellite-borne X-ray telescopes over the past decade or so have already produced a massive body of data. The Einstein observatory qucikly established that most quasars are powerful X-ray emitters, giving off from 10^{43} to $10^{47} ergs^{-1}$ between 0.5 and 4.5 Kev (Tananbaum et al, 1979). Only a few QSOs have yet had their X-ray fluxes measured at enough energies to yield any real "spectroscopic" information in that band and only a few QSOs have been monitored often

enough in the X-ray to allow conclusions about their variability in this band (Matilsky et al, 1982). The known QSOs, BL lacs and Seyferts. Only the brighter ones have been surveyed so far, and only a few of the very brightest have as yet been subjected to any detailed study. BL Lac objects are usually fairly moderate X-ray emitters (Biermann et.al, 1981), although confirmation of the association of specfic X-ray sources with BL Lacs really did not begin until 1978 when MK421 and MK501 were firmly identified (Mushotzky et.al 1980) Particular, long-term monitoring of AGN at X-ray wavelengths has been carried out for only a few objects (see also Abramowicz, 1988). One of the best case is BL 1219+305 (Wilson et.al, 1979) consists of a light curve which spans four years and show some possible outbursts. In most of other studies, the X-ray light curves are based on only a few points (e.g., 3 points for 3C345, Bregman et.al, 1986). Comparing optical data for BL 1218+305 obtained in Asiago with the X-ray measurement by Wilson et.al., (1979) one can find a correlation between active periods for this sources at these two wavebands. The X-ray outburst took place at the beginning of 1974 while the optical one was a hundred days later. Beregman et.al., (1986) discussed the results of comparing X-ray optical-infrared and radio variability data for 3C345. The beginning of the radio outburst coincides with the X-ray measurements and the increase in the X-ray flux is about the same as the increase in the 15 GHz radio flux. They did not find any apparent correlation between the X-ray and optical-infrared fluxes. Unless variations occur much more rapidly at X-ray frequencies than at optical and infrared frequencies, the X-ray emission is probably associated with the radio emitting region rather than with those regions emitting in the infrared or optical.

Abramowicz (1988) gave a clear review in short-term X-ray variability. He pointed out the short-term X-ray variability usually occurs on all of the relevant timescales. Pound et.al (1987) have illustrated this by discussing three generic types of X-ray variability, Similar to the Rosemary Hill type (but omitting the third). The example of the first Rosemary Hill type is the rapid variability of NGC4051 (Lawrence et.al, 1985). The source varies with a timescale $\leq 1h$ and with large amplitude. The variability is essentially continuous. Some "outbursts" can be seen. The same type of behavior is shown by MCG-6-30-15. McHardy and Czerny (1986) concluded from their analysis of the light curves of the seyfert galaxy NGC5506 that the observed variations which have amplititudes of up to 30 percent and timescales of hours, can be explained as a random distribution of events with random

amplitudes. The example of the second Rosemary Hill type is the variability of NGC4151 which shows secular trends, rather than rapid fluctuations. The fourth Rosemary Hill type is represented by the variability of III Zw 2, where a large flare was found in the X-ray light curves: the flux increased by a frctor of 3 in about 1500 sec and then decreased again to nearly the initial level in a futher 4000 sec. Most recently, Turner and Pounds (1988) reported distinctive short term variability in the soft X-ray excess of the seyfert galaxy Mkn 335. This is the first observation of this kind and it strenghtens the proposed identification of the soft X-ray excess as being of thermal origin and coming from an accretion disk.

2. The Broad Emission Lines

There are many theories of the structure of the broad emission lines(BEL) region and no general consensus of its physical composition has emerged. Most of these theories involve the motion of many low-mass clouds. The cloud's physical size is hypothesized to be less than $1AU$. With $\sim 10^{-9}M_{\odot}$, the whole BEL region is thought to contain between 1 and $100M_{\odot}$ (Nemiroff,R.J., 1988).

The major observational feature which BLR theories strive to explain kinematically is the shape of the BLR spectral emission lines. The lines are seen to have logarithmic shapes away from their peaks, with widths that imply motion of the the order of $10^4 kms^{-1}$. Most theories use the macroscopic motion of the clouds to explain these velocities. The discrete Doppler shift from each cloud creates a cumulative emission line that is much broader than the hypothesized temperature of the individual clouds would imply.

The intensity of the broad emission lines (BEL) observed in many AGN is proportional to the flux of ionizing radiation (Kwan et.al, 1979, 1981) which is believed to come directly from the accretion disk. This is the current explanation. Therefore, variations of the intensity of BEL may be an indicator of non-stationary accretion processes occurring directly inside the disk. However, it is not possible at present to make a direct quantitative link, as the kinematics and internal physics of the so called "broad emission lines clouds", where the emission lines originate, is still a metter of dispute among experts. Even the very existence of such clouds is sometimes questioned and it has been suggested that the emission line might instead originate at the surface of the accretion disk itself (Shields, 1977), at some high velocity stars passing nearby, or due to action of "duelling"

winds (Mardaljevic et.al, 1988). For general review of AGN and BLR properties, see Witta (1985) or Weedman (1986), and references therein; much of the current discussion is based on these reviews. Abramowicz(1988) gave a investigation and the most convincing and well established theoretical discussion of the broad emission line emitting region is that given in a series of articles by Collin-Souffrin (1986) and her collaborators (e.g., Joly et.al, 1985). Observations of variability of BEL have recently been reviewed by Peterson(1988).

Abramowicz and Lasota (1985, unpublished) studied the case of NGC 1566 using the (then unpublished) data of Alloin et.al (1986). Taking the mass to be $5 \times 10^7 M_\odot$ (in accordance with an earlier estimate by Alloin et.al 1985) and the efficiency to be $\eta = 0.06$ they concluded that the accretion rate averaged over the whole cycle was about $0.3\dot{M}_E$ and that the amount of matter accreted during one burst was about $10^{-2} M_\odot$. This suggests that variability was not caused by a change in the supply rate due to the the capture of a single star during each outburst (random capture of four unusually low mass stars in an almost periodic fashion has a small probability). They argued that the most natural explanation of the periodic outburst of NGC 1566 is the existence of a limit cycle produced by accretion disk instabilities.

3. Periodic light variation

According to Rosemary Hill classification, there are some QSOs belived to have peroidic light variations. Smith (1965) research the light curve of the quasar 3C273, he indicated the possible existence of nearly periodical brightness variations.Naearly periodic variation in the optical luminosity of the quasar 3C345 was suggested by Kinman et.al, (1968) and later confirmed by Smith and Wolstencroft (1970). The existence of periodicity in the brightness variation of 3C446 and 3C454.3 was suggested by Lu and Hunter (1969) and later by Kinman (1970). Jurkevich et.al (1971) repoted a periodic component with $p = 350^d$ for 3C120. Sillanpaa et.al., (1988) reported the OJ 287 exhibits periodic outbursts at intervals of 11.6 yr. Visvanathan (1973) discovered, using Fourier analysis, that the brightness of OJ 287 varies with a surprisingly short period $p = 29.4$ minutes. This was confirmed by Frohlich (1973), but questioned by Kiplinger (1974). Other examples are NGC 4151 (Pacholczyk, 1972) , 3C371 (Babadzanjanz, 1975), NGC 1275 (Lutyi and Pronik 1975), BL Lac in optical (Ozernoy and Usov, 1977), BL Lac in redio (Gorshkov and

popov, 1972) and OJ 287 in radio (Hagen-Thorn et.al., 1977). This long list of successes in finding periodicities may be two optimistic. The recent analysis of all existing data for 3C345 by Kidger and Beckman (1986) shows that there is no periodicity which is free from doubt. In particular, they exclude the long periods of 1000-2000 days obtained by Barbieri et.al.(1985). A recent paper by the Rosemary Hill group (Webb et.al., 1988) used only the data gathered by the same instruments and reduced by the same procedures. It discussed three objects in detail: 3C120, 3C345 and 3C446. The sinusoidal components found for 3C120 with a period of 1245 yr and the components for 3C345 with periods of 11.4 and 5.6 years did not agree with any periodic components suggested by other authors. The conclusion of the paper was that identification of periodic components in a finite data set does not prove the existence of "real"periods in the source. Barbieri et.al. (University of Padova preprint 1988) carried out a similar study with the Asiago data and reached a similar conclusion. They then discussed the Rosemary Hill data for ON231 (Webb et.al., 1988) and performed a Fourier analysis using the program of Deeming (1975). They found the same periods as the Rosemary Hill group. However, when they repeated the procedure with the Asiago data for the same source (which is as extensive as the Rosemary Hill data) none of the periods which they found agreed with those found by Webb et.al.. As a last step they took all of the data reported in the literature. All periods disappeared except a 27 years period- the interval between two almost identical outbursts found for this source a long time ago (Pollock et.al., 1974).

The Nature of the optical observations is not convenient for making periodicity searches: there are unequal intervals of time between observations and annual gaps in the data, together with the normal observational uncerntainties and the relativity short baseline of the data set. The same difficulties may explain the conflict between the results obtained by the EXOSAT and Einstein observatory X-ray satellites. Zamorani et.al (1984) using the Einstein observatory data, concluded that for roughly half of their sample of bright quasars they should have been able to detect variations of the order of 30 percent in amplitude and with timescales shorter than 10^4 seconds but, in fact, did not see any such variations. A similar conclusion, that short-term variability in optical selected Seyfert galaxies is rare, has been reach by Urry et.al.(1987), who also used the Einstein observatory data. On longer timescales (months, years) Urry et.al. found that variability is more

common. However, recent EXOSAT results have called these conclusions into question. These results do not indicate long-term variability and suggest that short-term variability is common at X-ray frequencies (Warwick 1986).

The different results obtained using Einstein Observatory and EXOSAT may reflect inherent difference between the sources observed, as the selection criteria were differnet: the EXOSAT survey used well-studied, X-ray bright, historically variable X-ray source, while the Einstein observatory survey was based on complete, optically selected samples. However, the differences may be of a purely technical nature connected with the fact that EXOSAT was capable of much longer observing times(for each observation) than the Einstein Observatory but had a shorter total life time. This stresses the importance of good selection criteria and frequent sampling in future space missions which plan to study variability of AGN (see e.g. Broadfoot, Duran and Stalio 1988 in the case of the Santa Maria satelite).

4. Short timescale in variability of AGNs

Short-time variations in luminosity provide the best upper limits for the sizes of AGN active regions. In the absence of special geometries and relativistic motions, it can fairly be concluded that significant variation over a time Δt implies a source no longer than $\Delta R = c\Delta t$. Particularly, the rapid optical variability is one of the important properties of BL. Lacertae objects. In general, the shortest time scale relates to the region close to the central power source and general constraints on emission mechanisms may be placed (Guilbert et al. ,1984).

There are many explanation about variablity in AGN, which are based on different models of AGN (They are accreting black hole, spinar, compact star clusters,etc). But, the best one is accreting black hole. According to this model, we can obtain the shortest observed timescale. The short term irregular flares is due to inhomogeneities in the falling matter. When some hot, dense lump fall into the inner part of accretion disk, where the most of luminosity is emitted, a flare should exhibit. Elliot and Shapiro (1974) argued, if this assumption is true, then we should have a relation between the luminosity and the shortest timescale. At first, they assume the luminosity L can not be greater than the Eddington value (i.e, radiation pressure on the infalling matter never exceeds the

gravitational force [Eddington 1921]):$L \leq L_E = 10^{38}(M/M_\odot)ergs^{-1}$. Then, the minimum time scale $t_{\min}$ should be greater than the light travel time across a distance equal to the Sohwartschild radius: $t_{\min} \geq r_G/C = 10^{-5}(M/M_\odot)S$. They derived the relation $\log\Delta t_{\min} > \log L - 43.1$. According to this condition, all observational points should be above the corresponding diagonal line in Fig.8.

But Impey et al.,(1982) found some cases violating the Elliot & Shapiro criterion (0235,3c446). They try to explain the fact with assunption of relativistic bulk motion. On the other hand, Abramowicz and Nobili (1982) gave another explanation. They argued, in thick accretion disk instead of thin disk, the luminosity can be as large as 100 times Eddington luminosity (Luminosity larger than this one will be unrealistic). They corrected the Elliot and Shapiro criterion as follows:

$$\log t_{\min} = \log\ L - 43.1 + \log(\tau/\lambda)$$

where $\tau = \pi(r_*^{3/2} + a)$, $r_* = 2r_{in}/r_G$. r_{in} is the radius of inner edge of thick disk, a is the dimensionless Kerr parameter. In extrem-Keer case, $a = 1$, $r_{in} = 0.5r_G$, so $\tau_{\min} = 2\pi$, $\log\ \tau_{\min} = 0.8$ and

$$\lambda = \frac{L}{L_{Edd}}$$

In thick disk, λ can reach $\lambda_{\max} = 100$, $\lg\lambda_{\max} = 2$, put $\log\tau_{\min}$, $\log\lambda_{\max}$ into previous equation, we have Abramowicz criterion,

$$\log t_{\min} \geq \log L - 44.3$$

In Fig.9, we can see 0235 and 3c446, 0J87, BL Lac are above the criterion line. These give one of strong arguement favorable to thick disk model of AGN.

Barr (1986) analyse the X-ray data and point out that X-ray emitting regions are responsible for the shortest variablity timescale.

5. A possibility explanation for variability of AGN

The variability in luminosity of AGN is complex. The best model which can explain these variability is accretion disk instabilites: dynamical, thermal, viscous (Abramowicz, et al., 1989). This is a special direction and there are many excellent works. The interested

one is reported by Abramowicz (1981, 1986). They found a bistability in accreting black hole model which can be a reason of variability. Most probably in this case accretion flow undergoes a limit cycle behaviour: it oscillates between high and low states. The existence of the limit cycle is due to general relativistic effects in the gravitational field of a black hole. The short term variability behaviour of AGN provides a strong arguement favorable to the model of thick accreting disk (Abramowicz & Nobili criterion). Until now, we have no perfect model for long term periodic variability of AGN in the frame of accreting black hole model. Some expective models, such as bistability, self gravitational disk, need to be investegated further.

All the Previous models have a common point i.e. variability is produced by AGN itself, we called also the variability is intrinsic. On the other hand, some people (Schneider, 1985, Paczynski,1986, Refsdal, 1979) reported a possible mechanism of variability which is not intrinsic to the accretion processes. They suggested that variability might not be a signature of the physics of AGN at all, but might originate "midway" due to influence of matter between us and the source. In the light of recent results which indicate that a large fraction of quasars is gravitationally micro-lensed (Schneider, 1987), they propose the time dependent amplification by microlenses to be a reasonable explanation for variability in at least some active galactic nuclei; in particular, their results support the recent hypothesis (Ostriker and Vietri,1985) the BL-Lac objects may be due to selective amplification of quasars. Gravitational microlensing ordinarily refers to the lensing effects of individual stars or other compact masses, typically with masses $10^4 M_\odot \leq M \leq 10^6 M_\odot$, which may be superimposed on the lensing by an entire galaxy. The microlensing can not explain all of complex phenomena of variability of AGN. It can interprete a few types variability according to the Rosemary Hill classification at least. For a moderate number of microlenses, typical theoretical light curves show sudden, double peaked outbursts in which the rise and decay times are quite symmetric. The bursts have very characteristic U-shapes between the peaks, and are separated by long quiescent periods. A quasi-periodic bursting may easily occur by chance. The predicted timescales for variation due to microlensing range from weeks to centuries, depending on the impact parameter and the relative velocities of the lens and source on the sky. In fact, we have not observed symmetric U-shopes of the light curve in observation data. It exists only in the theory and is in lower optical

depth case, because the shapes of the light curve is dependent on the optical depth of the lensing galaxy. In theoretical models dense star fields in the lensing galaxy are found to produce irregular flickering without much change in apparent magnitude and without periodicities. This agrees, very nicely, one might think, with the fourth and first types in the Rosemary Hill classification. The possible gravitational lense amplification of the broad line region (BLR) of active galactic nuclei by stars in foreground galaxies is reported by Nemiroff (1988). For various possible kinematic structures of the BLR, the line shape changes caused by microlensing are generated and classified. The probability of spectral line distortion is at least equal to the probability of amplification of the inner continuum region, and in some cases can even slightly exceed it.

Variation in the apprent luminosity of active galactic nuclei might be caused by microlensing (Watson 1988). In particular, the observed enhancement of the central continuum in comparison with the larger, spectral line emitting region might arise because the central continuum region in the unlensed source is comparable or smaller than the Einstein radius and is thus magnified (Ostriker et al., 1985) whereas the line emitting region is larger than the Einstein radius ($\sim 10^6\sqrt{M/M_\odot}$cm). Of course, microlensinng model can not still interprete many characteristics in variability of AGN. Abramowicz (1987) has concluded some important detailed differences.

Part II Gravitational Microlensing

1. Historical Introduction

The concept of gravitational lensing can be traced back to the early 1800's, specifically to Soldner (1801). Combining Newtonian gravitational theory with the particle theory of light, Soldner predicted that a star could be imaged twice if another star lay close to the light path to the observer. Oliver Lodge proposed in 1919 that light could be focused through a gravitational lense. Following this suggestion, Frost, E. B. (director of Yerkes observatory in 1923) outlined a program to search for lens effects among stars. Chwolson (1924) anticipated that the light of distant stars grazing the limb of a foreground star would be see by an observer aligned with the two stars as a ring around them. It is possible that the luminous arc discovered in 1987 by R.Lynds and V.Petrosian is actually a "Chwolson ring" image of a galaxy. Einstein (1936) made a short calculation and rediscivered the possible existence of the Chwolson ring, now called the "Einstein ring". Others soon began to think about gravitational lensing. Tikhov (1937) worked out many of the mathematical properties of a point lens acting on a point source. Zwicky (1937a,1937b, 1957) became convinced that galaxies could eclipse each other and hence acts as lenses. He estimated that the probability of observing this effect was very high. Nevertheless, interests in the gravitational lensing phenomenon arose only after Yu. Klimov (1963), S. Liebes (1964), S. Refsdal (1964), and F. Link (1967) independently of each other published detailed calculations of the dioptric properties of gravitational lens images. Bourassa and Kantowski (1975) calculated the dioptric and photographic properties of images produced by distributed mass lenses and showed that such lenses can produce multiple images from the same object. Occasionally, the object itself is seen through the body of the lens. This may be the reason why in the literature it is usually stated that a gravitational lens produce at least three images.

In the early 1970's, papers on stellar gravitatioanl lensing were relatively few. There seemed, however, to be a growing realization that gravitational lensing should be seen if some models of the mass distribution in the nuiverse were correct. Press and Gunu (1973) showed that if the universe were uniformly populated with certain types of objects, and the density of such objects were comparable to the visible mass, several gravitational lens effects should be observable. Maeder (1973) showed how the resulting flux from a binary system could be altered by gravitational lensing. The detection of the first extra-

solar system gravitational lens event came in 1979 with the discovery by Walsh, et al., of two gravitationally induced images of the same quasar 0957+561. The two images were interpreted as that of a single quasar whose light is split by a galaxy along the line of sight. Since then, at least ten lens candidates have been put forward (Blandford, 1987), all of them caused by lenses of galactic mass or greater. These cases have come to be know as macrolensing.

In 1979 microlensing began to gain popularity. Chang and Refsdal (1979, 1984) showed that a single star, with the addition of the gravitational shear (discussed later) of the host galaxy, could split the image of a quasar into very close components and either magnify or diminish the flux from the original quasar image. Gott (1981) discussed the possibility that the haloes of spiral galaxies could be composed of low mass stars that could themselves lens background quasars. The paper predicted the likelihood and time scale of such events, and suggested that observations of quasar 0957+561 might show this microlensing phenomenon. More recently, Paczynski (1986) calculated the effect of many stars in a galaxy acting at once as a lens. These effects were shown to be much more complicated than that due to each stellar lens individually. The corresponding light curves were calculated and displayed.

Since the discovery of macrolensing systems, the number of papers written on gravitational lensing has increased dramatically. Although most papers attempt to model the mass distribution needed for macrolens systems, There has been a major conspicuous attempt to understand the effects of microlensing. To date, however, no unambiguous microlensing detection has been made.

2. The General Theory of Gravitational Lens

Although the General Relativity light bending prediction lies at the heart of gravitational lensing, the subject does not directly involve any frontier or state-of-the-art issues in physics; in principle, all is well understood. Nevertheless, theoretical work on gravitational lensing has proven to be a rich and illunminating undertaking. there are at least four major problems on which gravitational lens theorists have focused their attention:

The first major area of concentration has been the development of improved methods for solving the lensing equations and, specificly, of calculating the effects of particular

model lenses. The original vector displacement formalism, which is conceptually easy to understand but somewhat awkward to work with in complex situations, has been supplemented with two other major alternatives. One of these is based on Fermat's principle (in optics) and makes use of the time delay surface in the image plane, defined as the time delay for a light speed signal propagating alone a geodesic from the source to the lens (image plane) and there being deflected onto a geodesic leading to the observer. Image form at extrema and saddle points of this surface with magnification and parities determined by the surface's local curvature. The other is based on Catastrophe Theory and identifies images as zeroes in a so called squared deviation function; it is particularly well suited to studying lensing of extended sources. In addition to these new formalisms, a technique for representing complex lensing situations in term of source plane caustics, lines which separate regions of the source plane which are imaged n times from those which are imaged $n+2$ times, and the corresponding image plane critical lines along which new pairs of images appear when a source crosses a caustic has allowed us much clearer physical understanding of realistic lens models.

A second major area of effort might be broadly described as lensing statistics. This includes problems of line-of-sight integration of lens event probabilities over cosmological distances and in the framework of standard Friedmann models, treatment of increasingly realistic statistical models of lens mass distributions (galaxies, clusters, ...), inclusion of the effect multiple lens scattering events, interaction of lenses with very different characteristic angular scales, the influence of selection biases (in quasar samples, for example) on lens detection, and so forth. Although this problem involves some rather fundamental theoretical issues (e.g., how good and approximation is the Robertson-Walker metric for this purpose in a universe which is highly inhomogeneous on many scales). Most of the work has been aimed at improving the realism of the calculations in more prosaic astrophysical way (galaxy mass distributions, sample selection biases,...).

A third major topic of theoretical interest in lens studies is called microlensing, or sometimes minilensing. These more or less equivalent terms refer to lensing by effectively point objects with masses so small that the characteristic angular scale is much (usually very much) smaller than observational resolution, perhaps small enough that proper motions are signification on human time scales. Lensing by the most fundamental of as-

tronomical objects, stars, falls into the category of microlensing. Theoretical work on microlensing has sought to calculate the properties of microlensing light curves (produced by variable magnification due to proper motion) in a statistical sense, magnification probability distributions, and the coupling of microlensing to macrolensing (such as that produced by the galaxy in which a microlensing star moves). The dependence of microlensing effects on "optical depth" [the surface mass density of microlensing objects in units of the lensing critical surface density (whice corresponds to a lens focused on the observer)] and on finite source size which suppresses microlensing effects as it becomes large cmpared to the characteristic microlensing angular scale has also been examined.

A fourth area of theoretical lensing studies which has attracted considerable attention and ingenuity is the invention and elaboration of possible astrophysical applications of gravitational lens studies. Starting with Refsdal (1964) seminal paper pointing out that lens observations might plausibly be used to determine Hubble's constant H_0 directly on very large scales, a wide variety of investigators have invented a wide variety of possible uses for lenses. Ways of determining the other two classical cosmological constants, q_0 and Λ have also been pointed out. Techniques for measuring the mass distribution of galaxies, galaxy clusters, and even larger scale systems have been devised. These are particularly important in the context of dark matter which cannot be easily studied by other means; indeed microlensing effects offer the only known technique for distinguishing between dark matter consisting of smooth distributions of elementary particles and more conuentional macroscopic astronomical objects (dead stars, black holes, etc.) by direct astronomical observations. Uses of lenses as cosmic telescopes [originally suggested by Zwicky(1937)] to study quasars or distant galaxies have also been explored as has their possible role in producing correlations on the sky of objects at very different distance. Although it is unlikely that all of the proposed lens applications will ever be realized in practice, it is the continuing expectation that some of them will be important that drives most of the work, observational and theoretical, on gravitational lenses.

A) Principles of Gravitational Lensing

The important effects of a gravitational lens are not only splitting of images and deflection of light rays, but also amplification, distortion and rotation of images, and time

delay between different images.

According to general relativity, gravitation act on light as well as upon matter. The results of this interaction is to deflect a photon away from a path that would appear straight as viewed by an observer at infinity. In this way, non-uniform gravitational fields can act as lenses.

In the gravitational lens system, the interesting question is that of the nature of the lensing object, i.e. forground galaxy. At the present, there are such objects as candidate: a) the galaxy (Narajan, R. et al., 1984), b) black hole (Paczynski, B. 1986), c) cosmic strings (Gott, J. R. 1986). But the more discussion are concentrated on galaxy. So far, there is only one example for the black hole or cosmic strings (Paczynski 1986).

A particular gravitational field that merits study in the way it deflects light is the field of a point mass. Far from a point mass, a linear approximation to GR is valid. The nagular deflection of a photon is vary nearly $i = 2R_s/R$, where R_s is the Schwarzschild radius of the point mass, and R, the impact parameter, is the distance of closest approach of the photon to the mass. It is a good approximation to assume that the photon is deflected discretely when it crosses the lensing plane (the plane containing the lensing mass perpendicular to the line connecting the source to the observer, see Refsdal 1964 on this point). If the lens (assumed spherical) has a finite radius L greater than R_s, a unique focal length can be defined. The geometry is show in Figure 10. The focal length is easily shown to be (Namiroff, 1987)

$$F = 538 \left(\frac{R}{R_\odot}\right)^2 \left(\frac{M_\odot}{M}\right) \ AU \qquad (A.1)$$

Table 1 shows the focal lengths for different astronomical objects. It is evident that an observer must be a distance greater than F away from the lens for the lens to be able to deflected light so that a source far behind it becomes visible. Alternatively, the source must be a distance F or greater from the lens so that an observer far behind the lens can see it.

A important mathematical consequence of gravitational lensing is the conservation of surface brightness (Misner, et al., 1973). This consequence derives directly from conservation of phase space in the boundle of rays coming to the observer. Continuous, uniform-brightness images of source objects seen by an observer have the same surface

brightness after passing a gravitational lens as before. What a lens does is distort the area of the solid angle of the image as seen by the observer. With the same surfeace brightness but different angular extent, an unresolved object can appear to have a different overall apparent brightness to an observer, for total source flux to be conserved, there must be observers who see an increased source flux due to gravitational lensing, and other observers who receive a decreased amount. For near exact observer-lens source alignment, there are observers that receive a substantially greater flux from the source than without a lens. there are, however, no positions that would receive a substantially smaller amount of flux than without the lens. As expected, gravitational lensing does not create flux, it merely distorts its distribution.

At perfect observer-lens-source alignment, a point source is distorted by a point lens into a circle: a thin angular ring centered on the source (to Einstein 1936). At this configuration the flux from the source to the observer is maximized. The angular radius of this circle is a scale unit which is naturally defined by the problem. This scale unit will be referred to as the Einstein Ring Unit (ERU). Note that only at perfect collinear alignment does the Einstein ring appear. If the alignment is not exact, two images of the soource appear. When the alignment is close to exact, the two images are separated by two ERU(Nemiroff, 1988).

There is also typicall a time delay between the two images. The magnitude of the time delay is of the order of the time it takes light to cross the Schwarzschild radius of the lensing mass. The images are not precise replicas of each other. One image is a scaled, inverted mirror image of the other. The difference in the apparent brightness of the images is always the original apparent brightness of the source (Liebes, 1964).

What happens to the image character when more than one lens is present? To discuss this in the context of the modern mathematical language of gravitational lensing, it is necessary to introduce the concepts of optical depth and shear. Optical depth can be defined in a gravitational lensing sense as the number of lensing massas per ERU. If there is a distribution with lenses spaced by only a couple of ERU or less, the net effect on the source light will be more complex than from the linear addition of the individual lenses.If the average separation between lenses is much greater than the ERU, it is usually a good approximation to consider the lenses one at a time and add their respective contributions.

In this case, however, only one lens will significantly affect the image flux.

If a large mass is near to a stellar lens in the lensing plane, the mass can distort the image characteristics of an individual lens in non-trivial ways. This can be the case when stars close to the center of a galaxy act on the flux from a distant quasar, the host galaxy of the star exerts a gravitational influence distorting the lens effect of the individual star. This effect is called a shear effect. Shear is important when a lens is within a few ERU of the near large mass. When the star is many ERU (of the massive object) distant, shear effects of the massive objects are minimal.

In the presence of high optical depth and shear terms, the location of the images and the calculation of their brightnesses become more complex. To calculate these one may invoke Fermat's principle (Blandford 1986). Fermat's principle states that real images take paths where the time of travel is an extremum, either maximixed or minimized (or both as with a saddle point). In the absence of lensing, the cirtical path is a straight line between the source and the observer, and the travel time is obviously a minimum. In the presence of lensing, time is showed in the vicinity of the gravitational fields of the lenses, making the critical paths more numerous and complex. It will be discussed more detail later.

B) Lens Formulas

The major purpose of this thesis is about microlensing and variability of AGN. Then, we give only a short discussion in gravitational lensing i.e. macrolensing.

There are three separate formalisms that are useful for different problems in gravitational lensing. They are vector firmalism, scalar formalism and propagation formalism. we discuss only concentration onto vector formalism and scalar formalism. Although the original vector formalism somewhat awkward to work with in complex situation, but it is conceptually easy to understand. The scalar formalism based on the new way called Fermat's principle and will derive directly the time delay. This is a new theoretical direction for studing gravitational lensing. The propagation formalism (the optical scalar equations) are useful in an inhomogeneous universe where are no well-dedined lens planes at which the light rays are bent. It can decide the evolution of the cross section of the congruence of light rays (Blandford 1987). We will neglect this discussion in my thesis.

We will consider the trajectory of the light ray passing at a distance R from the center

of the field. Schwarzschild metric:

$$g_{\mu\nu} = \begin{pmatrix} -e^x & & & \\ & e^y & & \\ & & r^2 & \\ & & & r^2\sin^2\theta \end{pmatrix} \qquad (B.1)$$

where $e^x = e^{-y} = \left(1 - \frac{2GM}{r}\right)$. We consider the path of a light ray in a centrally symmetric gravitational field. As in every centrally symmetric field, the motion occurs in a single "plane" passing through the origin; we chose this plane to be the plane $\theta = \pi/2$. This path is determined by the eikonal equation

$$g^{\mu\nu}\partial_\mu\psi\partial_\nu\psi = 0 \qquad (B.2)$$

where ψ is the eikonal. Substituting metric into (B.2), we find the following equation:

$$\left(1 - \frac{2GM}{r}\right)^{-1}\left(\frac{\partial\psi}{\partial t}\right)^2 - \left(1 - \frac{2GM}{r}\right)\left(\frac{\partial\psi}{\partial t}\right)^2 - \frac{1}{r^2}\left(\frac{\partial\psi}{\partial\phi}\right) = 0 \qquad (B.3)$$

By the general procedure for solving the Hamilton-Jacobi equation, we look for a ψ in the form

$$\psi = -\omega_0 t + L\phi + \psi_r(r) \qquad (B.4)$$

where ω_0 is the frequency of the light, L is the moment of the impusle, and $\psi_r(r)$ is an undertermined function. From (B.4), we obtain

$$\frac{\partial\psi}{\partial t} = -\omega_0, \qquad \frac{\partial\psi}{\partial r} = \frac{\mathrm{d}\psi_r(r)}{\mathrm{d}r}, \qquad \frac{\partial\psi}{\partial\phi} = L.$$

Substituting these formulae into (B.3), we find the derivative $\frac{\mathrm{d}\psi_r(r)}{\mathrm{d}r}$ and thus:

$$\psi_r(r) = \int\left(1 - \frac{2GM}{r}\right)\sqrt{\omega_0^2 - \frac{L^2}{r^2}\left(1 - \frac{2GM}{r}\right)}\mathrm{d}r. \qquad (B.5)$$

The trajectory itself is determined by the equation $\frac{\partial\psi}{\partial L}$, combined with (B.4) and (B.5), so that

$$\phi = \int\frac{L/r^2}{\sqrt{\omega_0^2 - \frac{L^2}{r^2}\left(1 - \frac{2GM}{r}\right)}}\mathrm{d}r.$$

Thus, we obtain a differential equation

$$\left(\frac{L}{r^3}\frac{\mathrm{d}r}{\mathrm{d}\phi}\right)^2 = \omega_0^2 - \frac{L^2}{r^2}\left(1 - \frac{2GM}{r}\right).$$

Therefore, we proceed with a series of tedious operations. We obtain the net bending angle,

$$\Delta\phi = \frac{4GM}{R}. \qquad (B.6)$$

We have chosen $C = 1$. eq.(B.6) has been deduced in an approximation to the full theory and is linear, bending angle due to different mass are additive, so formalism based on this formaula seen to be set in the framework of linearized G.R.,at least as concerns the effects of clumpiness of matter in the universe. The bending angle does not depend on the photon's frenquency. The different null geodesics from a light source can pass on opposite sides of the deflecting object and intersect each other after deflection, so an observer collecting these light rays will see several images coming from apparently different directions.

Vector Formalism.

The geometrical construction of gravitational lensing is shown in Fig.11. The lens equation for a single lens follows from simple geometry (Blandford, 1987),

$$\theta_{\mathrm{s}} D_{0s} + \alpha(\theta_{\mathrm{I}}) D_{Ls} = \theta_{\mathrm{I}} D_{0s} \qquad (B.7)$$

where θ_{s} is the angular position of the source, θ_{I} is the angular position of the image. This equation can be written into another convenient form,

$$\theta_{\mathrm{I}} - \theta_{\mathrm{s}} = \frac{D_{Ls}}{D_{0s}}\alpha(\theta_{\mathrm{I}}). \qquad (B.8)$$

The bending angle α can be computed by superposing the deflections due to each element of the lens,

$$\alpha(\theta_{\mathrm{I}}) = 4D_{0L}\int \mathrm{d}^2\theta \frac{\Sigma(\theta)(\theta_{\mathrm{I}} - \theta)}{|\theta_{\mathrm{I}} - \theta|^2}, \qquad (B.9)$$

where Σ is the surface mass density of the lens. Due to the universe is not Euclidean, the distances used in the lensing equation (for example D_{0s}, D_{Ls} etc) should not be Euclidean distances. In a smooth Friedmann universe with current density fraction $\Omega_0 = 2q_0$ (where

q_0 is the deceleration parameter) of the critical density for closing the universe and use the Einstein-Desitter model in which $\Omega_0 = 1$, the angular diameter distance is given,

$$D_{ij} = \frac{2}{H_0} \frac{(1+z_i)^{1/2}(1+z_j) - (1+z_i)(1+z_j)^{1/2}}{(1+z_i)(1+z_j)^2} \qquad (B.10)$$

where H_0 is Hubble constant, z is the redshift of source and lens. The most probable lens position is near $z_L = 0.5$ where $D_{Ls}/D_{0s} \sim 0.5$ whereas by $Z_L = 1.5$, $D_{Ls}/D_{0s} \sim 0.1$.

An equivalent geometrical construction is given by a bending angle diagram, shown in Fig. 12, where the deflection angle is plotted as a function of the image position on the lens plane on which the curve $\theta_I - \theta_s$ is superposed. The images are located at the intersections of the curve and the line. Note that for a non-singular gravitational potential, the deflection angle will be $\propto M/r$ at large radii, and $\propto \Sigma_0 r$ at small radii, where Σ_0 is the central surface density. As long as the potential is non-singular and circularly symmetric, only one or three images will be generated unless the mass distribution is very contrived. Singular potentials will generally capture one image in the singularity of the potential.

Amplification

Gravitational bending of light rays may not only lead to multiple imaging, but also changes the apparent luminosity of a source. We should discuss the amplification shortly. The variable $\mathbf{r}$ is used instead of the θ in above lens equations (the construction is shown in Fig. 13), and $\alpha(\mathbf{r})$ can be written as a gradient of the scalar function $\psi(\mathbf{r})$, $\alpha(\mathbf{r}) = \nabla\psi(\mathbf{r})$, where

$$\psi(\mathbf{r}) = \int \Sigma(\mathbf{r}') \ln|\mathbf{r} - \mathbf{r}'| \mathrm{d}^2 r' \qquad (B.11)$$

and lens equation (B.7) can be written

$$\mathbf{x} = \mathbf{r} - \alpha(\mathbf{r}) \qquad (B.12)$$

This equation can be expressed in term of another scalar function as

$$\mathbf{x} = \nabla\phi \qquad (B.13)$$

where

$$\phi(\mathbf{r}) = \frac{|\mathbf{r}|^2}{2} - \psi(\mathbf{r}) \qquad (B.14)$$

In term of ϕ, the Jacobian matrix is

$$A \equiv \frac{\partial \mathbf{x}}{\partial \mathbf{r}} = \begin{pmatrix} \frac{\partial^2 \phi}{\partial x^2} & \frac{\partial^2 \phi}{\partial x \partial y} \\ \frac{\partial^2 \phi}{\partial y \partial x} & \frac{\partial^2 \phi}{\partial y^2} \end{pmatrix} \tag{B.15}$$

The determinant of A is given by

$$\det A = \phi_{xx}\phi_{yy} - (\phi_{xy})^2 = 1 - \Delta\psi + [\psi_{xx}\psi_{yy} - (\psi_{xy})^2]$$

where $\Delta \equiv \partial^2/\partial x^2 + \partial^2/\partial y^2$ denotes the two-dimensional Laplacian. If one defines $\mu = \psi_{xy}$, $\lambda = \frac{1}{2}(\psi_{xx} - \psi_{yy})$, one seens that the determinant can be reexpressed as

$$\det A = (1 - \frac{1}{2}\Delta\psi)^2 - \lambda^2 - \mu^2 \tag{B.16}$$

and the trace is given by

$$\mathrm{tr} A = \Delta\phi = 2 - \Delta\psi \tag{B.17}$$

where

$$\Delta\psi(\mathbf{r}) = \int \Sigma(\mathbf{r}')\Delta \ln|\mathbf{r} - \mathbf{r}'| \mathrm{d}^2 r' \tag{B.18}$$

$\Delta\psi(\mathbf{r})$ has been found (Schneider, 1984) $\Delta\psi = 2\pi\Sigma(\mathbf{r})$, which gives

$$\det A = (1 - \pi\Sigma)^2 - (\lambda^2 + \mu^2) \tag{B.19}$$

$$\mathrm{tr} A = 2(1 - \pi\Sigma) \tag{B.20}$$

The first term in (B.19) is a local quantity, describing the effect of material in the light beam; it is called Ricci-focussing, while $\lambda^2 + \mu^2$ is a non-local quantity, called shear. (B.20) was first derived by Young (1981). Schneider proved $\det A \geq 0$ and $\mathrm{tr} A \geq 0$, which implies that the amplification factor

$$I = (\det A)^{-1} \geq 1 \tag{B.21}$$

Particularly, for the rotationally symmetric case,

$$0 < \det A \leq 1,$$

so an observer see a non-deamplified image. This proves the general fact that every geometrically thin, transparent lens leads to at least one image of a source which amplification

factor is greater than or equal to one. This is not violate flux conservation (Schneider, 1984).

For a circlar lens, the amplification is

$$A = \frac{\theta_I}{\theta_s}\frac{\mathrm{d}\theta_I}{\mathrm{d}\theta_s}$$

it consists of two parts, θ_I/θ_s is the tangential spreading of the image, The $\mathrm{d}\theta_I/\mathrm{d}\theta_s$ is due to the focusing or defocusing of the source in the radial direction.

For different lenses, the formulas of amplification are difference (Abramowicz, lecture in GL).

parity of image

When we discuss the time delay and the orientation of images, we will use the idea of parity. The partial parity of an image in any direction is + if it has the same orientation as in the source and –if it has been reflected. Hence each image has a parity label (radial parity, angular parity), and a total parity which is positive if the partial parities have the same sign and negative if they have opposite signs. The partial parities are the signs of the eigenvalues of the second rank tensor which describes the distortion of the images relative to the source (it will be seen later).

Scalar Formalism : Fermat's Principle.

The main mathematical principle used to calculate image location and intensity is Fermat's principle: real image travel on paths for which the light travel times is a local extremum.

In the weak field limit ($\phi \ll 1$), the metric near the lens is

$$\mathrm{d}S^2 = -(1+2\phi)\mathrm{d}t^2 + (1-2\phi)\mathrm{d}x^\alpha \mathrm{d}x_\alpha + o(\phi^2) \qquad (B.22)$$

where ϕ is the Newtonian gravitational potential of the lens. The equation for the geodesic following by a light rays is simply $\mathrm{d}S^2 = 0$ which we can integrate along the trajectory to determine a time along the path. If the lensing stars are considered to be confined to a plane between the observer and the source, we can assign a number to every point on the

plane describing the light travel time from the source to the observer passing through the given point. If we then consider this number to be a fictitious height above the plane, we can drow a relative light travel time surface. When the surface shows a local minimum, for example, the time it takes for light to reach the observer is at an extremum, and an image forms there. For the small, positive optical depths considered here, only minima and saddle points can occur.

For a given path, there are two source of time delay (Schneider, 1985). The geometrical contribution is just the extra path length traveled by the light when it is deflected from a geodesic in the background world model by a large mass. The second contribution , viz., the local gravitational time delay attributable to the presence of that mass, is familiar from the radar-ranging experiments. carried out in the solar system (e.g., Reasenberg et al. 1979; Weinberge 1972). These two contributions to the time delay in the observer frame is

$$t_{geom}(\theta_{\mathrm{I}};\theta_{\mathrm{s}}) = \frac{(1+z_L)D_{0L}D_{0s}}{2D_{Ls}}(\theta_{\mathrm{I}}-\theta_{\mathrm{s}})^2 \qquad (B.23)$$

$$t_{grav}(\theta_{\mathrm{I}}) = -2(1+z_L)\int \mathrm{d}s\phi(\theta_{\mathrm{I}}) \qquad (B.24)$$

where z_L is the redshift of lens, other quantities are shown in Fig. 2. The integral of the Newtonian potential along the line of sight is a two- dimensional potential with the projected surface density as its source. The renormalized time delay is defined by Blandford (1986),

$$\tau = \frac{D_{Ls}}{(1+z_L)D_{0L}D_{0s}}t \qquad (B.25)$$

and define a two-dimensional relativistic potential $\psi(\theta_{\mathrm{I}})$ by

$$\psi(\theta_{\mathrm{I}}) = \frac{2D_{Ls}}{D_{0L}D_{0s}}\int \mathrm{d}s\phi(\theta_{\mathrm{I}}) = \frac{4D_{Ls}D_{0L}}{D_{0s}}\int \mathrm{d}^2\theta'\Sigma(\theta')\ln(\theta_{\mathrm{I}}-\theta') \qquad (B.26)$$

where $\Sigma(\theta')$ is the surface density (gcm^{-2}) of matter at relative position θ'. The potential ψ then satisfies the two-dimensional Posson equation

$$\nabla_2^2\psi = \frac{\partial^2\psi}{\partial\theta_{I1}^2}+\frac{\partial^2\psi}{\partial\theta_{I2}^2} = \frac{8\pi D_{oL}D_{Ls}\Sigma}{D_{0s}} = \frac{2\Sigma}{\Sigma_c} \qquad (B.27)$$

where the derivatives are with respect to cartesian axes in the image plane. The quantity Σ_c is the critical density at which a uniform sheet of matter would just focus radiation from the source at the observer (Turner, Ostriker, and Gott 1984).

The total time delay is obtained by adding the geometrical and gravitational contributions. In these cosmologically scaled units,

$$\tau(\theta_{\mathbf{I}};\theta_{\mathbf{s}}) = \frac{1}{2}(\theta_{\mathbf{I}} - \theta_{\mathbf{s}})^2 - \psi(\theta) \qquad (B.28)$$

where $\tau(\theta_{\mathbf{I}};\theta_{\mathbf{s}})$ is the time surface. By Fermat's principle, for a given source position $\theta_{\mathbf{s}}$, the images are located at the stationary points of $\tau(\theta_{\mathbf{I}};\theta_{\mathbf{s}})$ with respect to variations of $\theta_{\mathbf{I}}$.

For the moment, we can choose our image plane coordinates to be centerted on the source position $\theta_{\mathbf{s}}$ so that

$$\tau = \frac{1}{2}{\theta_{\mathbf{I}}}^2 - \psi(\theta_{\mathbf{I}}) \qquad (B.29)$$

In the absence of intervening mass ($\psi = 0$), τ is simply a paraboloid and the single image is located at the minimum, $\theta_{\mathbf{I}} = 0$. As mass is gradually introduced (with $\psi < 0$) the arrival-time surface will be raised and new extrema will eventually be created (maxima, minima, and saddle points) corresponding to new inages. Figure 14 shows a typical sequence of contour plots with increasing lens mass.

Topological classification of time surface

Now consider the scale (extrinsic) curvature tensor

$$K_{ij} = \tau_{,ij} = \delta_{ij} - \frac{\partial^2\psi}{\partial\theta_{Ii}\partial\theta_{Ij}} = \frac{\partial\theta_{si}}{\partial\theta_{Ij}}. \qquad (B.30)$$

K_{ij} is also the Hessian of the transformation $\theta_{\mathbf{I}} \rightarrow \vec{\theta_s}$. The mapping from the source plane to the image plane is described by the magnification tensor

$$A_{ij} = K_{ij}^{-1}$$

It is clearly, if the time surface is locally flat (small curvature) the image will be strongly amplified. The magnification tensor is symmetric, so its diagonalized form can be written as

$$K_{ij} = \begin{pmatrix} \kappa + \mu & 0 \\ 0 & \kappa - \mu \end{pmatrix} \qquad (B.31)$$

where $\kappa = 1 - \Sigma/\Sigma_c$ is the expansion or the convergence (in some articles) and μ is the shear. In terms of this decomposition, the magnification of the image is given by

$$A = (\kappa^2 - \mu^2)^{-1} \qquad (B.32)$$

We can use the eigenvalues of the magnification tensor to classify the parity of the image. The partial parities of the image are defined to be equal to the single of the two eigenvalues, and the total parity is the sign of the product of the eigenvalues. Thus at a minimum of the time surface, the parities is (+,+). At a maximum has total parity (−,−). While a saddle point has total parity (+,−) or (−,+). Fig.15 interpret the standard bending angle diagram for a circularly symmetric lens (Yong et al., 1980)in terms of the parities of the images and the nature of the extrema (see also Narayan et al., 1984). In fact, all minima of time surface must be amplified bacause the $(+,+)$ parity requirement implies $|\mu| < \kappa < 1$ so the magnification satisfies $A = (\kappa^2 - \mu^2)^{-1} > 1$.

By examing the crossing contours of the time delay, we can classify the allowed parity combinations if the time delay asymptotically becomes parabolic. When there is only one image, the only extremum is a minimum and there are no crossing contours of the surface. If there are three images, then there are two topologically distinct cases. The first is called a limacon, and its limiting case is a black hole which generates two images of different parity. The second is called lemniscate, and its limiting case is a cosmic string, generates two images of the same total and partial parities. If we allow five images, there are six different non-degenerate geometries. Total cases are shown in Fig.16.

As a result of using fermat's principle and the topology of the time surface, Burke (1981) suggested the odd-number theorem. Provided that there are no discontinuities in the time surface (that is to say, we have a non singular, transparent potential), there is always an odd number 2n+1 of images, of which n+1 have positive total parity and n have negative total parity. This is obvious in terms of the time surface because there is one positive parity image in the absence of the lens and the addition of the lensing mass produces new images in pairs of opposite parity. The odd-number theorem is of course not valid if there are singularities in the lens, as with black holes or strings, or if there is obscuration of images. But it is most disturbing that we usually observe an even number of images. Five results of this discrepancy have been advanced, non of them compelling. They have been collected by Blandford (1986).

3. Caustics and Catastrophes.

It was claimed that the new science, catastrophe theory, was much more valuable to

mankind than mathematical analysis (Arnold 1986): While Newtonian theory only considers smooth, continuous processes, catastrophe theory provides a universal method for the study of all jump transitions, discontinuities, and sudden qualitative changes. Catastrophes was based on Whitney's singularity theory. This is a professional direction in mathematic and we can not review it in detail here. It can be used in gravitational lens to explain the transition from one topology to another through the merger/creation pairs of images.

caustics and critical lines

In order to understand the imaging characteristica of a lens, it is useful to study the structure of its caustics and critical lines. The family of spokes in the source plane defines an evenlope, which is the locus of points where two intersecting spokes become parallel. This is the caustic. Source points on the caustic map onto a curve that is a slight deformation of the original Einstein ring, in the image plane. This is called a critical curve. This way of dividing up the source plane using caustic curves and the image plane using the associated critical curves is quite general. The configuration of caustic and critical curves was only defined by lens itself and so it depends on the model. The source oneself in a passive position where is in vinicity to the caustic or on the caustic. The source can not defined the configuration of caustic. A spoke will be mapped onto an almost straight line segment in the image plane where the distance of the image from the critical curve is directly proporational to the distance of the source point from the caustic measured along the spoke. A point just inside the caustic will lie on two nearly parallel spokes and will be mapped onto a pair of image points separated tangentially almost parallel to the critical curve.

For typical elliptical lens, there are two caustics, dividing the source plane into regions of multiplicity 1, 3 and 5 respactively (see Fig. 17). The change in multiplicity when the source crosses a caustic occurs through the creation/destruction of a pair of merged images on a critical line in the image plane. The image panels $a - d$ in Fig.17 correspond to the four source position in the source plane, starting from the center. Panels a and b are cases with five images but, in practice, only four images will be seen since the central image tends to be much fainter than the others (Narayan, R., et el., 1988).

When the background source is not a pointlike quasar but an extended galaxy, the images can be observably distorted into highly elongated "arcs", particularly when the source lies on a caustic (Grossman and Narayan 1988). Fig.18 shows several configurations that could lead to arcs with a typical elliptical lens which models a typical galaxy. With the discovery of the first arcs (Soucail et el., 1987, Lynds et al., 1987), several astronomers (notably Paczynski 1987) suggested that they could be gravitationally imaged galaxies.

The above description is for a general caustic, that is to say, a fold caustic. In addition, there can be singular points on the caustic line that represent so-called cusp caustics. These lead to three bright merging images when the source is inside the cusp and a single bright image when the source is on the outside. In the lens model considered here, the tangential caustic has four cusps and the radial caustic has none.

Catastrophe

We have seen that the configuration of caustic on the source plane and critical line on the image plane depend on the model of lens, and image characteristics can be defined by them. But, when a moving source crosses a caustic, the new phenomena will be created. In order to explain this phenomena of the jump transition, astronomers used catastrophe theory. As a continuation of topological distinguishable arrival-time surface, the result of catastrophe phenomena is the transition from one topology to another through the merger/creation of pair of images.

The simplest catastrophe is the fold catastrophe, which corresponds to caustics tracing a smooth curve in the source plane. A source on one side of a fold generates two images which straddle a critical line in the lens plane, which on the other side it generates no images (see Fig.19). as the source crosses the fold, the two images merge producing strongly amplified images. Locally, the time delay surface can be written

$$\tau(\theta_I) = \frac{1}{3}ax_I^3 + \frac{1}{2}bx_I^2 + \sqrt{bc}x_I y_I + \frac{1}{2}cy_I^2 \qquad (2.3.1)$$

where $a > 0$, without loss of generality. a, b and c are derived from a Taylor expansion of the Newtonian potential about the image point, and $a + b \leq 2$ is required for a positive surface density. The image position are

$$x_I = \pm\frac{1}{\sqrt{a}}\left[x_s - \sqrt{\frac{b}{c}}y_s\right]^{1/2}, y_I = \frac{1}{c}y_s - \sqrt{\frac{b}{c}}x_I. \qquad (2.3.2)$$

which means the mapping is from source plane to image plane.

The magnification of each image is

$$A = \frac{1}{2acx_I} = \frac{1}{2c\sqrt{a}(x_s - \sqrt{\frac{b}{c}}y_s)^{\frac{1}{2}}}. \tag{2.3.3}$$

For $x_s > (\frac{b}{c})^{\frac{1}{2}}y_s$ there are two images, and for $x_s < (\frac{b}{c})^{\frac{1}{2}}y_s$ there are no images. When $x_s = (\frac{b}{c})^{\frac{1}{2}}y_s$ the two images merge at $x_I = 0$ with infinite amplification. Thus, the line $x_I = 0$ is a critical line, and $x_s = (\frac{b}{c})^{\frac{1}{2}}y_s$ is a caustic.

The next useful catastrophe is the cusp, which generates either three images or one image. The time delay surface can be expanded locally in the from

$$\tau(\theta_I) = \frac{1}{4}ax_I^4 + \frac{1}{2}bx_I^2y_I + \frac{1}{2}cy_I^2, \tag{2.3.4}$$

with images located at the solutions of the equations

$$x_s = ax_I^3 + bx_Iy_I, y_s = \frac{1}{2}bx_I^2 + cy_I. \tag{2.3.5}$$

The magnification is

$$A = \frac{1}{(3ac - b^2)x_I^2 + bcy_I}. \tag{2.3.6}$$

The critical line and the caustic are the curves for which the magnification diverges:the critical line is a parabola,

$$y_i = \frac{b^2 - 3ac}{bc}x^2 \tag{2.3.7}$$

and the caustic is

$$y_s^3 = \frac{27c^2}{8b}\left(1 - \frac{2ac}{b^2}\right)x_s^2 \tag{2.3.8}$$

For sources "inside" the caustic there are three images, and for sources "outside" there is one image. When $\theta_s = 0$ the three images merge at $\theta_I = 0$ leaving one infinitely amplified image at the same location. As the caustic is approached, the images become elongated parallel to the critical line (see Fig.20). Note that a cusp catastrophe is the only way to produce an isolated, highly magnified image–a fold catastrophe is not enough (Blandford 1986).

We have considered a source confined to a plane at constant redshift. If we allow the redshift to vary as well, it will create the more complex caustic. We will no discuss here. It has never in the theory of lensing.

4. Microlensing

The most spectacular effect of gravitational light deflection is the generation of multiple and/or strongly distorted images of distant galaxy and quasara due to the lens-like action of foreground galaxies and clusters. However, it is also well-known that gracitational micro-lensing due to compact objects (black holes, stars, brown dwarfs, jupiters, galactic halo) in a foreground galaxy is of great astrophysical importance (Gott, 1987). Then, "gravitational microlensing" ordinarily refers to the lensing effects of individual stars or other compact masses, typically with masses $10^6 M_\odot \geq M \geq 10^{-4} M_\odot$, which may be superimposed on the lensing by a entire galaxy. That is, microlensing can be viewed as the effect of the deviation from a uniform distribution of matter (or the "granularity") that occurs because the mass of galaxy is (at least partly) in the form of compact masses. Chang and Refsdal (1979) seem to have first recognized that the relevant astronomical parameters are such that microlensing may reasonable be expected to play a role in the gravitational lensing by galaxies.

The characteristic length scale for microlensing is the Einstein radius a_0 for the single mass. For significant gravitational lensing by an individual compact mass, the rays of light must pass near the mass –within a distance roughly equal to its Einstein radius. For cosmological, the Einstein radius is roughly

$$a_0 \simeq 5 \times 10^{16} \sqrt{M/M_\odot}\ cm \tag{2.4.1}$$

which corresponds to an angle

$$\theta_0 \simeq 10^{-6} \sqrt{M/M_\odot}\ arc\ sec \tag{2.4.2}$$

for a compact lensing mass M in terms of the solar mass $M_\odot$.

If a large fraction of the light from a distant source is to be affected by lensing due to the single mass, a similarly large fraction of the rays must pass within a_0 of the mass.

Hence, the requirement for the angular size of the source θ_s is

$$\theta_s \leq \theta_0 \tag{2.4.3}$$

for significant microlensing. The central, optical continuum emitting regions and the X-ray emitting region of quasars may satisfy eq.(2.4.3) for $M \simeq M_\odot$. In contrast, there is no evidence that the emmitting regions of extragalactic radio sources can be small enough to satisfy eqn.(3) unless $M > 100 M_\odot$ [if lensing masses within our own galaxy are considered, θ_0 is increased to approximately a milli-arc second but the probability for lensing along a randomly chose line of sight is small ($\simeq 10^{-5} - 10^{-6}$)].

The typical scale of angular separation of subimages is $10^{-6} \sim 10^{-3}$ arcseonds (for too small to be resolved at present).

Vietri and Ostriker (1985) and Nityananda and Ostriker (1984) introduced and developed a very useful concept of optical depth to microlensing. When optical depth is small, it gives a probability that one star strongly affects the intensity of a distant source of radiation. The optical depth for the occurrence of microlensing can be estimated from the angular cross section for microlensing, $\sigma \sim \pi\theta_0^2$, and the number of stars per unit angular area n. The optical depth is (Blandford, 1987)

$$\tau \sim f\Sigma/\Sigma_{crit} \tag{2.4.4}$$

where $\Sigma_{crit} \sim 0.4g\ cm^{-2}$ is critical surface density of the galaxy, and f is the fraction of the local mass in stars, and Σ is the local surface density of the galaxy. In the outer parts of galaxies, $\Sigma \ll \Sigma_{crit}$ and $f \ll 1$ so that galaxies are optically thin; but in the central regions, $\Sigma > \Sigma_{crit}$ and $f \sim 1$, so that the optical depth exceeds unity and the problem becomes non-linear due to multiple scatterings. If we model the galaxy by an isothermal sphere, the central optical depth is $\tau \sim 10$. The impact parameter with respect to the star is $b \sim 10^{16}\sqrt{M/M_\odot}\ cm \gg r$, where r is the radius of the star. This condition allows the microlensing potential to be treated as that of a point mass. When the optical depth τ is greater than a few tenths, the simulataneous lensing by a number of masses must be calculated. Questions to be answered by such calculations are, how rapid are the time variations in the observed flux? How do the results depend upon the size of the source, upon the amount of matter in compact masses and upon the amount of matter in a completely smooth distribution (gas, neutrions, etc)?

If the angular size of the source is much larger than the scale of the deflections then microlensing becomes unimportant. When the lensed objects are quasars, we can estimate whether or not the source size scale are small enough for microlensing to occur. Quasar radio and optical emission lines come from regions with scales $\sim 3pc \gg 10^{16}\ cm$, which means that microlensing will not occur, but "millilensing" might. The size of the optical continuum source is unknown. If the UV bump is roughly black body radiation from the inner regions of an accretion disk, then the size is 10^{15} to 10^{16}cm, which would allow microlensing to occur. Howevre, time variability on the scale of months to years implies a source size of $\sim 10^{17}$ cm which preclude it. The X-ray flux can vary on scale of weeks to days, which may imply an emission region small enough for microlensing to be important.

An attractive aspect of microlensing is the prediction of time variations. That is, its magnification effect should change on a time scale of roughly

$$t_m = \frac{a_0}{V_\perp} \tag{2.4.5}$$

where $V_\perp$ is the characteristic relative velocity perpendicular to the line-of-sight between the source, observer and the lensing mass. Due to galactic rotation $V_\perp$ should be at least 300km/s and many reasonably be about 1000km/s in many case due to the random motion of galaxies. Time scales $t_m \simeq 10\ yrs$ are then short enough to be sought even for $M \simeq M_\odot$. The characteristic "rise time" for the magnification is roughly

$$t_r \simeq \frac{a_s}{V_\perp} \tag{2.4.6}$$

where a_s is the size of the source, and can be much shorter than t_m when $a_s \ll a_0$. If may also be a useful signature of microlensing.

On the other hand, since θ_0 is the characteristic angular size for any changes of the image due to microlensing, multiple images due to microlensing cannot be expected to be resolved. From a observational viewpoint,the effect of microlensing is thus simply to alter the apparent luminosity of the image.

Although the effect of microlensing in enhancing the apparent luminosity of a source can be comparable to that of the entire galaxy, the unambiguous identification of microlensing can be expected to be difficult and this has so far proved to be the case. Impressive evidence for microlensing has recently been reported (Watson 1988) and it may well withstand future scrutiny. Because the relevant time scales tend to be measured in years and

gravitational lenses have been detected for only a few multiples of this time scale, it can reasonably be expected that date from the monitoring of lensed images will begin to yield a significantly improved assessment of the astronomical impact of microlensing.

Another phenomenon which we might call"millilensing" can be caused by objects whose masses lie between stellar and galactic masses such as globular clusters, giant molecular clouds, and hypothetical halo black holes with masses of order $10^6 M_\odot$. In this range of masses, the characteristic scale of the deflection angle is milliarcseconds. They will only produce multiple images if they have surface density $\Sigma > \Sigma_{crit}$. Globular clusters certainly satisfy this condition, but the fraction of galactic mass in these objects is small, so the optical depth will be small and globular cluster lensing will be correspondingly rare. Giant molecular clouds have the opposite problem, because although they contain a large fraction of the mass, they are not dense enough to cause multiple imaging. Local condensations within molecular clouds, however, may exceed the critical surface density. The dark mass in galactic halos may be contained in black holes with masses $\leq 10^6 M_\odot$: heavier objects will fall into the galactic center through the effects of dynamical friction. Limits on the incidence of millilensing will eventually set limts on the mass density of this mass range.

5. The Principles of Microlensing

There are two models for microlensing. First called low optical depth model and second called large optical depth model. The boundary between two models is the density of deflectors in the forground galaxy, i.e., optical depth. The optical depth $\tau < 0.4$ is for first model and > 0.4 will be for second model. Although low optical depth model is not applicable in fact, it provide a basic way to study microlensing.

At low optical depth, we can consider one star at a time, and the star can be modelled as a point mass. Chang and Refsdal(1979,1984) showed that a single star (or several stars) close to the light path can influence the image properties of the double quasar considerably, for instance by splitting an image into a group of sub-images with angular separations of about $10^{-5} arcs$ (far too small to be resolved at present). Since the sub-images may be difficult or impossible to resolve, the most important observational effect will be the change of flux density which may change over timscales of months or years due to proper

motions, the image splitting and flux changes, etc. Due to stars (with mass M_s) can play an important role for sources with diameter $\leq 0.3ly.(M_s/M_\odot)^{1/2}$ if the star density close to the light path is high enough.

The microlensing geometry

The geometry of the model of low optical depth is indicated in Fig. 21. One might at first think that the Einstein-deflection arising from the nearest star can be neglected since it is only $\sim 10^{-6}$ times the galaxy deflection ($M_G/M_s \sim 10^{12}$). A suitable form for the transformation of the (ξ, η) plane into the (x,y) plane for the light rays from a point source is the following:

$$\begin{aligned} x &= \xi + \gamma\xi - \xi/(\xi^2 + \eta^2) \\ y &= \eta - \gamma\eta - \eta/(\xi^2 + \eta^2) \end{aligned} \tag{2.5.1}$$

where

$$\gamma = 4GM_G(1 + z_G)(L - \lambda)\lambda/c^2\xi_G^2 L \tag{2.5.2}$$

The solutions $[\xi_i(x,y), \eta_i(x,y)]$ of these equations represent one group of sub-images seen close to the star S by an observer located at (x,y). The inversion of these equations leads to fourth order equations in ξ and η and that one can have two to four solutions for a given x,y. This means that up to four different light rays passing close to S can reach the same point in the observer's plane, so that the observer will see a group of 2-4 images(angular separation $\sim 10^{-5} arcs$).

The Jacobian transformation is zero:

$$J(\xi, \eta) = \frac{\partial(x,y)}{\partial(\xi,\eta)} = 0 \tag{2.5.3}$$

defines the critical curves in the (ξ, η) plane (see Fig.22). The transformation of these curves into the observer's plane by eq.(2.5.1) define the caustics in the (x,y) plane (see Fig.23). They depend on the values of γ. Within the point source and geometrical optics approximation the flux density is infinite along the critical curves in the (x,y) plane. In practise however the flux density remains finite due to the finte size of the source. The caustic are also of great interest since the number of sub-images of a point source can only change if the observer crosses a critical curve.

Rough estimates of the transverse velocities Q,S and the observer lead to an observer's observer's velocity relative to P(x=0,y=0) of about $1,000 kms^{-1}$ (see Fig.4 and Fig.6 in Refsdal,1979).

Flux Densities

From simple geometrical opticas it follows that the observed flux density of sub-image i is

$$F_i = J^{-1}(\xi_i, \eta_i) F_0 \tag{2.5.4}$$

Where F_0 is the flux density which would have been observed without and lens effect from the galaxy or the star. Due to the very small angular separations between the sub-images in one group ($\sim 10^{-5} arcs$) they can not be resolved with present equipment. We shall therefore mainly be interested in the total flux density F_T from a group of sub-images,

$$F_T(x,y) = \sum_{i=1}^{N} (\xi_i, \eta_i) = F_0 \sum_{i=1}^{N} J^{-1}(\xi_i, \eta_i), \qquad N \leq 4 \tag{2.5.5}$$

The corresponding flux if only the galactic deflection is taken into account by F_0'. It is then easily seen from geometrical optics that

$$F_0'/F_0 = \left| \frac{\partial(x,y)}{\partial(\xi,\eta)} \right| = |1 - \gamma^2|^{-1} \tag{2.5.6}$$

The main features of the function F_T/F_0' were shown in Fig.24. We see that very high flux densities are found along and on the insides of the critical curves. the high flux values and the discontinuity at the critical curve is of great observational interest since compact sources can show large and rapid variations of flux density when the observer crosses a critical curve.

Typical Light Curve and Topological

The hight F_T values close to the critical curve (J=0) were, of course, to be expected, since a vanishing of the jacobian for at least one of the images means an infinite flux(within the point source and geometrical optices approximation). For sources which are small but finite, one can show that the maximum value of F_T which occurs when an observer passes

a critical line is proportional to $D^{-1/2}$, where D is the diameter of the source, The same type of dependence was found for the spikes discussed by Benson(1979). If a source crosses a fold at t_0, the observed flux decays (or increase) as $|t-t_0|^{-1/2}$. If the source enters a cusp the flux rises again as the source approaches the second fold, giving rise to a typical light curve. see Fig. 25.

Microlensing at small optical depths can be understood also with the scalar formalism (Blandford and Kochanek,1987): the character of subimages depends on the form of the time delay surface prior to microlensing.

If the unperturbed image is at a minimum of the time surface, the isochronal is deformed into a limacon with the maximum located on the microlens, that absorbs the image. Thus there remain two images, one at a minimum and one at the saddle point. If the microlens is not point-like but extended, the captured image is so strongly deamplified to be still unobservable [Subramanian et al, 1985).

If the unperturbed image is at a maximum of the time delay surface, one finds that the unperturbed isochronal is distorted into a lemniscate with two maxima and a saddle point: one of the maxima images is absorbed by the microlens and is unobservable. There two toplogical were shown in Fig. 26.

As a degenerate case, the saddle point could merge with the original maximum, annihilating it and leaving only the maximum captured by the microlens.

The second case is the most likely for multiply imaged systems, since maxima are usually associated with dense galactic cores, where the optical depth to microlensing is higher.

Extended Source

For extended source, the solid angle covered by sub-image i of an infinitesmally small source element is

$$d\Omega_i = J^{-1}(\xi_i, \eta_i) d\Omega_0 \tag{2.5.7}$$

Where $d\Omega_0$ is the corresponding solid angle without any lens effect. The flux density

$$dF_i = J^{-1}(\xi_i, \eta_i) dF_0 \tag{2.5.8}$$

Hence, the surface brightness is not changed by the lens effect, a well-known result. Total flux density F_T can be found by integrating over the source

$$F_T = \frac{\int\int_{source} \sum_{i=1}^{N} J_i^{-1} dx\ dy}{\int\int_{source} dx\ dy} F_0 = \frac{\int\int_{images} d\xi\ d\eta}{\int\int_{source} dx\ dy} F_0 = \frac{\Omega}{\Omega_0} F_0 \qquad (2.5.9)$$

Since J_i may be zero at some points in the source, the integral is difficult to calculate with high accuracy. Refsdal(1984) given a approximationlly way, $F_T \simeq F_d(t)$,

$$F_d \simeq F_0'\ d^{-1/2}, \quad 0 < d < 1 \quad (normalized\ \ units)$$

$$F_d = 0 \qquad\qquad d < 0$$

where d is distance from the source to the critical curve in the source plane. As expected, the amplitudes of the flux variations get smaller and the time scales larger when diameter D of source increases. When $D \leq 0.1\ lt\ yr.$, the typical light curve like U shape can be created when crossing a critical line(see also Fig.25). At this time, function F_T/F_0' has two maximum.

6. A Description of the Microlensing

In the previous chapter we described the effects of small optical depth ($\tau < 0.4$) to microlensing. In this limit only one star (or none) strongly affects properties of the image formed by a galaxy. This seems to be the only case that may be treated analytically.

A real galaxy is made of stars and some contiuously distributed mass: interstellar matter and possibly some exotic particles (dark matter). A detailed structure of a macroimage may depend on the masses and surface density of stars which split the macroimage into a large number of microimages, separated by some micro-arcsec. Even if we cannot tesolve this structure, it may affect brightness of the macroimage and contribute to its variation in time.

A bundle of light rays propagating through a galaxy with high optical depth ($\tau > 0.4$) is subject to two different effects influencing its cross sectional area: matter in the beam leads to a convergence (Ricci focusing), whereas the shear leads to a distortion of the shape of the ray bundle(Misner, et al 1973).

Let us to use the theory of transparent lenses has been developed by Bourassa and Kantowski(1975). The lens equation is

$$\theta^Q = \theta - (D_{ds}/D_s)\alpha \qquad (2.6.1)$$

with the deflection angle given by

$$\alpha = 2c^{-2} \int_{-\infty}^{\infty} \nabla\phi \; dl \tag{2.6.2}$$

From (2.6.1), we have

$$\frac{\partial\theta_i^Q}{\partial\theta_j} = \delta_{ij} - \left(\frac{D_{ds}D_d}{D_s}\right) \frac{\partial\alpha_i}{\partial x_j} \tag{2.6.3}$$

where $x_j = D_d\theta_j$ is physical length in the deflector plane. From (2.6.2), we find

$$\frac{\partial\alpha_i}{\partial x_j} = \frac{2}{c^2} \int_{-\infty}^{\infty} \frac{\partial^2\phi}{\partial x_i \partial x_j} \; dx_3 \tag{2.6.4}$$

where x_i, x_j are in the plane of sky and x_3 along the light beam. But,

$$\frac{\partial^2\phi}{\partial x_1^2} + \frac{\partial^2\phi}{\partial x_2^2} + \frac{\partial^2\phi}{\partial x_3^2} = 4\pi G\rho \tag{2.6.5}$$

which may be integrated along the line of sight to give

$$\int_{-\infty}^{\infty} \frac{\partial^2\phi}{\partial x_1^2} \; dx_3 + \int_{-\infty}^{\infty} \frac{\partial^2\phi}{\partial x_2^2} \; dx_3 = 4\pi G\Sigma = 4\pi G \int_{-\infty}^{\infty} \rho \; dx_3 \tag{2.6.6}$$

If we set

$$\begin{aligned} \kappa &= (4\pi G\Sigma/c^2)(D_{ds}D_d/D_s) \\ \lambda &= (2/c^2)(D_{ds}D_d/D_s) \int_{-\infty}^{\infty} \frac{\partial^2\phi}{\partial x_1^2} \; dx_3 - \kappa \\ \mu &= (2/c^2)(D_{ds}D_d/D_s) \int_{-\infty}^{\infty} \frac{\partial^2}{\partial x_1 \partial x_2}\phi \; dx_3 \end{aligned} \tag{2.6.7}$$

we may write equation (2.6.3) as

$$\frac{\partial\theta_i^Q}{\partial\theta_j} = \begin{pmatrix} 1 & 0 \\ 0 & 1 \end{pmatrix} - \begin{pmatrix} \lambda & \mu \\ \mu & -\lambda \end{pmatrix} - \begin{pmatrix} \kappa & 0 \\ 0 & \kappa \end{pmatrix} \tag{2.6.8}$$

This is the transformation from a small source onto a small image. We may rotate the θ_i coordinate system to generate a tranformation,

$$\frac{\partial\theta_i^Q}{\partial\Theta_j} = \begin{pmatrix} 1 & 0 \\ 0 & 1 \end{pmatrix} - \begin{pmatrix} -\gamma & 0 \\ 0 & \gamma \end{pmatrix} - \begin{pmatrix} \kappa & 0 \\ 0 & \kappa \end{pmatrix} \tag{2.6.9}$$

The third term expresses the convergence of the been due to matter in the beam. The second term is the beam shear term caused by externally imposed potentials. The amplification of the image(given by the Jacobian of the $\theta_i^Q \rightarrow \Theta_j$ transormation) is

$$A = [(1-\kappa)^2 - \gamma^2]^{-1} \tag{2.6.10}$$

where $A > 0$ for a positive parity image and $A < 0$ for a negative parity image.

If a light beam manages to slip between indvidual stars in a galaxy, then we have a vacuum solution with $\Sigma = 0$ leading to $\kappa = 0$. Then

$$A = (1 - \gamma^2)^{-1} \tag{2.6.11}$$

It is interesting that all images with $|A| < 1$ have $|\gamma| > \sqrt{2}$ and must have negative parity.

We may consider the effects of stars with the lensing equation,

$$\xi^Q = \begin{pmatrix} 1+\gamma-\kappa & 0 \\ 0 & 1-\gamma-\kappa \end{pmatrix} \xi - \sum_k \frac{m_*^k}{M_\odot} \frac{\xi - \xi^k}{|\xi - \xi^k|^2} \tag{2.6.12}$$

$$\theta_0^2 = (4GM_\odot/c^2)(D_{ds}/D_s D_d)|1 - \sigma_c|^{-1} \tag{2.6.13}$$

Where stars of mass m_*^k are located at ξ^k, and has established the deflection angle $\xi^Q = \theta^Q/\theta_0$ and $\xi = \Theta/\theta_0$. θ_0 is the angular size of the ring around a 1 $M_\odot$ star if it has a light source exactly behind it for the edmensionless lens equation. Note that

$$\kappa = \pi D_d^2 \theta_0^2 (\Sigma/M_\odot) = \pi\ r_0^2 (\Sigma/M_\odot) \tag{2.6.14}$$

so that κ represents the number of solar masses of surface density enclosed in a ring of angular diameter θ_0 or of physical diamater $r_0 = D_d\theta_0$. $\kappa = \sigma = \sigma_s/(1 - \sigma_c)$ is dimensionless surface mass density in stars and is equal to the optical depth. Assuming all stars have the same mass $M = M_\odot$, they have a Poisson distribution on the image plane with a constant average surface mass density Σ_s, and there may be a continuous distribution of "dark matter" with a constant surface mass density Σ_c. The corresponding dimensionless surface mass densities are σ_s and σ_c, as defined by Paczynski(1986). $\sigma = 0.1$ for low optical depth, $\sigma \sim 0.4$ for a moderate optical depth.

If there is an additional smooth mass distrbution of surface density κ and an externally applied shear γ, then the amplification expected is

$$A = [(1 - \kappa - \kappa_*)^2 - \gamma^2]^{-1} \tag{2.6.15}$$

The radius of i image,

$$r_i = r_G(D_d/D_s) \tag{2.6.16}$$

Then the half-energy radius is $1.18r_i$, and the surface mass enclosed by the half-energy ellipse of the lensed beam is

$$M_i = 1.385(r_i/r_0)^2\kappa_* A(M_\odot)$$

and the number of stars thus enclosed is

$$N_i = 1.385(r_i/r_0)^2\kappa_* A(M_\odot/M_*)$$

when stars of mass m_* are involved ($m_* = 1M_\odot$ here).

- A trial with $\gamma = 0, \kappa = 0, \kappa_* = 0.5$, Then the amplfication is A=4. Beams with $\sigma = r_i/r_0$ from 0,2 to 9.0 (giving $N_i = 0.11$ to $N_i = 224$) were fired through a series of randomly generated star fields. For $N_i > 25$,the distribution function was approximatly Gaussian with $\sigma(A)/A = 0.9N_i^{-1/2}$. With few stars in the beam, the distribution of amplification is very far from Gaussian.
- Young(1981) did numerical experiments with various quantities of γ, κ and κ_*. They find that sufficiently large light beams the star field acts like a smooth mass distribution. When $N_i > 25$, the distribution function of amplifications tends to a Goussian. For small N_i the mean amplification remains equal to that for a smooth mass distribution with the same surface density as the stars.
- The picture changed dramatically when optical depth (or σ) exceeded ~ 0.5. In this case it was no longer possible to identify the originally undistorted image.
- The area of images expands enormously when the optical depth approaches unity. Since the number of micoimages is comparable to the number of stars, the amount of computing increase rapidly when the optical depth becomes large.
- The number of caustic depend on optical depth in foreground galaxy. When source or observer crosses the critical line in source plane or observer plane, the high amplification event(HAE) would been created. Due to exist relative motion between source and galaxy, and stars in the galaxy can move with ramdom. Then, observed light curve are complex and irregular. The time scale of variation depend on these complex motion and velocity, and also depend on optical depth. The statistical methode are also formulated to assess the time variation of the surface brightness due to the random motion of the masses that cause the microlensing(Deguchi et al 1988).

7. A Summary account on the Microlensing

The possibility that individual stars in faraway galaxies may affect gravitational lensing properties of these galaxies has been studies by Chang and Refsdal(1979,1984), Gott(1981), Young(1981), Vietri and Ostriker (1983), and Nityananda and Ostriker(1984). The effects of small optical depth to gravitational lensing were analyzed in considerable detail. In this limit only one star(or none) strongly affects preperties of the image formed by a galaxy. This seems to be the only case may be treated analytically.

However, in case of strong gravitational lensing, when a galaxy is responsible for the presence of more than one image, the brightest one must be formed in a region of large optical depth to microlensing.

Young(1981) studied the case of large optical depth, and applied Monte-Carlo method considering an extended source whose light passes through a star field in a galaxy. In most of his models the angular size of a quasar was large than the angular spacing between stars in the lensing galaxy. He investigated the shape of the images, but did not give the amplification factors and the statistics.

The finite size of the source probably is the key consideration for the occurrence of microlensing by individual stars. For the intensity from a particular location, Deguchi(1988) find that the parameter which governs the importance of microlensing is $\delta = (a_0/a)^2 \tau \ln[3.05(N)^{1/2}]$, where a_0 is the characteristic impact parameter for lensing by a single star, a is the size of the source, τ is the optical depth for lensing, and N is the number of stars being considered.

Paczynski(1986) tried to solve numerically the lens equation at large optical depth. He assumed that the angular size of a quasar is much smaller than the angular spacing between stars in the lensing galaxy. In order to find all images, he gave the positions and amplification factors of the subimages. But his method has the following disadvantages:

- it can be applied only to point source, while the source size is very important in some applications of microlensing theory;
- the method does not guarantee to find all the images(the number of solutions of the lens equation not known a priori);

- calculations have to be performed for every source position, then the method does not allow statistics(and is very time consuming).
- By neglecting the shear term from the smoothed out galaxy he showed that the only free parameter in the problem is σ, the normalized surface mass density in stars.
- The models of Paczynski(1986) covered a very small range of lens parameter, and the models of Young(1981) almost certainly did not have enough stars. In a study covering a large region in parameter space(surface mass density, shear, mass function of the stars) it is important to know how many stars need to be included in, and how much computing power is required.
- He only considered the relative transverse velosities of the stars. It is not convenience to study variability time scale for observer.

Kayser, et al(1986) extended Paczynski's work in sereral ways. The features of that work are :

- extend source are considered;
- They allowed to exist a shear term. 3 free parameters have been considered, the normalized density σ, the normalized shear parameter γ and the normalized radius $\tilde{R}$ of the source.
- They neglected relative velocities of the stars and consider the effective transverse velocity arising from motion of observer, source and the bulk velocity of the the stars. This approximation is more realistic, and it simplifies the calculations and the discussion of the results.
- Of particular astrophysical interest are the high asymmetric peaks in the light curves which occur when a compact source crosses a critical curve. When comparing models with and without shear, but with the same σ, the shear term causes a much higher frequency of such high peaks for small σ.
- The error introduced by considering only a limited number of microimages is estimated;
- the total amplification factor is obtained for a whole range of source positions simultaneously;
- the positions of the microimages cannot be obtained, it is claimed that this not is not

important, since we cannot resolve microimages with the present techniques.

- Predicted variations in flux for the microlensing of finite-size sources have been obtained for $\tau \leq 0.4$.

Schneider and Weiss(1987) extended the previous models to large optical depths, determining the amplifications for extended sources with high accuracy, in a scheme useful for statistical consideration(the number of stars considered is up to 10^4). The features of this work and the best accepted results of these simulations are the following:

- Their computational scheme allows to treat rather high optical depth (> 0.4) or eqnivalently a large number of objects in the star field ($\leq 10^4$ stars).
- caustic and critical lines strongly tend to cluster in their respective planes; as a consequence, the amplification function is flat on large regions of the source plane.
- Whereas for moderate optical depth the typical light curve of a source moving relatively to the lens is characterized by rather quiet behaviour most of the time, interrupted by sudden outbursts, sources behind a dense star field show very irregular flickering, without dramatic changes of their apparent luminosities. It can be difficult to separate intrinsic source variations from microlensing effects in observed systems.
- They pointed out even for much lower optical depth(≤ 0.1) the effect of multiple stars can not be neglected. This is due to the tendency of critical line to cluster.
- The region covered in the source plane is usually of the order of, or less than, $10\xi_0$ (ξ_0 = Einstein radius in the source plane), possibly too small to cover the largest features of the light curve.

Kayser et al(1989) explore the effect of considering microlenses with different masses, they consider a two- component model compased of massive stars and low mass objects(low mass stars, brown dwarfs, or Jupiters) with mass raties 1:10 and 1:100. The result is that different masses induce different length scales and the clustering and bridging of caustics and critical lines are enhanced.

At large optical depths, the idea of a caustic network becomes less useful. Folds may no longer completely dominate the cross sections so that the A^{-2} cross section law may be violated. The variations become much smoother and it is difficult to separate intrinsic

variations from the effects of microlensing. The overall effect may be described by a point spread function, with a central Gaussian core and a power law tail$\propto \theta^{-4}$ where θ is the distance from the central intensity peak. This is in reasonable agreement with numerical simulations (Blandford 1987).

At the present time, many of cases of microlensing have been modeled in detail, but no perfect model has been applied to all the cases.

Part III. Light Curves

The shape of caustic and critical lines located on source plane and image plane respectively were defined lensing galaxy oneself. Many micro-caustics and micro-critical lines will been created by individual stars in foreground galaxy. Their number and global distribution depend on lensing models and optical depths. When source are crossing the caustic, the high amplification event can been created. If the size of source extended large enough, this HAE would loss efficacy. In addition, dut to exsit relative motion beteen source and galaxy, and the motion of the individual stars. Then, if we stressed the possibility that the variability of some QSOs may be due to the amplification cauesd by microlensing, the analysis of variability would beome to complex. The variability time scale expect from microlensing can be obtained in term of lens model (include optical depth and mass distrbution), source size, and relative transverse velocity. So, no an united model and way have been applied to all the cases of microlensing. Almost every candidate of microlensing correspond to with several difference model and difference explanation.

1. Probability Considerations and Time Scales

For the effective operation of microlensing event, we must first check that the probability of their occurrence is high enough. This depends on how many microlensing stars in the galaxy(or galaxy cluster) may be expected within the region of area, Σ, about z_0^i(where z_0^i is the position of the ith image), wherein the effects of microlensing are significant. This number can be computed from the product of Σ and the surface density,n_s, of such stars in the vicinity of this region. We are assuming here that the source size is much smaller than Σ; for a larger source, n_s will get multiplied by the source size itself. Note that the only scale occurring in the microlensing problem is provided by l_0, and on expressing relevant distances in units of l_0, the equations have no explicit reference to the microlens. Consequently, the area of influence is simply some multiple of πl_0^2,i.e.,$\Sigma = f^2(\pi l_0^2)$(Subramanian 1985). $1.3 \leq f \leq 4.5$.

The number of stars, N, which can fall inside Σ is given by

$$N \approx \frac{1.8}{r_c} f^2 \left(\frac{\sigma_v}{300 kms^{-1}}\right)^2 \left(\frac{D_{ds}}{D_s}\right) \frac{(n^2 - x^2)^{1/2}}{(n^2+1)^{1/2}(1+x^2)} \qquad (3.1.1)$$

Here r_c is the core radius of the lens galaxy in units of arc seconds, and x is the distance of the image from the lens center in units of r_c, σ_v is the velocity dispersion defined in Young

et al(1981).

The characteristic time scale t_0 has been obtained by Deguchi et al(1988),

$$t_0 = \frac{a/2\tau v_0 ln(3.05\sqrt{N})}{[\tau + (a/a_0)^2/4ln(3.05\sqrt{N}]^{1/2}} \tag{3.1.2}$$

where a_0 is the characteristic impact parameter for lensing by a single star, a is the size of the source, τ is the optical depth for lensing, and N has been expressed in (3.1.1). For the usual case of interest-source sizes smaller than a_0- the time scale is typically somewhat shorter [by the factor $2\tau \ln(3.05\sqrt{N})$] than the time it takes a star to traverse a distance equal to the size of the source.

2. Transverse Velocity and the Normalized Parameters

Let the source have a transvers velocity $\mathbf{v}_q = d\mathbf{s}_q/dt_q$ measured in the source plane, the deflector a transverse velocity $\mathbf{v}_d = d\mathbf{s}_d/dt_d$ measured in the deflector plane, and the observer a transverse velocity $\mathbf{v} = d\mathbf{s}_{obs}/dt_{obs}$ measured in the observer plane.

The projections of length differentials onto the source plane are

$$d\mathbf{s}_d^{'} = -\frac{D_q}{D_d} d\mathbf{s}_d \tag{3.2.1}$$

$$d\mathbf{s}_{obs}^{'} = \frac{D_{dq}}{(1+z_d)D_{obs}} d\mathbf{s}_{obs} \tag{3.2.2}$$

and the velocity of the source relative to the critical curves measured in the source plane is

$$\mathbf{v}' = \mathbf{v}_q - \frac{1+z_q}{1+z_d}\frac{D_q}{D_d}\mathbf{v}_d + \frac{1+z_q}{1+z_d}\frac{D_{dq}}{D_d}\mathbf{v}_{obs} \tag{3.2.3}$$

In the observer plan, the effective velocity of the transverse source motion is

$$\mathbf{v}_e = \frac{1}{1+z_q}\mathbf{v}_q - \frac{1}{1+z_d}\frac{D_q}{D_d}\mathbf{v}_d + \frac{1}{1+z_d}\frac{D_{dq}}{D_d}\mathbf{v}_{obs} \tag{3.2.4}$$

This is the velocity of the source relative to the critical curves with time measured by the observer. The deflector velocity $\mathbf{v}_d$ can be separated into 3 components

- the center of mass velocity of the defector (galaxy), $\mathbf{v}_1$;
- The bulk velocity of the local star field relative to the center of mass, $\mathbf{v}_2$;
- The relative star velocities.

Neglecting the third component it is easily seen that

$$\mathbf{v}_d = \mathbf{v}_1 + \begin{pmatrix} 1-\sigma_c-\sigma_s+\gamma' & 0 \\ 0 & 1-\sigma_c-\sigma_s-\gamma' \end{pmatrix} \mathbf{v}_2 \tag{3.2.5}$$

For realistic cases it should usually be a good approximation to neglect the relative star velocities (Kaystr and Refsdal 1986). It also simlifies the discussion considerably since the critical curves and the ray plot diagrams would be time dependent if these velocities were included.

For a general situation, compare Kayser and Refsdal(1983),Pacynski(1981) and Kayser et al(1986) introduce the follwing units.

- Normalized length unit in the deflector plane

$$z_0 = (4Gc^{-2}DM/|1-\sigma_c|)^{1/2} \tag{3.2.6}$$

  This is the radius of the critical curve (Chang and Refsdal,1984) around an isolated star embedded in continuously distributed matter of dimensionless surface density σ_c. For $\sigma_c < 1$ it is also the radius of the luminous ring seen from the symmetry axis.

- Normalized length unit in the source plane

$$\zeta_0 = z_0(1-\sigma_c)D_q D_d^{-1} \tag{3.2.7}$$

  This is the projection of z_0 onto the source plane.

- Normalized length unit in the observer plane

$$\zeta_0' = z_0(1-\sigma_c)D_q D_{dq}^{-1}(1+z_d) \tag{3.2.8}$$

- Normalized surface density in stars,

$$\sigma = \frac{\sigma_s}{1-\sigma_c} \tag{3.2.9}$$

  where σ_s is dimensionless surface density of stars.

- Normalized shear parameter

$$\gamma = \frac{\gamma'}{1-\sigma_c} \tag{3.2.10}$$

  where γ' has been defined in Kayser et al. (1986)

- Normalized lens equation

$$\xi = \text{sign}(\sigma)S(z) + \begin{pmatrix} 1+\gamma & 0 \\ 0 & 1-\gamma \end{pmatrix} z \tag{3.2.11}$$

- The amplification is given by

$$A = |(1-\sigma)^2 - \gamma^2|^{-1} \tag{3.2.12}$$

Above quantities are basic model parameters in microlensing and been used into numerical simulation.

3. Single Star Light Curves (Low optical depth events)

Single star light curves have been studied previously by Liebes (1964), and Refsdal (1964). Liebes and Refsdal calculated analytically the basic effects of a single star on a point source behind it. Maeder (1973) considered a binary system with one star gravitationally lensing the light from the other star. Bontz (1979) calculated source changes that result from the lensing of a massive opaque lens. Chang and Refsdal (1979, 1984) considered the light curves of a star in a galaxy acting in conjunction with the gravitational field of its host galaxy (equivalent to working at large shear).

They adopted effective transverse velocity $\mathbf{V}_e$ (it has been shown at (3.2.4) of the source (contribution from observer velocity, deflector velocity and source velocity), and the real diameter of the source object R.

$$R \approx 0.05 D' \ lt\ yr \tag{3.2.13}$$

For $V_e \approx 1000 kms^{-1}$ and $R \approx 0.001 ly$, time scale $t \sim 0.3\ yr$. For point source and extrended source (various R value), the typical light curves show in Fig.27.

From Fig.27, we find that the amplitudes of the flux variations get smaller and the time scales larger when D' increases. By the largest D' value we still see, however, that a 5% increase in $\sim 30\ yr$ is possible. If we consider flux variation of $< 1\%$ as insignification we find that significant flux variation can only occur for $D' < D'_{crit} = 20$. From equation (3.2.13) we see that this corresponds to

$$R < R_{crit} = 1\ lt\ yr \tag{3.2.14}$$

Stars as deflectors can therefore only give significant flux changes for R smaller than about 1 $lt\ yr$.

As for the position and appearance of the extended images, we note that a large increase in the flux of an image is always connected with a large deformation, and that the separate images which appear of a point source often smear together for large D' values.

For small D' values the rapid flux changes when the observer crosses a critical line is of utmost interest. The typical U shape can be created at that time. So, U shape can be created only when the size of source and optical depth are small enough, but the shear is strong enough. We have found that the maximum value of F_T/F_0' when crossing a critical line is usually about ($D' \leq 0.1$)

$$\frac{F_T}{F_0'} \approx \frac{2}{\sqrt{D'}} \tag{3.2.15}$$

The time scale for the disappearence or appearence of the bright images is

$$t = D'\Delta t \tag{3.2.16}$$

where $\Delta t = 30\ yr$ for $V_e \sim 1000 kms^{-1}$.

The very rapid X-ray fluctuations (we think intrinsic) of some quasars (time scale some hours), which have been reported from the Einstein satellite, do indicate that the R-value of the X-ray source is less than $5 \times 10^{-4}\ lt\ yr$; that is $D' < 0.01$. Large changes in F_T caused by the lens effect could then occur within some months.

More recently Nottale (1986, NTL) considered the effect of a foreground star, acting alone on a background circular quasar of uniform brightness. NTL modeled a spectific light increase of the quasar 0846+51W1. Nemiroff (1987) studied in detail the light curves for a single lens acting on a uniform circular source. These light curves are symmetric about Δm_{max}. The diameter of the source R is starting from 1.2 $lt\ yr$ to 1.8 $lt\ yr$., $\Delta M_{max} = 1,\ 2$, and 5 are represented in their results respectively.

Paczynski (1986a) calculated the probable effect of single stars in our own galaxy lensing stars in nearby ones. He calculated and displayed single-star light curves for a wide range of magnitude brightenings due to a single star lensing a point source. The time scales in this new model can become shorter than $0.3yr$ defined by Chang and Refsdal (1979, 1984). any star in a nearby galaxy has a probability of 10^{-6} to be strongly microlensing

at any time. The lensing events last $\sim 2\ hr$ if object has a mass of $10^{-6}M_{\odot}$, and they last $\sim 2\ yr$ for objects of $100M_{\odot}$. The typical $\Delta m_{max} \sim 1$.

4. Double Stars Light Curves

Double star lensing was first studied by Barnothy (1986), who invoked it to explain the then mysterious pulsar phenomenon. Bartels (1981) derived many of the analytical properties of the two point mass lens. Schneider and Weiss (SW 1986) have recently explored further many of the asymmetric properties of the two point mass lens. SW examined both analytical and numerical aspects of the two point mass lens acting on an extended source over a specific range of lens and source parameters. SW also calculated some light curves as an extended source underwent image creation events. They showed that the light curves for these systems were not just the simple linear addition of two single star light curves.

The most dramatic differences between double star light curves and single star ones occur when the two stars are separated by a distance of the order of an ERU. Here the ERU refers to that of the combined mass of the double star lens. If the two stars are much closer than an ERU, such as their separation being ERU/10 or less, they typically affect source as would a single star of combined mass.

SW defined an normalited radius of the source R and a parameter X about distance. Here we do not describe detailly these two parameters. In the special model described by SW $X = 0.5$, R starting from 0.0 (for point source) to 0.05 (for extended source). The light curve is shown in Fig.28. We should see again from this Fig., the magnitude can decrease with increasing R, and time scale can be longer with increasing R. The cases in Fig. 28 is when they cross a critical line or a cusp.

5. Light Curves at Large Optical Depth

The light curves at large optical ($\tau > 0.4$) was more interested in astrophysics. The initial, limited numerical computations using Monte Carlo type methods due to Yong (1981) have been criticized for limited sampling, and several investigators have performed further computation (also of the MOnte Carlo type). Paczynski (1986) examined the case

of the microlensing of a point source and obtained the time variation in the flux due to the random motion of the compact masses. At any time, there are numerous images of the source that are separated by angles that typically are measured in micro-arc seconds (for $1M_{\odot}$ masses) as discussed above section. Hereafter, many works on this topic have been done by Schneider and Weiss (1987), Kayser et al. (1986), Schneider (1988), Wambsganss et al. (1988), Kayser et al. (1989). In these works, a wide range of parameters were covered.

The optical depths was up to 0.8 or, equivalently, a large number ($\leq 10^4$) of stars.

The normalized source size b were chosen as 0.0125, 0.025 and 0.0375 or, equivalently real size $6 \times 10^{14} cm$, $1.2 \times 10^{15} cm$ and $1.8 \times 10^{15} cm$ respectively.

In general, the effective velocity V was about $1000 kms^{-1}$.

There are basically two time scales, relevent for light variations. The first one is the typical rise time to a peak in the amplification. This corresponds to a displacement of R of the source across a critical line. The characteristic "rise time" for the manification is roughly (Waston 1988)

$$t_r \approx \frac{R}{V}$$

The second time scale one is the time betweem two peaks. This time is much more subject to large statistical fluctuations and is therefore less useful than the rise time t_r. A mean time between peaks can be represented

$$t_m = f \cdot t_0 \approx \frac{a_0}{V}$$

where $t_0 = X_0/V$, $X_0 = a_0 D_s/D_d$, $a_0 = (4GMD_dD_{ds}/c^2D_s)^{1/2} \approx 10^{16} cm$, and the factor f is ~ 4 for $\sigma = 0.2$, ~ 1 for $\sigma = 0.5$, ~ 0.2 for $\sigma = 0.8$; it thus depends sensitively on the specific lens model.

We chose several typical light curves to show in Fig.29a-l and Fig.30. These figures correspond to models described in Table 2.

One of the most surprising results of the computation is visiable in all cases: there is a strong tendency of critical structure to cluster. The consequence of this clustering is directly related to observation. Since there are large regions of the source plane where the complification function is very flat a source movimg relative to the lens can have a much more flatter light curve than one would expect from simple independent point masses

considerations. In addition, since the patterns of the critical lines are frequently much large than, say, a Chang-Refsdal critical region, one can also obtain flat light curves at considerable amplification.

Whereas for moderate optical depth (Fig.29a, b, g, h, i) a typical light- curve is characterized by rather quiet behaviour most of the time. Interrupted by sudden "outburts", sources behind dense star fields tend to show a very irregular flickering, without very dramatic changes of their apparent luminosity.

The sensitivity to source size, the rapid rise time for small sources, and the longer characteristic length a_0 for variations are evident. The smallest source size $b = 0.0125$ for the cases of high optical depth corresponds to $\sim 6 \times 10^{14} cm$. If the continuum source is not smaller than this, large changes of brightness cannot be expected. In fact, if the source is a factor ~ 10 larger than the value given above, the expected light curves should be rather smooth.

Supposing that the relevant transerve motions is given by the transverse velocity V_d of the local star field, relative to the line-of-sight to the quasar, one obtains for solar mass objects

$$t_0 \approx \left(\frac{V_d}{1000 kms^{-1}}\right)^{-1} 7.5yr$$

$$t_r \approx \left(\frac{a_0}{10_{15} cm}\right)\left(\frac{V_d}{1000 kms^{-1}}\right)^{-1} months,$$

and

$$X_0 \approx 10^{17} cm$$

hence, for a source of size $\sim 10^{15} cm$ the solid curves in Fig. 29a and b are applicable. The time scale to implies that one should observe intensity paeks of that source, on the average, every $\sim 30\ yr$; however, as discussed by Schneider, this number is subject to large statistical spread. Time scale $t_m \approx 10\ yrs$ are then short enough to be sought even for $M \approx M_\odot$.

The results for high optical depth (e.g., case e,f,and l) show that one can obtain very high amplification factors of a source, but without large intensity changes similar to outburst, but more with a flicker of the source, i.e. brightness variations of $\sim 0.5 mag$. All of Δm_{max} in models were $< 5 mag$.

As a extending of these works, Kayser et al. (1989) considered microlensing due to an ensemble of compact objects with different masses by means of numarical simulations. They find that different length scale are induced by the different masses and that the large scale structures. ("clustering") of the caustics/anti-caustics are enhanced. If the compact source of the quasar continuum is small enough ($\leq 10^{-3}$ pc), low mass objects like brown dwarfs and even Jupiters should lead to detectable variations in the brightness of quasars.

6. Light Curves as Compared With Observation

We finally ask whether light variations similar to those shown in Fig.29 and Fig.30 have actually been observed. Consider first the timescales involved. The time scale for rapid luminosity rise (and decline) t_r is a factor c/V larger than the light acrossing time in the source. Hence, if the relevant source component moves relativistically, these two time scale agree. The only direct evidence of relativistic motion in AGN comes from VLBI observations of superluminal sources. Note that the fraction of superluminal sources among compact radio sourcs is high (Porcas, 1985). Of course, it is unknown how many AGN have relativistically moving source components, but there is no reason to assume this fraction to be small. Thus, it is no a problem to account for variability time scales by lensing.

Lens-induced variability should cause light curves which are symmetric on the average. We do not see any evidence for pronounced asymmetry in the optical light curves (see Pica and Smith, 1983). The same is true for the radio light of BL Lac (Johnston et al., 1984), a source for which relativistic motion is established (Mutel et al., 1981).

Another prediction of models, which can be seen from Fig.29, is that sources which are lensed by star field of moderate ($\tau \sim 0.5$) optical depth should show phases of high "activity", with rather quiet phases in between. This has been observed for several sources; e.g., BL Lac was very active between 1969 and 1973, but quiet from 1974 to 1980, where it become active again.

The quasar 1156+295, one of the most extremely variable objects, was very inactive from 1950 to 1977, but active earlier in the century and after 1977.

QSO 2237+0305 is an excellent candidate for microlensing (Schneider et el., 1988, Kayser and Refsdal 1989, Wambsganss et al., 1988). The model light curves represented in

Wambsganss et al., (1989) show luminosity variations of the order of 1 $mag.$ in a time scale as short as a few years. The differences in the observed luminosities of QSO 2237+0305 between the measurements in 1986 and 1987 are -0.11, $+0.24$, -0.23, -0.20 $mag.$ for the images A, B, C, D, respectively (Schneider et al., 1988). These changes are most likely due to microlensing.

There is a munber of very promisimg candidates for lens-induced variability in the sample of blazars given by Angel and Stokman (1980). The light curve of the superluminal radio source 3C 345 looks very similar to above model light curves. From observation data (Fig.5), it indeed shows a succession of strong bursts, which could be interpreted as double peaked, U-shaped and symmetric. This would point to a moderate optical depth. After 1975, however, there have been no bursts, but only an irregular flickering with large amplitude. This rules out lensing as the mecahnism since that would imply a sudden change of the number of stars in the lensing galaxy in 1975.

The BL Lac object 0235+164 is not only highly variable, but there is an object very close to its line-of-sight which may be a galaxy in which micro lensing occurs. The microlensing models with different mass predict that, for medium optical depth, there should be phases of activity alternating with phases where the sources do practically not vary. This is observed in a couple of cases, e.g. 1156+295, which is one of the most violently variable quasars, was very active after 1977, but quiet from 1950 to 1977; from historical plates it is known that this object was active earlier this century.

So far, the best example for microlensing is BL Lac object 0846+51W1. Arp et al. (1979) reported the observation of an eruption of this object, which shows several peculiarities: (1) It is a violently variable object, it was observed to have brightened by ~ 4 mag in less than a month, and then decreased by more than 1 mag in two days. (2) It lies only $12''$ south of a spiral galaxy with redshift 0.072, itself's member of a group. (3) While at maximum light outburst, the optical spectrum is that of a BL Lac object, it looks like a QSO when fainter, the identification of lines C_{IV} 1549 and C_{III} 1909 yielding a redshift $z = 1.86$. (4) The colors are redder than any quasars; moreover, there are suggestions that the optical spectral index vary with magnitude, the object appearing bluer ($\alpha = 1.63$) at brightest and redder ($\alpha = 2.83$) at faintest level. Nottale (1986) suggested that these characteristics may be accounted for in a simple model where most of the

variability is not intrinsic to the object, but instead due to the gravitational amplification by a star lying in the intervening galaxy at $z = 0.072$. Moreover, the application of the theory of microlensing to this object allows to estimate of the mass of the lensing star, and to measure directly the dimensions of the various emission regions in the QSO. Fig.31 shows the fit of the observational data by the predicted light curve, It is fit very nicely for both theory and observation data. The value of the last undetermined constant, i.e. f/V depends on the magnitude at faintest level. Arp et al.'s data show that it lies between $V_{5000} = 20$ and 21, which implies $f/V = 50$ to 120 days, i.e. two to four months for the line of sight to cross the critical radius. With $A_{max} \approx 4mag$ (observed data), they find for $f = 10^{-3}pc$ (critical radius); $R \approx 5 \times 10^{-5}\ pc$ for the virtual beam in the lens plane, yielding for the QSO continuum emitting region: $R \approx 4 \times 10^{-4}\ pc = 10^{15}\ cm$, a value in good agreement with current determinations from X-ray or optical intrinsic variability.

The color seems to vary with luminosity. They suggested that this could be due to the QSO internal structure: a central blue steller object embedded in a larger redder object.

The light curve showed additional fluctuations with respect to the main burst. While this could be due to intrinsic variability of the QSO we may also interpret them as due to the passage of the star in front of substructures of the central emitting region.

Conclusions

Gravitational microlensing may, at least in some cases, be the reason for violent variability in AGN. But a major problem in the dection of microlensing variations of background AGN is distinguishing them from intrinsic AGN variations. There is a danger that a single diagnostic may be identified as intrinsic variability. There are two methods to distinguish the two types of variations.

The first method was originally discussed by Gott (1981). He suggested that the simultaneous observation of multiple macroimages of the same AGN could help separate the two types of variability. Specifically, if the time delay between images is known, one can compare the images and assume that intrinsic AGN variations occur in all images, while microlensing effects occur in each image individually. The subtraction of one image brightness from another (including the time delay) should therefore isolate microlensing variations (more accuratelly: isolate those effect that occur along the line-of-sight) and cancel intrinsic effects.

One problem with this analysis is that the optical depth to at least one of the images must be high. The rapid variations at high optical depth would therefore make it difficult, in practice, to find the time delay and recover information about the source or lenses.

Another clever method was suggested in Greiger, Kayser, and Refsdal (1986). They suggested that multiple observers might be of use in distinguishing between the two source of variability. If several observers were separated by 0.1 AU or more, they should all measure the same intrinsic variations but observe different microlensing variations. Microlensing effects would make themselves known through a relative time delay in the variability measured by the different observer. This would be caused by the slightly different aligments among observers, lens, and source.

A less fancy method of distinguishing intrinsic variability from microlensing variability involves monitoring both the BLR emission lines and the continuum simultaneously. Since the center of the BLR is usually the larger contributor to the line changes, and since the center of the BLR is hypothesized to be coincident with the continuum region, an observer might expect to see microlensing-induced variations occur in both the lines and the BLR at the same time. Intrinsic changes in AGN brightness might be expected to be seen first in the continuum region, and later propagate through the BLR (see, for example, Ulrich

et al., 1984). The time scale for continuum variations to propagate outward through to the BLR is of the order of days to weeks.

A mostly subjective method for discerning microlensing variations is to inspect AGN light curves for microlensing signatures. If candidates for low optical depth microlensing are investigated, one should have a good idea, from the record of theoretical research, what microlensing light curve signatures are to be expected. A major confounding factor with this method is observer bias. It is possible that any light curve with a peak would looks like a microlensing event to an observer eager enough for discovery. Finally, if we could combine all the cumulative diagnostics at once, we may yet a single reliable diagnostic. Unfortunately, only a single event has been put forward to date, and this event was the result of a single diagnostic (Nottale 1986).

Although models of microlensing have been developed at a high speed, the variability of AGN can be explained by microlensing are a few. It is very difficult to prove that this is indeed lens-induced variability. We obtained some basic idea about variablity of AGN. The time scale for a high amplification event is given by the time it takes a source to cross a caustic. The predicted timescale for variation due to microlensing range from weeks to centuries, Paczynski (1986) researched microlensing by the galactic halo and suggested the lensing events last $\sim$ 2 hr if a typical "dark halo" object has a mass of $10^{-6}M_{\odot}$. The time scales depend on the impact parameter b, source size R, optical depth τ, and relative velocity V. The maximum amplification $\Delta m_{max} \leq 5\ mag$. When the size of source is small enough, and optical depthe is small too, light curves can have very characteristic U-shapes between the peaks. The properties of variability of AGN can be explained by microlensing are at most $\Delta m_{max} \leq 5\ mag$ and irregular flickering without much change in apparent magnitude and without periodicities. This agrees with the fourth and first types in the Rossemary Hill classification.

Abramowicz (1987) gave a review an variability of AGN. He points out there are some important detailed differences: (1) Variability of the intensity of the spectral lines cannot be explained by lensing, especially when some other lines do not change or when, as sometimes happens, there is a correlation betwen variability in lens and in the continuum. (2) Gravitational lensing cannot explain secondary maxima or the fact that many outbursts have a much shorter rise time than decay time. These features are characteristic of damped

oscillations caused by an instability. Double peaked outbursts are not common.

One should not be surprised by the difficulties to identify microlensing events: the situation resembles that in normal optics. The investigation of a lens can not be better than the understanding of the light that we shine through it. An outstanding problem in gravitational lens reasearch is our ignorance of the physics of quasars and other AGN. Clearly, if lensing is a dominants effect, then quasar physics and lens theory are inseparable.

However, astronomical applications of microlensing are extensive and there are many gratifying results. Microlensing can be an important tool to the informed observer. There is much information it can tell us, and many ways it could manifest itself. It detected, microlensing could prove to be an valuable resource in the quest to understanding the universe around us.

Figur Captions

Figure 1: The picture of light curve of 3C 273. Adopted from Smith (1965) ≪Qusi-Stellar Objects and Grav. Collapse≫ p.225.

Figure 2: Magnetic residuce ΔB of 3C 345 as a function of phase ϕ assuming a period of $321^d.5$ and taking $\phi = 0.0$ at J. D. 2439049 7. Adopted from Kinman, T. D., et al, Ap. J. **152**, 357.

Figure 3: A tipical active–nucleus light curve , the U-band curve for the Seyfert galaxy NGC 3516. Adopted from Dibar, E. A. et al, 1984, Sov. Astro. **28(1)**. Jan-Feb., 7.

Figure 4: Light curve of OJ 287. Adopted from Sillanpää, A., et al, 1988, Ap. J. **325**, 628.

Figure 5: Light curve of 3C 345 spanning a 15 year period from 1965. Adopted from Kidger, M. P., and Beckma, J. E., 1986, A.Ap. **154**, 288.

Figure 6,7: Theoretiacl timescales and observed timescales. Adopted from Abramowicz M. A., and Szuszkiewicz, E., 1988, preprint of SISSA.

Figure 8: The minimum time scale of variablity is plotted against total luminosity for a selection of quasars, Seyfert nuclei, and BL Lac objects. The absence of any points in the shaded region indicates that presently observed fluxvariablity is consistent with black hole accretion models for these objects. Supermassive stars should lie well above the shaded region, while giant pulsars could populate both the shaded and unshaded regions. Adopted from Elliot, L., et al., 1974, Ap. J., **192**, L3.

Figure 9: Seven active galactic nuclei on the Log$L$ versus log t plane. The heavy line corresponds to the origianl Elliot-Shapiro relation ($\lambda = 1 = \tau$). Three thin lines give absolute lower limits for t_{min} in the cases $\lambda = 1, 3, 10, 30, 100$ ($\log \tau = 0.8$ is assumed on these lines). For almost all the objects $\lambda >> 1$. This rules out thin accretion disks. Observational points in the dark region would contradict the black hole model. Adopted from Abranowicz, M. A., & L. Nobili, 1982, Nature **300**, 506.

Figure 10: The lensing geometry, b is impact parameter, R is spherical lens radius, along the axis, the distance from the lens is defined to be F, the minimum focal length of the lens.

Figure 11: Diagrams of light ray paths in a typical lens. The solid lines show the true path of the light rays from the sources S to the observer O as they are deflected in the lens plane L. The observer sees the images I_1 and I_2 of the sources as if light had followed

the path of the dashed lines. The lensing equation is shown to be the geometrical construction derived from the distances D_{oL}, D_{Ls}, D_{os}) and the angles (θ_I, θ_s α) in the problem. The sources S, which has a real position at θ_s, is seen at the image position θ_I due to a deflection at the lensing mass by angle α.

Figure 12: A bending angle diagram for a typical spherical lens, characterized by a linear rise at small radius, and a $1/r$ drop off at large radii. To construct the image positions for a source at position θ_s, the line θ_I–θ_s is drawn on the bending angle diagram, and the images (A, B and C) are at the intersections of the bending angle curve and the line.

Figure 13: The geometry of gravitational bending of light. Adopted from Schneider., 1984, A. Ap., **140**, 119.

Figure 14: Contours of arrivial time $\tau(\theta_I;\theta_s)$ in the θ_I plane for a simple elliptic galaxy lens in which the surface density is increased. The source is located at the centers of the four diagrams, images are located on L, H and S. Surface density is 1, 2, and 3 represented by b c and d respectively. Adopted from Blandfoord, 1986, Ap. J. **310**, 568.

Figure 15: The think line shows the bending angle α as a function of impact parameter θ_I for a typical circularly symmetric lens. Adopted from Blandford, 1986, Ap. J. **310**, 568

Figure 16: Crossing contours for three image topologies and for five image topologies.

Figure 17: Position of source and images. Adopted from Narayan, R. 1988, Lecture Notes in Physics **330**, p.32.

Figure 18: Position of extended source. Adopted from Narayan, R. 1988, Lecture Notes in Physics **330**, p.32.

Figure 19: Fold catastrophe. The images atart on opposite sides of the fold, and merge when the source is on the fold caustic where they are infinitely amplified. When the source has crossed the catastrophe there are no images.

Figure 20: Cusp catastrophe. Adopted from Blandford, 1986, Ap. J. **310**, 568.

Figure 21: The geometry of low optical depth lens. Adopted from Chang and Defsal 1979, Nature **282**, 561.

Figure 22: Critical curves in the deflector plane for various values of γ. Adopted from Chang and Refsdal 1984, A. Ap. **132**, 168.

Figure 23: Critical curves in the observer plane (or in the source plane) for various values of γ, with the source (observer) in the origin. Adopted from Chang and Refsdal 1984, A.

Ap. **132**, 168.

Figure 24: Total flux from one image (group of subimages) of a point source located in the origion P' for various values of γ. F_0' is the flux which would have been observed, if only the galactic deflection had been taken into account (the star neglected).

Figure 25: Amplication signature of microlensing event. After the source crosses the fold at t_0 (at which time the amplification is formally infinite), the observed flux decays as $|t - t_0|^{-1/2}$, and similarly the flux rises again as the source approaches the second caustic at time t_1.

Figure 26: Crossing contours for microlensing at a minimum and a maximum. The black region covers one of the maxima, which is unobservable because it is inside the star.

Figure 27: Light curves with different values of D'. The real diameter of the source object Q is given by $D'r_0L/\lambda$. *a*, point sourc; *b*, D'=0.5–$D' = 1.0$; *c*, $-D' = 20$–D'=4.0, $-D' = 10.0$. Adopted from Chang and Defsal 1979, Nature **282**, 561.

Figure 28: Light curves of an extended source of radius R which crosses a) a critical line and b) a cusp. Adopted from Schneider and Weiss, 1986, A. Ap. **164**, 237.

Figure 29: The magnification Δm as a function of the source position along straight lines through the source plane, for the cases a–l described in Table 2. The solid lines correspond to a source size of b, whereas the dotted and dashed lines correspond to source size of $10b$ and $5b$ respectively. THe unit of length along the x-axis is x_0. Cosidering these curves as light curves, the unit of time along the x-axis is t_0. Adopted from Schneider and Weiss, 1987, A. Ap. **171**, 49.

Figure 30: Model light curves. Adopted from Watson, W. D., Lecture Notes in Physics 1988, **330**, p.202.

Figure 31: Fit of the main burst of the light curve observed by Arp et al, (1979), by the microlensing model described by Nottale (1986). Adopted from Nottale, L. 1986, A. Ap. **157**, 383.

Table 1: Focal Lengths of the Astronomical Objects.

Table 2: Description of the Models.

References

Abramowicz, M. A., and Piran, T., 1980, Ap. J. Letter, **241**, L7

Abramowicz, M. A., Calvani, M., and Madau, P., 1987, Comments Astrophys. **12**, 67

Abramowicz, M. A., Calvani, M., and Nobili, L., 1980, AP. J., **242**, 772

Abramowicz, M. A.,et al., 1986, in Quasars, eds. G.Swarup and V. K. Kapahi, (Reidel, Dordrecht), P. 371

Abramowicz, M. A., 1987, in Variability $\cdots$, ed A. Treves., P.137

Abramowicz, M. A., Nobili, L. 1982, Nature **300**, 506

Abramowicz, M. A., and Zurek, W. H., 1981, Ap. J. **246**, 314

Abramowicz, M. A., et al., 1986, Marcel Grossmann Meeting on G. R. 1467

Abramowicz, M. A., et al., 1989, preprint in SISSA. 45A

Abramowicz, M. A., Szuszkiewicz, E., 1988, prepint in SISSA 79A

Abramowicz, M. A., 1989, Lecture in SISSA

Altshuler, D. R., and Wardle, J. F. C., 1976, M. N. R. A. S. **82**, 1

Angione, R. J., 1973, ibid., **78**, 353

Angel, J. R., and Stockman, H. S. 1980, Ann. Rev. Astron. Astrophys. **18**, 321

Arp, H. et al., 1979, Ap. J. **230**, 68

Arnold, V. I., 1986, Catastrophe Theory

Barbieri, C. et al., 1985, Astron. Astrophys. **142**, 316

Barbieri, C. et al., 1983, Men. S. A. It. **54**, 617

Barnothy, J. M., 1968, A. J. **73**, S164

Bartels, G. G., 1981, Thesis, Hamburg University.

Benson, J. R., et al., 1979, Ap. J. **227**, 360

Babadzanjant, M. K., and Belokon, E. T., 1975, in Variable Stars and Stellar Evolution, IAU Symp. NO. 67, p.611

Bourassa, R. R., Kantowski, R. 1975, Ap. J., **195**, 13

Bontz, R. J. 1979, Ap. J. **233**, 402

Biermann, P. et al., 1981, Ap. J. Lett. **247**, L53

Bregman, J. N., et al., 1986, Ap. J. **301**, 708

Blandford, R., et al., 1986, Ap. J. **301**, 568

Blandford, R. 1987, 13th Jerusalem Winter School on Dark Matter in th Universe.

Burke, W. L. 1981, Ap. J. Lett. **244**, L1

Chang, K., 1984, A. Ap. **130**, 157

Chang, K., and Refsdal, S. 1984, A. Ap. **132**, 168

Chang, K., and Refsdal, S. 1979, Nature **282**, 561

Canizares, C. R., 1982, Ap. J. **263**, 508

Cannon, R. D., et al., 1971, M.N.R.A.S., **152**, 79

Collin-Souffrin, S., 1968, A. Ap. **166**, 27

Dent, W. A., and Balonek, T. J., 1980, Nature **283**, 747

Deguchi, S., et al., 1988, Ap. J. **335**, 67

Deeming, T. J., 1975, Astrophys. Space Sci., **36**, 137

Dibai, E. A., 1984, Sov Astron. **28**,(1) Jan.-Feb. 7

Eddington, A. S., 1921, Zs. f. Phys., **7**, 351

Elliot, J. L., Shapiro, S. L. 1974, Ap. J. **192**. L3

Einstein, A., 1936, Science, **84**, 506

Frohlich, A., 1973, IAU Circ. NO.2525

Foy, R., et al., 1985, A. Ap., **149**, L13

Gott, J. R., 1981, AP. J. **243**, 140

Gott, J. R., 1986, Nature **321**, 420

Greiger, B., Kayser, R., and Refsdal, S., 1986 Nature **324**, 126

Gorshkov, A. G., and Popov, M. V., 1972, Astron. Zh. **49**, 722

Guilbert, P. W., et al., 1984, M.N.R.A.S. **205**, 593

Grossman, S. A., and Narayan, R. 1988, Ap. J. Lett. **324**, L37

Grieger, B., et al., 1988, A. Ap. **194**, 54

Hewitt, A., and Burbidge, G., 1987, Ap. J. Suppl. Series **63**, 1

Hackney, et al., 1975, A. J. **80**, 895

Hagen-Thorn, V. A., et al., 1977, Pis'ma Astron., th. **3**, No. 2

Impey, C. G., et al., 1982, M.N.R.A.S., **200**, 19

Johnston, K. J., et al. 1984, Ap. J. **277**, L32

Joly, M., et al., 1985, A. Ap. **152**, 282

Jurkevich, I., et al., 1971, Astro. Space Sci. **10**, 402

Kinman, T. D., 1970, Report at Symp. IAU. NO.44, Uppsala

Kinman, T. D., 1968, Ap. J. **152**, 357

Kidger, M. R. et al., 1968, A. Ap. **154**, 288

Kikuchi, S. et al., 1968, A. Ap. **190**, L8

Kwan, J., and Krolik, J. H., 1979, Ap. J. Lett. **233**, L91

Kwan, J., and Krolik, J. H., 1981, Ap.J. **250**, 478

Kilinger, A. L., 1974, AP. J. Lett. **191**, L109

Klimov, Y. G., 1963, Soviet Phys., **8**, 119

Kayser, R., and Refsdal, S., 1989a, Nature **338**, 745

Kayser, R., and Witt, H. J. 1989b, A. Ap. **221**, 1

Kayser, R., and Refsdal, S., Stabell, R. 1986, A. Ap. **166**, 36

Kayser, R., Weiss, A., Refsdal, S. and Schneider, P. 1989, A. Ap. **214** , 4

Kayser, R. and Refsdal, S., 1988, A. Ap. **197**, 63

Kayser, R. and Refsdal, S., 1983, A. Ap. **128**, 156

Lawerence, A. et al., 1987, M.N.R.A.S. **217**, 685

Liebes, S. J., 1964, Phys. Rev. **133B**, 835

Link, F., 1967, Bull. Astr. Inst. Czech., **18**, 215

Lutyi, V. M., and pronik, V. I., 1975, in variable Stars and Stellar Evolution, IAU Symp. No. 67 (Reidel Dordrecht), p.592

LU, P. K. and Hunter, J. H., 1969, nature **221**, 755

Lynds, R. and Petrosian, V., 1987, Bull. AAs, **18**,1014

Lyutyi, V. M., 1979, Sov. Astron., **23**, 518

Maeder, A., 1973, A. Ap. **26**, 215

McGimsey, B. Q. et al., 1975, A. J., **80**, 895

Minser, C. W. et al., 1973, Gravitation

Medd, W. J. et al., 1972, Mem. R. A. S., Vol.**77**, Pt.3

Matilsky, T. et al., 1982, Ap. J. Lett. **258**, L1

Mardalajevic, J. et al., 1988, Ap. Lett. **26**, 357

Mchardy, I. and Czerny, B., 1987, in Variability $\cdots$, ed. A. Treves, p.59

Misner, C. W. et al., 1973, Gravitation, San Francisco: W. H. Freeman

Mutel, R. L. et al., 1981, Nature **294**, 236

Mushotzky, R. F. et al., 1980, Ap. J. Lett. **239**, L5

Narayan, R. et al., 1984, Nature **310**, 112

Narayan, R. et al., 1988, Lecture Notes in Physics, **330**, 593

Nityananda, R. and Ostriker, J. R., 2984, J. Astr. Ap. **5**, 235

Nottale, L., 1986, A. Ap., **157**, 383

Ozernoy, L. M. and Usov, V. V., 1977, A. Ap., **56**, 163

Ostriker, J. P., Vietri, M., 1985, Nature **318**, 446

Paczynski, B., 1987, Nature **325**, 572

Paczynski, B., 1986a, Ap. J., **304**, 1

Paczynski, B., 1986, Ap. J., **301**, 503

Paczynski, B., 1986, Nature, **321**, 419

Pacholcyk, A. G., 1972, in External Galaxies and Quasi-Stellar Objects IAU Symp., No.44, p.168

Pica, A. J. and Smith, A. G., 1983, Ap. J., **272**, 11

Pica, J. T. et al., 1980, A. J., **85**, 1442

Pringle, J. E., 1981, Ann. Rev. Astr. Ap., **19**, 137

Penston et al., 1974, M. N. R. A. S., **169**, 357

Pounds, K. A. et al., 1987, M. N. R. A. S., **224**, 443

Peterson, B. M., 1988, P. A. S. P., **100**, 18

Poecas, R. W., 1985, in Active Galactic Nuclei, ed by J. E. Dyson.

Press, W. H. and Gunn, J. E., 1973, Ap. J., **185**, 397

Refsdal, S. 1966, M. N. R. . S., **132**, 101

Refsdal, S. 1964a, M. N. R. . S., **128**, 295

Refsdal, S. 1964b, M. N. R. . S., **128**, 307

Refsdal, S. 1970, Ap.J., **195**, 357

Refsdal, S. 1964, Mon. Notices of the Royal Astro. Soci., **128**, 307

Reasenberg, R. D. et al., 1979, Ap. J. Lett., **234** , L219

Rieke, G. H. et al., 1972, Ap. J. Lett., **177**, L115

Schneider, P. and Weiss, A., 1986, A. AP., **164**, 237

Schneider, P., 1984, A. Ap.,**140**, 119

Schneider, P., 1986, Ap. J.,**300**, L31

Schneider, P., 1987a, A. Ap.,**183**, 189

Schneider, P., 1987b, Ap. J. ,**316**, L7

Schneider, P., 1987c, A. Ap.,**179**, 71

Schneider, P., 1987d, A. Ap.,**179**, 80

Schneider, P. and Weiss, A., 1987, A. Ap.,**171**, 49

Schneider, P.and Weiss, A., 1988a, Ap. J., **330**, 1

Schneider, P., 1988b, A. J.,**95(6)**, 1619

Schneider, P., 1985, A. Ap.,**143**, 413

Schneider, P. and Schmid-Burgk, J., 1985, A. Ap., **148**, 369

Schneider, P., 1987, Ap. J. Lett.,**316**, L7

Seyfert, C. K., 1943, Ap. J., **97**, 28

Schmidt, J., 1968, Nature, **218**, 663

Sillanpaa, A., 1988, Ap. J., **325**, 628

Sanduleak, N. and Pesch, P., 1984, Ap. J. Suppl. Series., **55**, 517

Smith, M., 1965 Quasi-Stellar Objects and Grav. Collapse.

Strittmatter, P. A. et al., 1972, AP. J. Lett., **175**, L7

Soucail, G. et al., 1987, A. Ap., **172**, 414

Stocke, J. T. et al., 1987, AP. J. Lett., **315**, L11

Subramanian, K. et al., 1985, Ap. J., **289**, 37

Shields, G. A., 1977, Astro. Lett., **18**, 119

Smith, M. et al., 1970, Astro. Space Sci., **8**, 471

Soldner, J., 1801, Berliner A. Jahrb **1804**, 161

Tikhov, G. A., 1937, Bull. Obs. Central a Poulkovo, **16**, 1

Tananbaum, H. et al., 1979, Ap. J. Lett., **234**, L9

Turner, T. J. and Pounds, K. A., 1988, M. N. R. A. S., **232**, 463

Turner, E. L. et al., 1984, Ap. J., **284**, 1

Ulrich, M. H. et al., 1984, M. N. R. A. S., **206**, 221

Bietri, M. and Ostriker, J. P., 1983, Ap. J., **267**, 488

Visvanathan, N. and Elliot, J. L., 1973, Ap. J., **179**, 721

Watson, W. D., 1988, Lecture Notes in Physics, **330**, 195

Warwick, R. S., 1988, in The physics of Accretion onto compact objects, ed. K. O.

MAson et al., (Springer, Berlin).

Wambsganss, J. et al., 1988, in Lecture Notes in Physics, **330**, 209

Wambsganss, J. et al., 1989, Preprint in Princeton University.

Wiita, P. J., 1985, Physica Reports, **123**, No.3, 117

Wills, D. et al., 1980, A. J., **85**, 1555

Weinberg, S., 1972, Gravitation and Cosmology (New York: Wiley)

Walsh, G. et al., 1979, Nature, **279**, 381

Webb, J. R. et al., 1988, A. J., **95**, 374

Wilson, A. S. et al., 1979, M. N. R. A. S., **187**, 109

Xie et al., 1987, A. Ap. Suppl. Ser., **67**, 17

Young, P. et al., 1980, Ap. J., **241**, 507

Young, P., 1981, Ap. J., **244**, 756

Zwicky, F., 1937a, Phys. Rev., **51**, 290

Zwicky, F., 1937b, Phys. Rev., **51**, 679

Zwicky, F., 1957, Morphological Astronomy, berlin: Springer-Verlag.

Focal Lengths of Astronomical Objects

Object	Typical Radius	Typical Mass	F
Sun	1 $R_\odot$	1 $M_\odot$	538 AU
O5 V Star	18 $R_\odot$	40 $M_\odot$	4630 AU
M5 V Star	0.32 $R_\odot$	0.2 $M_\odot$	275 AU
White Dwarf	6000 km	1 $M_\odot$	0.04 AU
Neutron Star	15 km	1 $M_\odot$	40 km
Jupiter	0.1 $R_\odot$	$10^{-3} M_\odot$	6000 AU
Earth	$10^{-2} R_\odot$	$3x10^{-6} M_\odot$	15000 AU
Asteroid	100 km	10^{20} gm	10 pc
Baseball	5 cm	1000 gm	30 Mpc
Dust Grain	10^{-5} cm	$4x10^{-15}$ gm	2600 Mpc
Proton	10^{-13} cm	$2x10^{-24}$ gm	650 pc

Table 1.

Model	a	b	c	d	e	f	g	h	i	j	k	l
κ_*	0.2	0.2	0.5	0.5	0.7	0.8	0.2	0.2	0.2	0.8	1.5	1.3
κ_c	0.0	0.0	0.0	0.0	0.0	0.0	0.5	0.3	0.2	2.0	0.0	0.0
γ	0.0	0.0	0.0	0.0	0.0	0.0	0.0	0.3	0.4	0.0	0.0	0.0
b	0.025	0.025	0.0125	0.0125	0.0125	0.0125	0.0125	0.0125	0.0125	0.0375	0.0125	0.0125
N_*	245	245	288	288	2520	8000	500	300	400	320	5400	4680
ε [%]	0.08	0.08	1.04	1.04	0.65	0.60	0.27	0.25	0.15	0.19	0.50	1.20
$\langle I_S \rangle$	1.56	1.56	4.00	4.00	11.1	25.0	11.1	6.25	5.00	0.31	4.00	11.1
$\langle I \rangle$	1.51	1.68	3.11	3.81	15.1	17.4	11.7	3.71	3.76	0.31	2.65	10.5
f_{sc}^{-1}	791.1	791.1	791.1	791.1	351.6	351.6	156.3	459.2	208.0	316.4	258.3	258.3
$\Delta m_{\min}$	0.0	0.0	0.0	0.0	1.0	1.4	1.4	0.6	0.6	− 4.0	− 0.2	1.0
$\Delta m_{\max}$	3.0	3.0	3.0	3.0	4.0	4.4	4.4	3.6	3.6	2.0	3.3	4.0
L_S	12.8	12.8	6.4	6.4	6.4	6.4	6.4	6.4	6.4	19.2	6.4	6.4

Table 2.

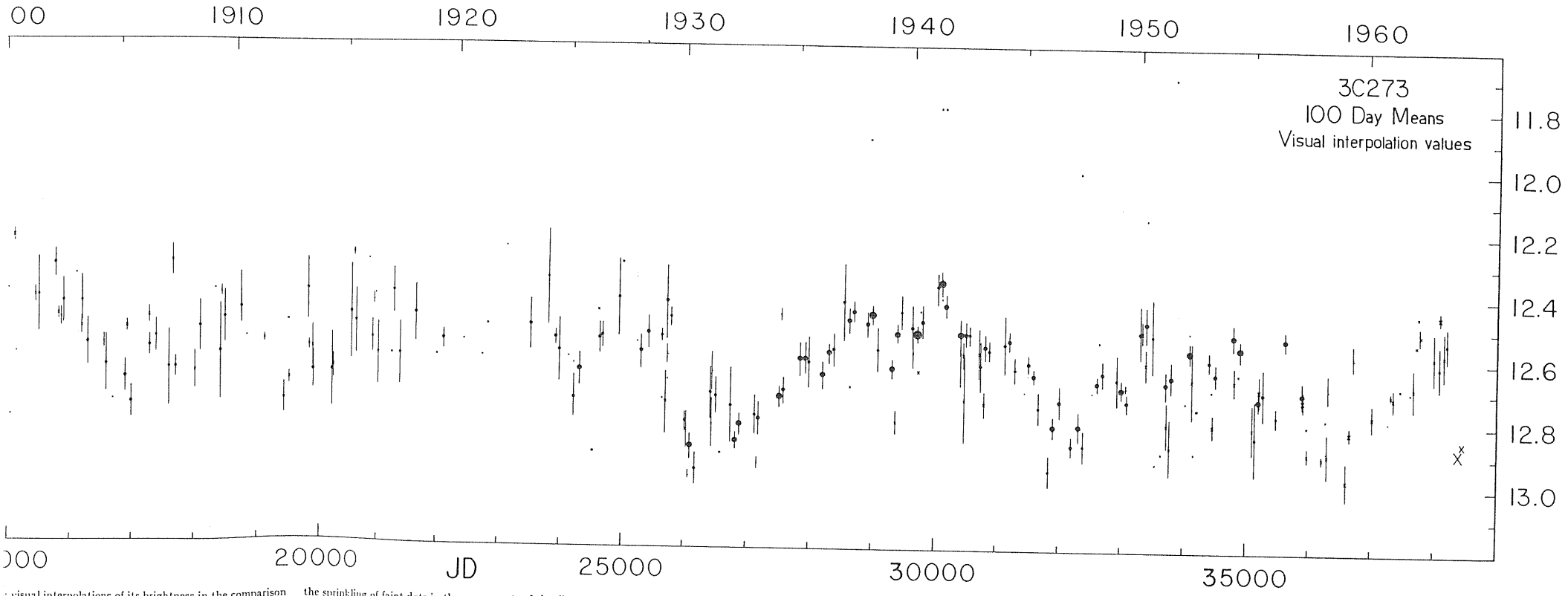

visual interpolations of its brightness in the comparison
100-day intervals of Julian date. Means in time within
lingly. Individual observations more than 0.5 magnitude
been included in the mean; shown separately, these giving the sprinkling of faint dots in the upper parts of the diagram.

A symbol without error bars refers to a single plate within a 100-day interval; the same size of dot with error bars indicates two plates; for three or more plates the area of each symbol is proportional to the number of plates entering the mean, with 45 the largest. Error bars are standard deviations about the mean for each 100-day interval of the particular plate series.

Dot symbols refer to Harvard plates, crosses to Heidelberg (before 1930) or Sonneberg (after 1930); +, M, K, and L correspond, respectively, to Russian, Maria Mitchell, Bamberg, and Lowell data.

Fig. 1

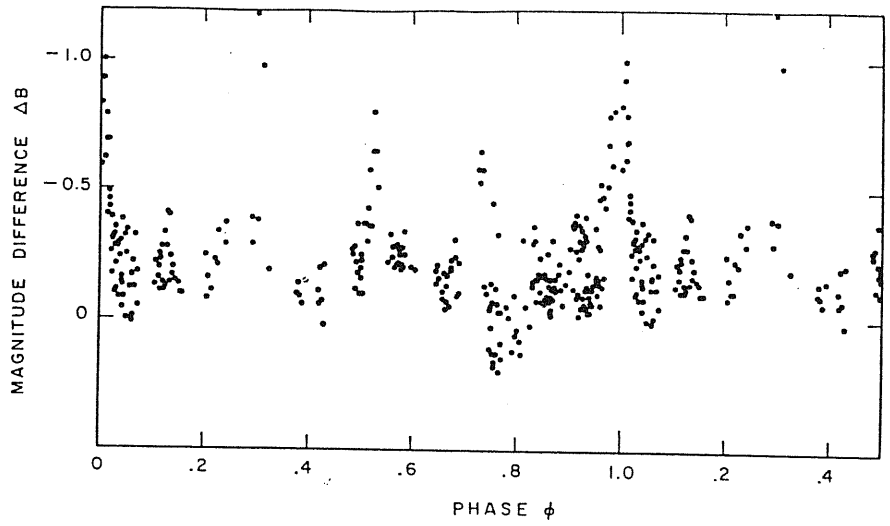

Fig. 2

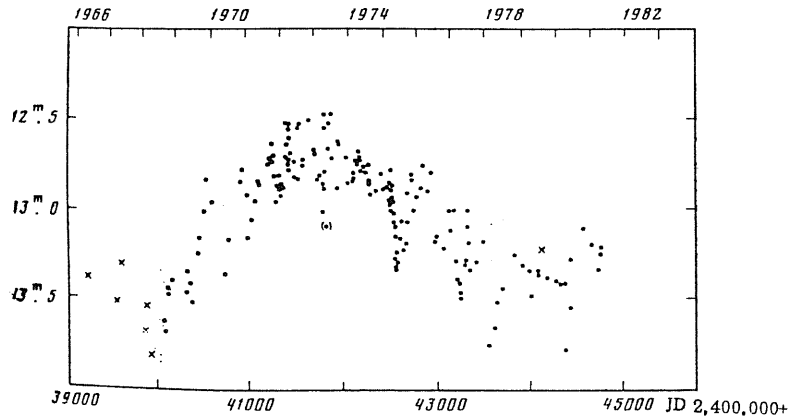

Fig. 3

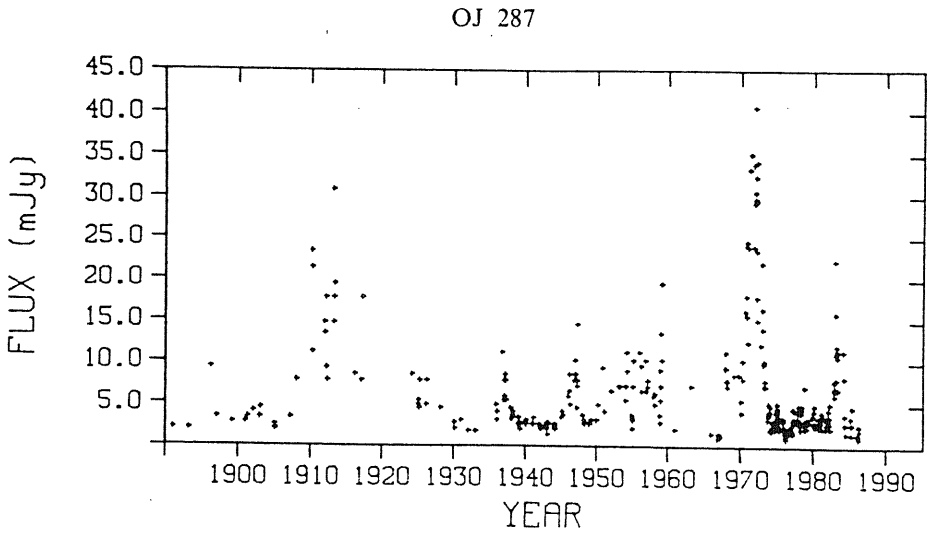

Fig. 4

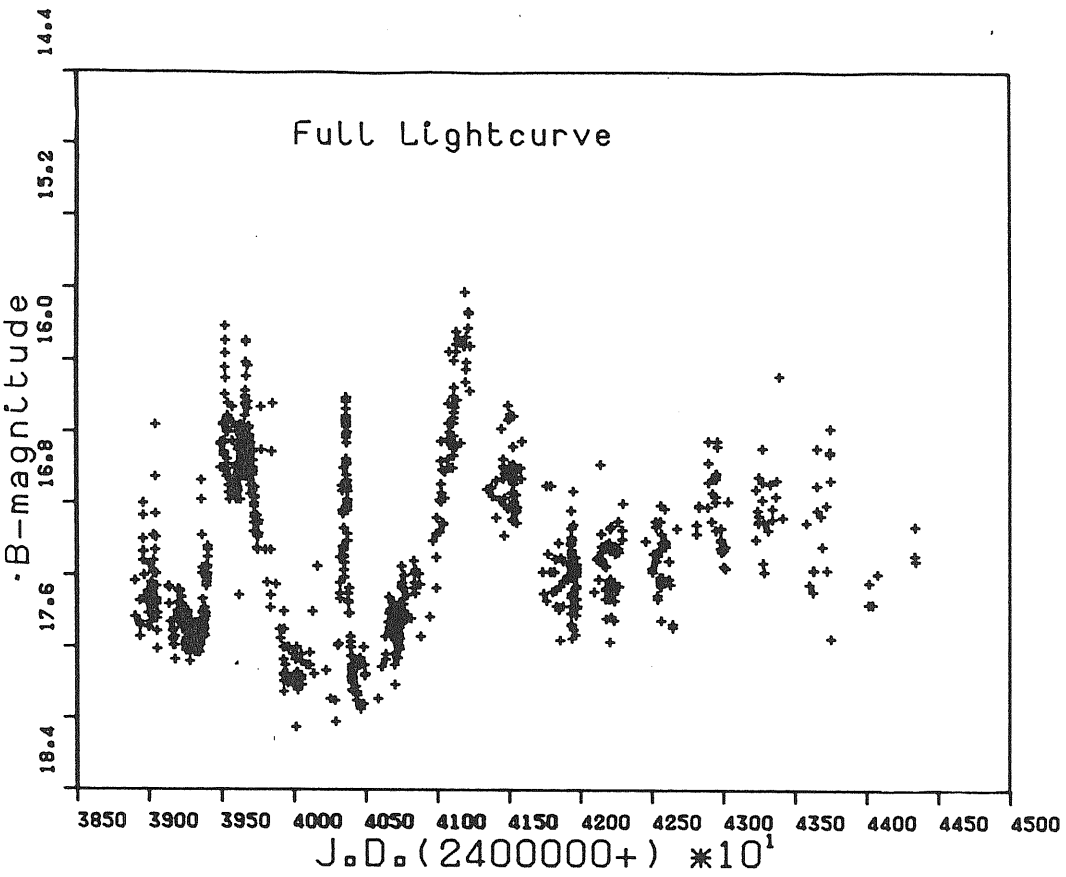
Full Lightcurve
B-magnitude
14.4
15.2
16.0
16.8
17.6
18.4
3850 3900 3950 4000 4050 4100 4150 4200 4250 4300 4350 4400 4450 4500
J.D.(2400000+) *10^1

Fig. 5

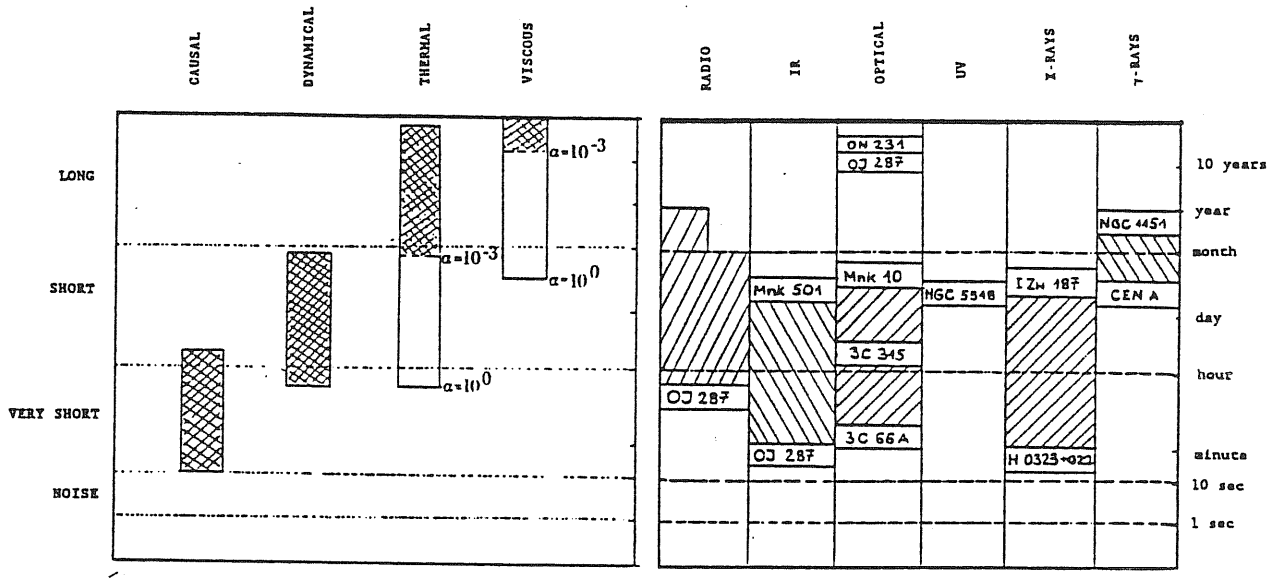
CAUSAL
DYNAMICAL
THERMAL
VISCOUS
RADIO
IR
OPTICAL
UV
X-RAYS
γ-RAYS
LONG
SHORT
VERY SHORT
NOISE
α=10^-3
α=10^-3
α=10^0
α=10^0
ON 231
OJ 287
Mnk 501
Mnk 10
3C 345
3C 66A
NGC 5548
1ZW 187
H 0323+022
NGC 4151
CEN A
10 years
year
month
day
hour
minute
10 sec
1 sec

Fig. 6, 7.

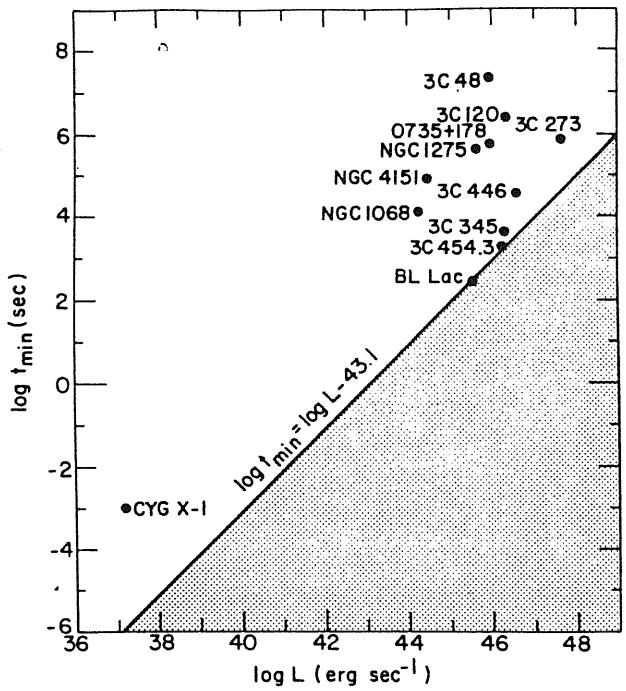
3C 48
3C 120
3C 273
0735+178
NGC 1275
NGC 4151
3C 446
NGC 1068
3C 345
3C 454.3
BL Lac
CYG X-1
log t_min = log L - 43.1
log t_min (sec)
log L (erg sec^-1)
8
6
4
2
0
-2
-4
-6
36
38
40
42
44
46
48

Fig. 8

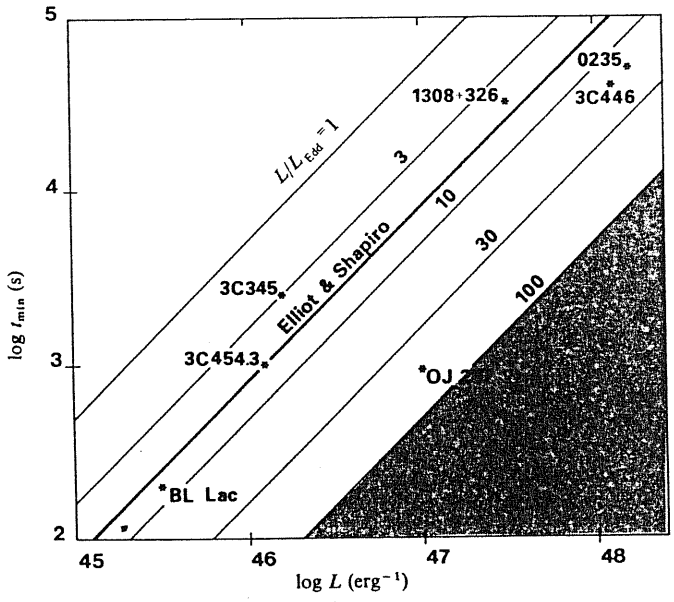
0235
3C446
1308+326
L/L_Edd = 1
3
10
30
100
Elliot & Shapiro
3C345
3C454.3
*BL Lac
log t_min (s)
log L (erg^-1)
5
4
3
2
45
46
47
48

Fig. 9

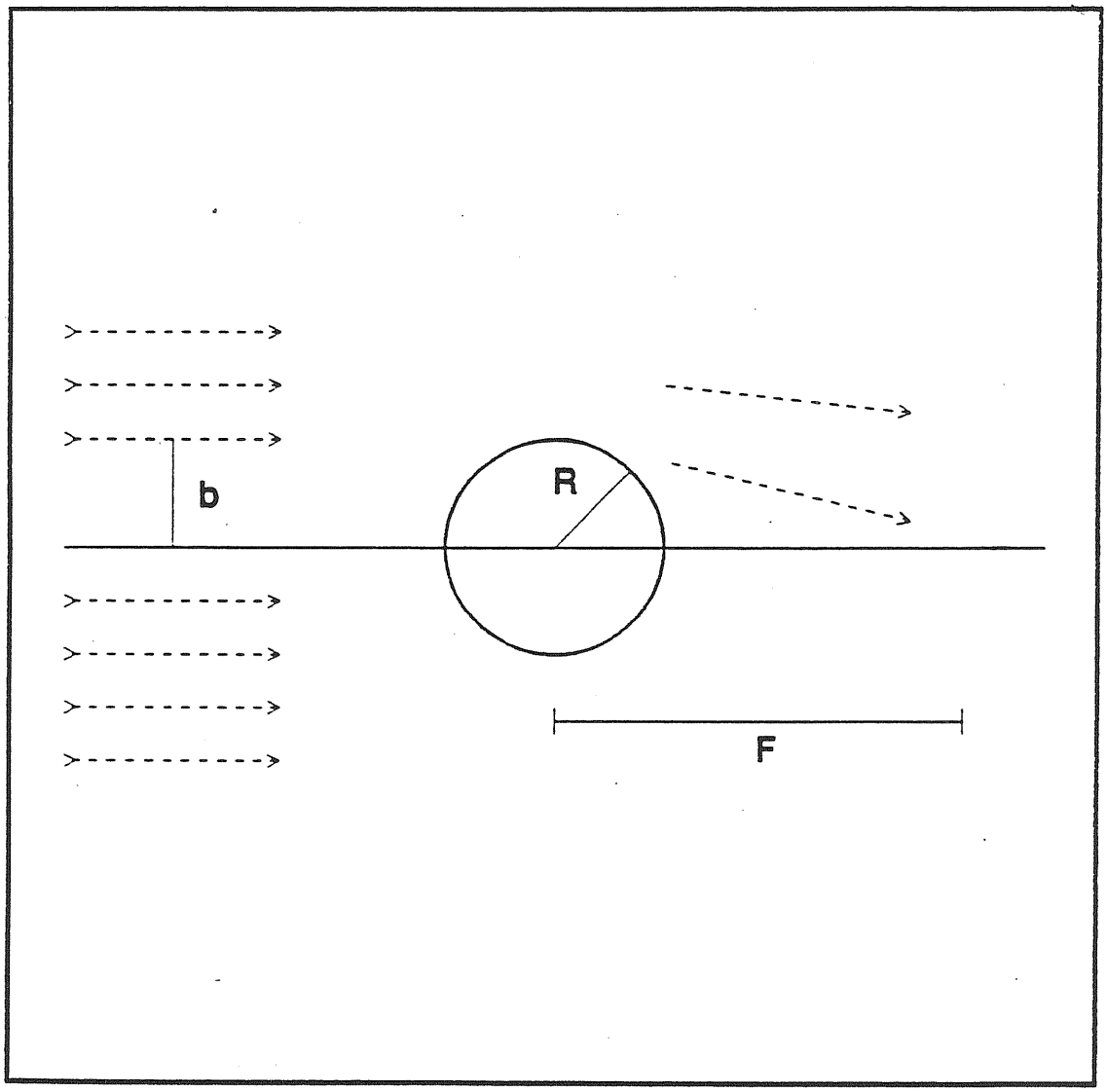

Fig. 10.

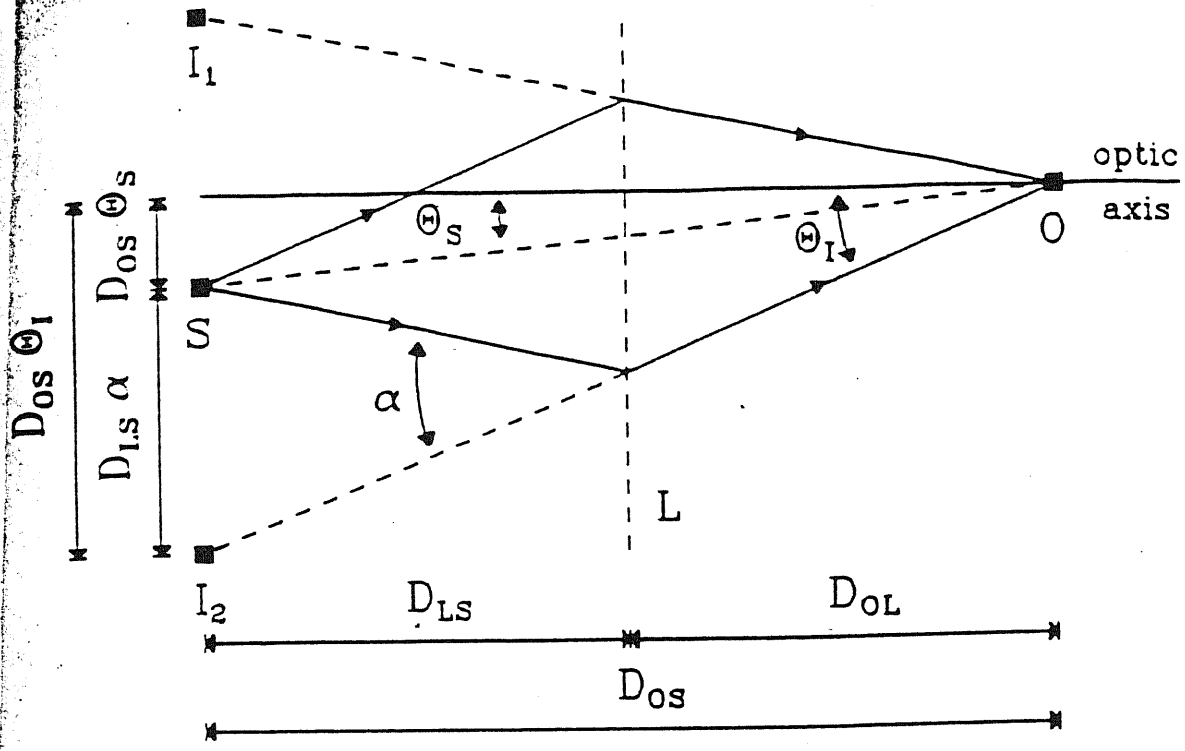
I1
optic
axis
O
S
L
I2
DLS
DOL
DOS
α
Θs
ΘI
DOS Θs
DOS ΘI
DLS α

Fig. 11.

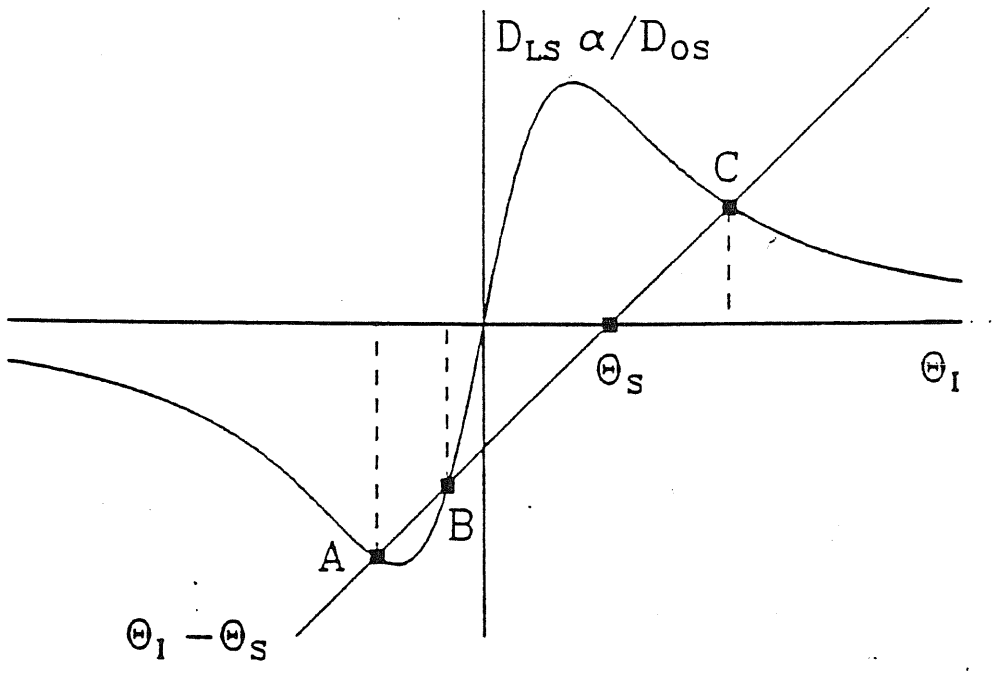
DLS α/DOS
C
Θs
ΘI
A
B
ΘI − Θs

Fig. 12

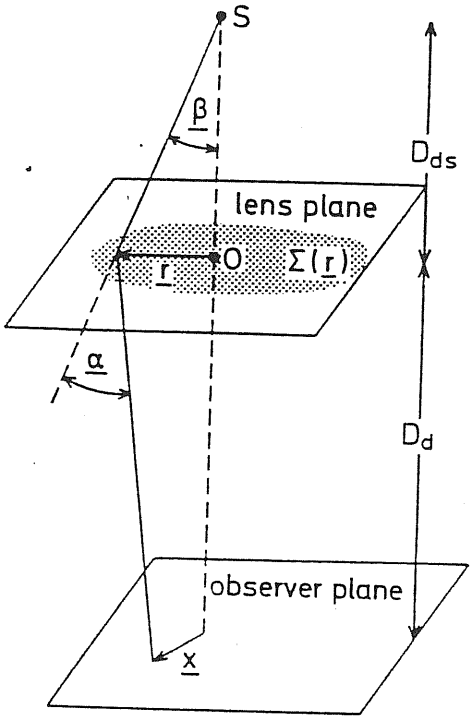

Fig. 13.

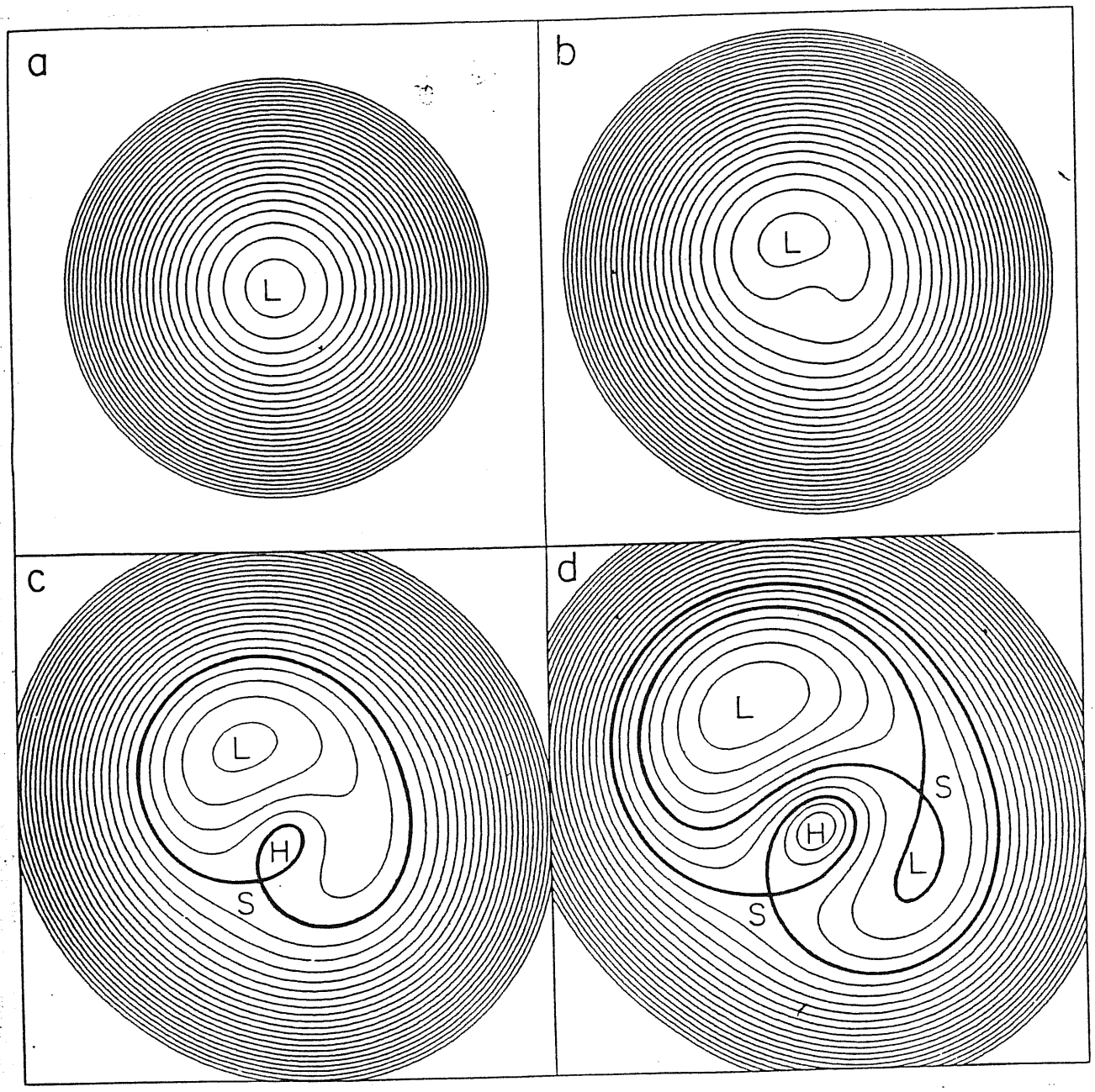

Fig. 14.

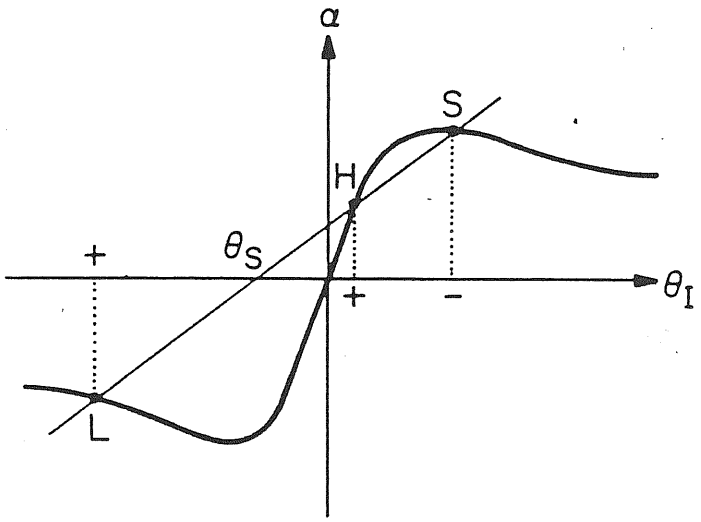

Fig. 15

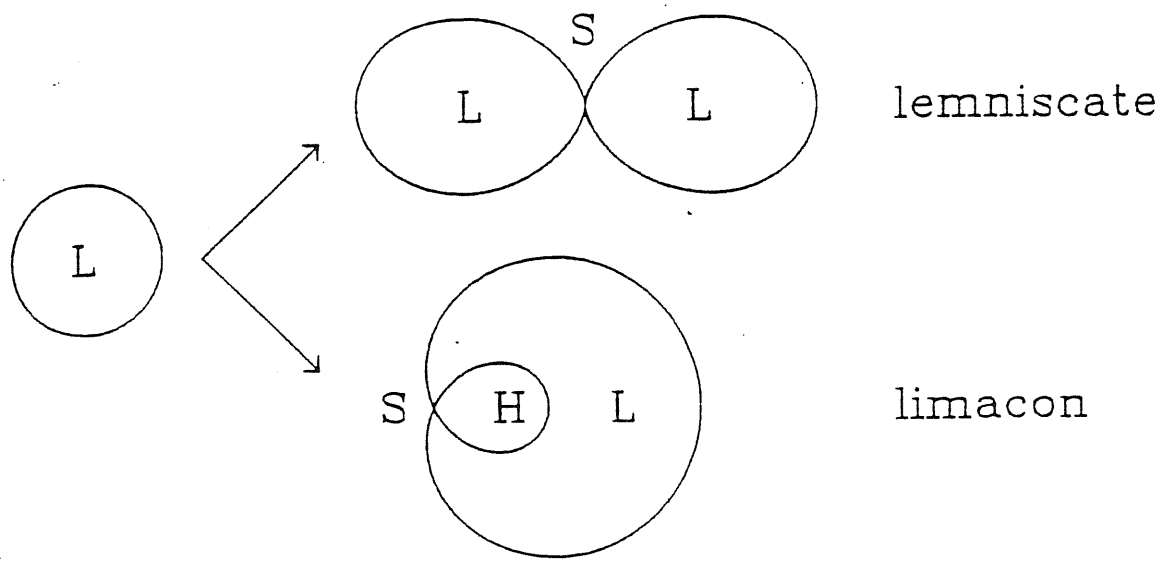

Crossing contours for three image topologies.

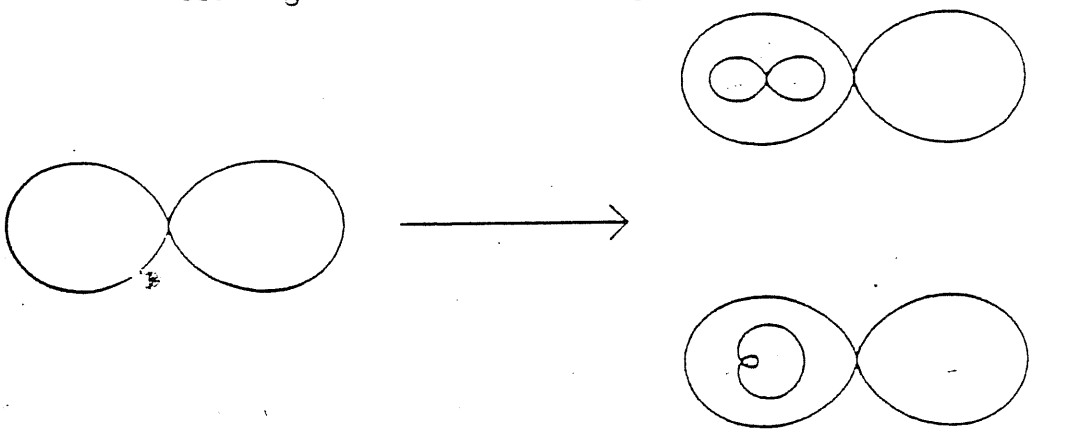

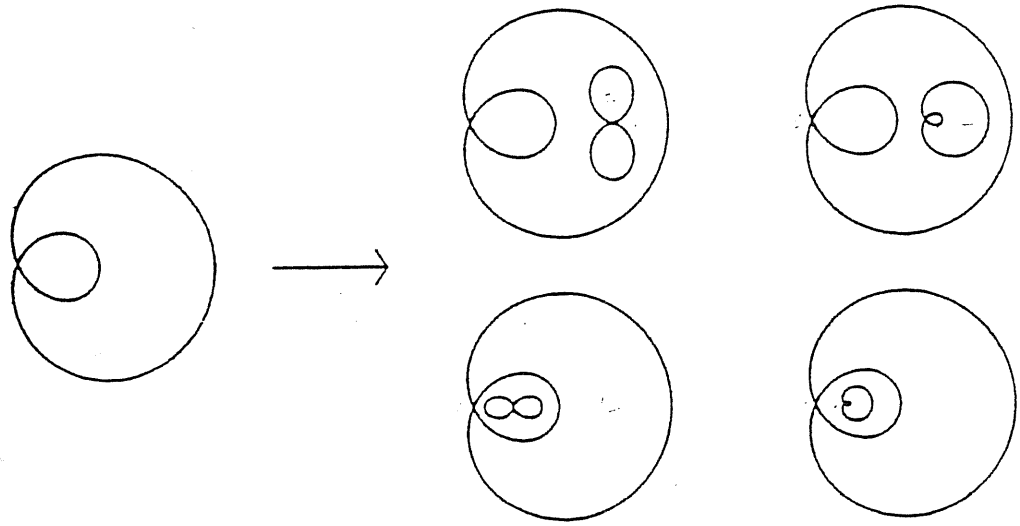

Crossing contours for five image topologies

Fig. 16.

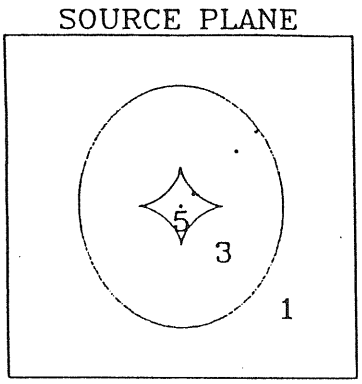

The inner and outer lines in the Source Plane are the tangential and radial caustics, which separate regions of image-multiplicity 1, 3, and 5. The inner and outer lines in the Image Panels are the radial and tangential critical lines. Panels a-d show image geometries corresponding to the four source positions (dots in the Source Plane), starting from the center. The angular scales in the Source Plane and Image Panels are not the same. The bottom panels show observed multiply imaged quasars that resemble the model configurations. A-D are quasar images and G represents the center of the lensing galaxy (if observed).

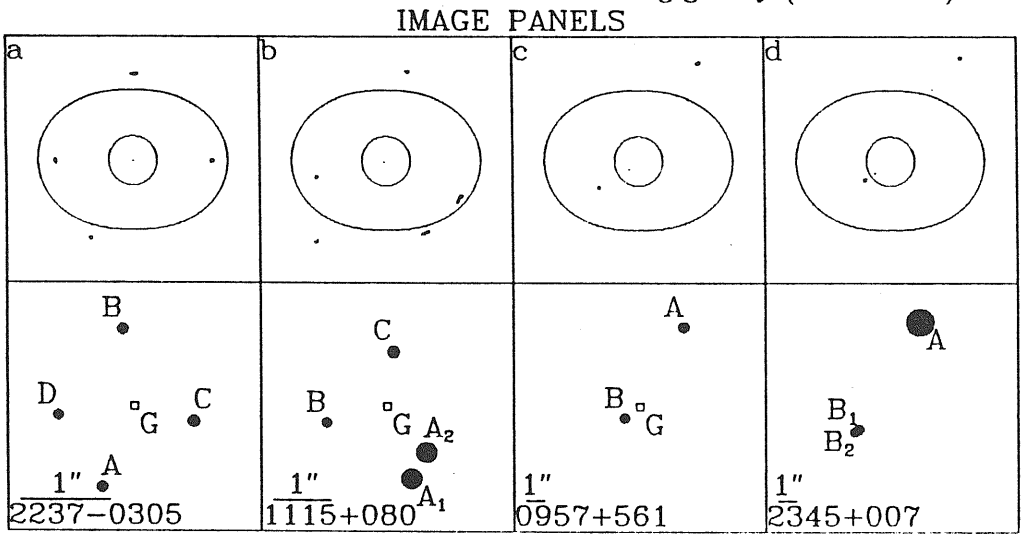

Fig. 17.

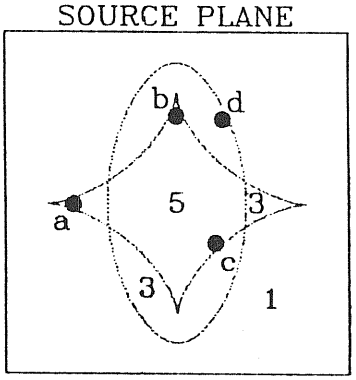

Elongated images of extended sources (filled circles) for four locations in the Source Plane. Image Panels a and b correspond to sources on cusps; three images merge tangentially on the tangential critical line to form a large arc. Panels c and d correspond to folds. In panel c, a small arc is produced by the tangential merger of two images, and in panel d a radially elongated image is formed. The lens potential corresponds to $r_c/\alpha_0 = 0.55$ (appropriate for a galaxy cluster, which is likely to have a less concentrated core relative to its bending than a galaxy) and $\epsilon = 0.1$.

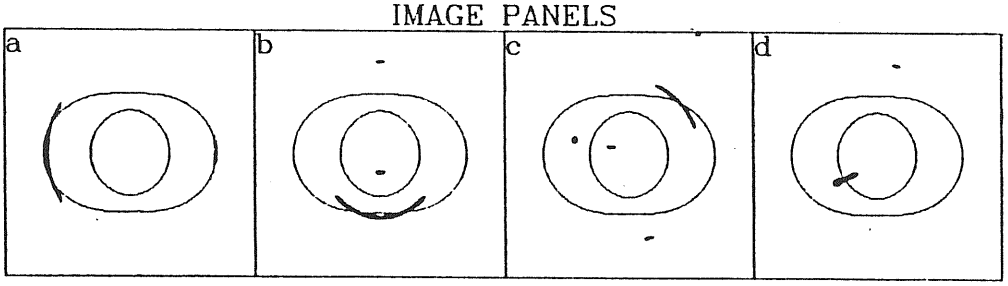

Fig. 18.

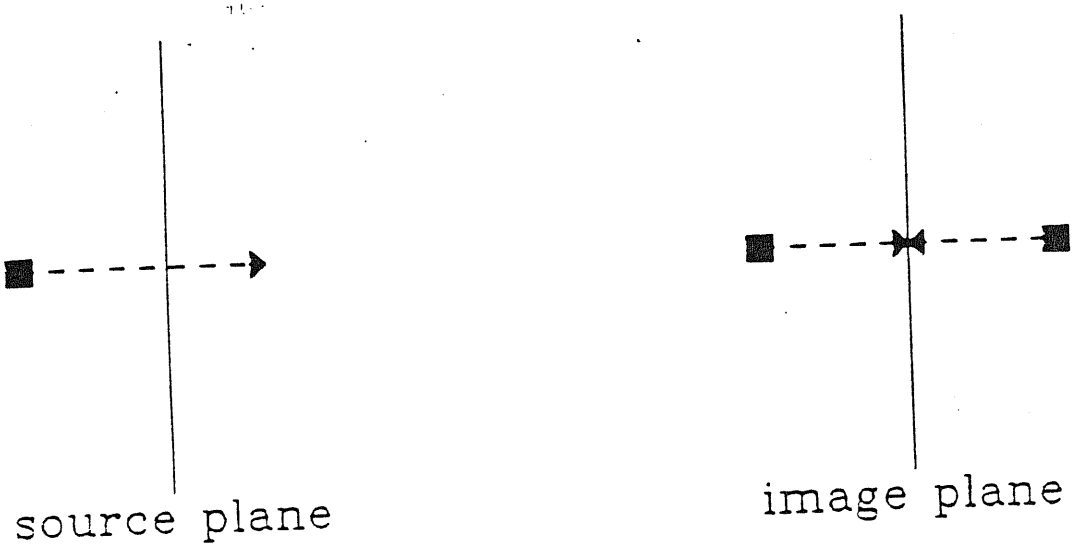

Fig. 19.

Fold Catastrophe. Diagrams of the source plane and image plane near a fold as a source crosses over the fold starting from the multiple imaging side. The images start on opposite sides of the fold, and merge when the source is on the fold caustic where they are infinitely amplified. When the source has crossed the catastrophe there are no images (locally, globally there must be at least one if the lens is non-singular).

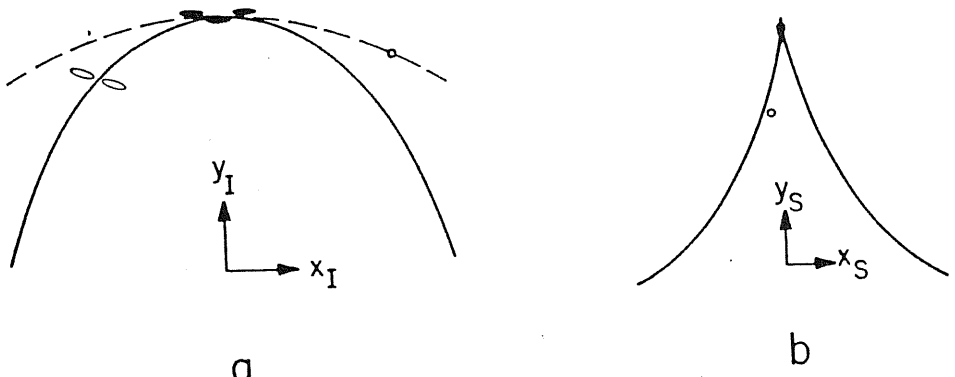

Cusp caustic in image plane (*a*) and source plane (*b*). The case displayed corresponds to a positive cusp. The solid ellipses show the locations and sh of the images when the source is very close to the cusp [solid circle in (*b*)]. The three images merge simultaneously along a direction tangential to the caustic when source is exactly on the cusp, and for a source just outside the cusp there is only one very bright image. Away from the cusp, the caustic in (*b*) behaves like a fold shown by the open circles and ellipses, when the source approaches and crosses the caustic line in this region, two bright elongated images merge and disapp while the third unbrightened image crosses the dashed single-image line. See Hogan and Narayan (1984) for a pictorial description of the fold caustic.

Fig. 20.

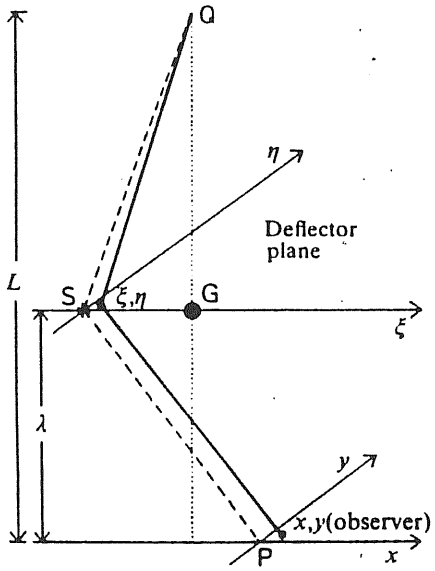

Light source Q with the affine parameter L large deflector G (galaxy) with the affine parameter λ and small deflecting mass S (star). The deflector plane (ξ, η) and the observer's plane (x, y) are normal to the line QG. For convenience we chose the origin of the (ξ, η) plane to be at S and the x axis to be parallel to the ξ-axis. The origin P in the (x, y) plane is obtained by considering a light ray QSP for which only the galactic deflection is taken into account. The solid line from Q through the points (ξ, η) and (x, y) represents the path a photon would take when the deflections from G and S are taken into account.

Fig. 21.

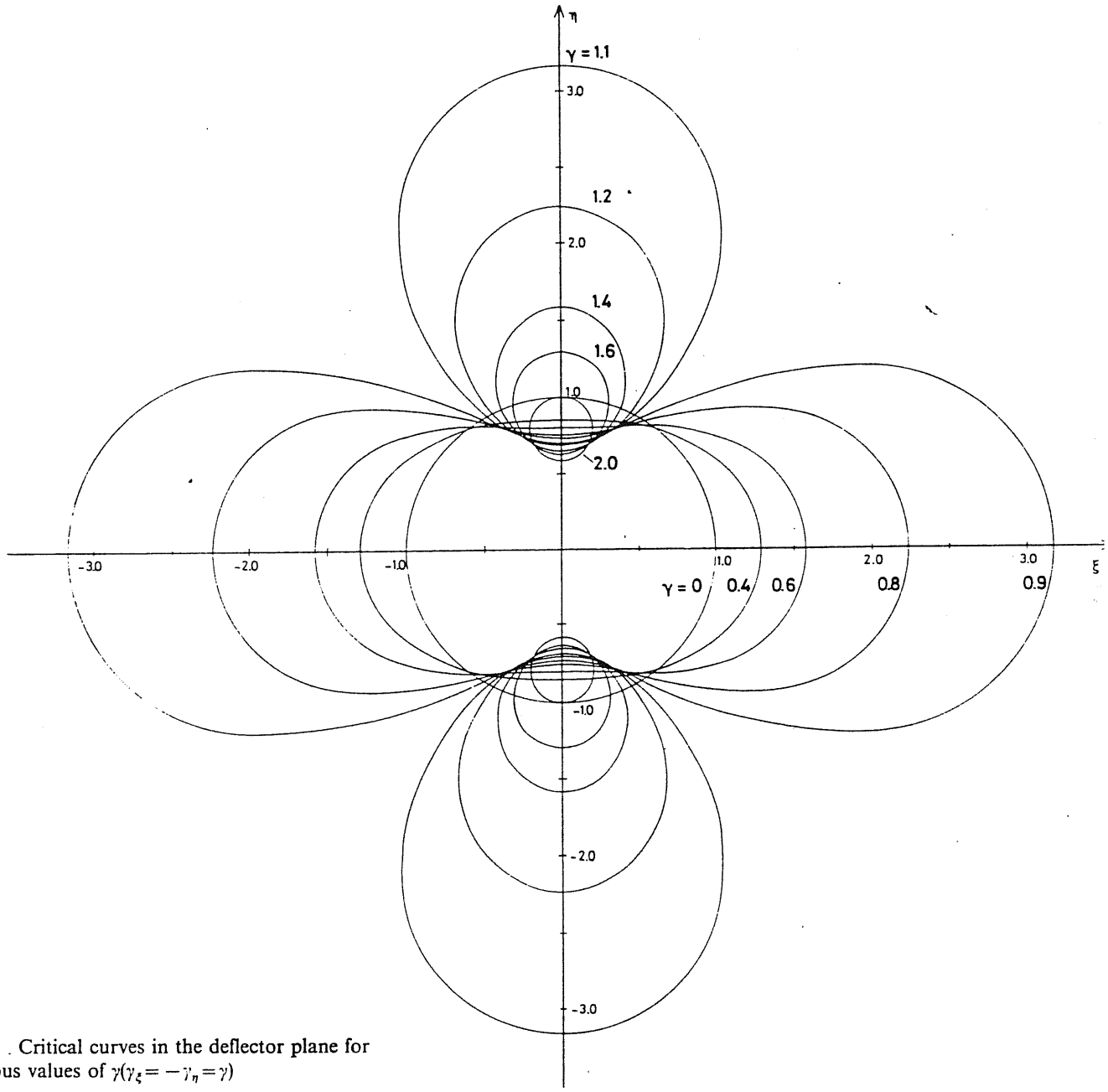

. Critical curves in the deflector plane for various values of $\gamma(\gamma_\xi = -\gamma_\eta = \gamma)$

Fig. 22.

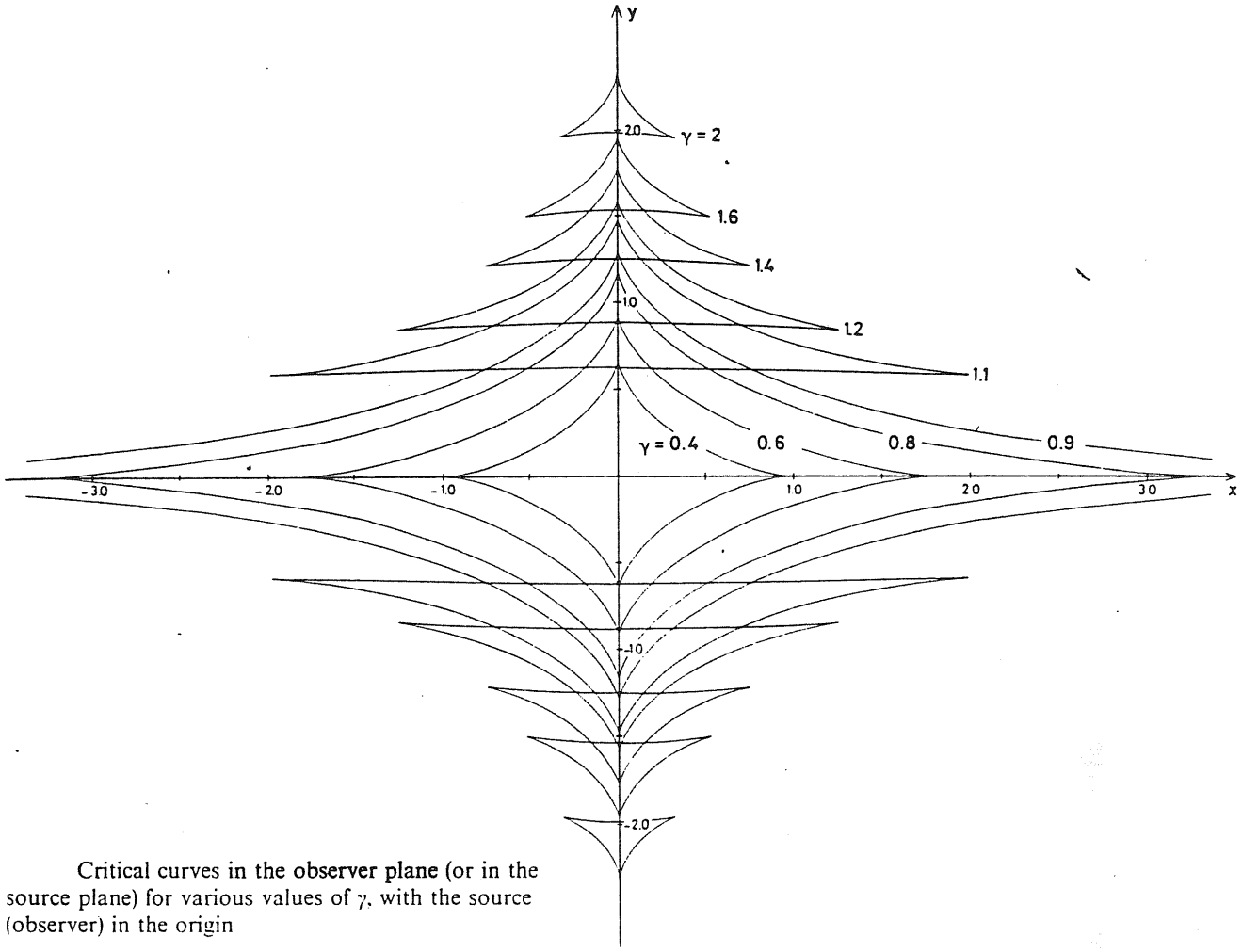

Critical curves in the observer plane (or in the source plane) for various values of γ, with the source (observer) in the origin

Fig. 23.

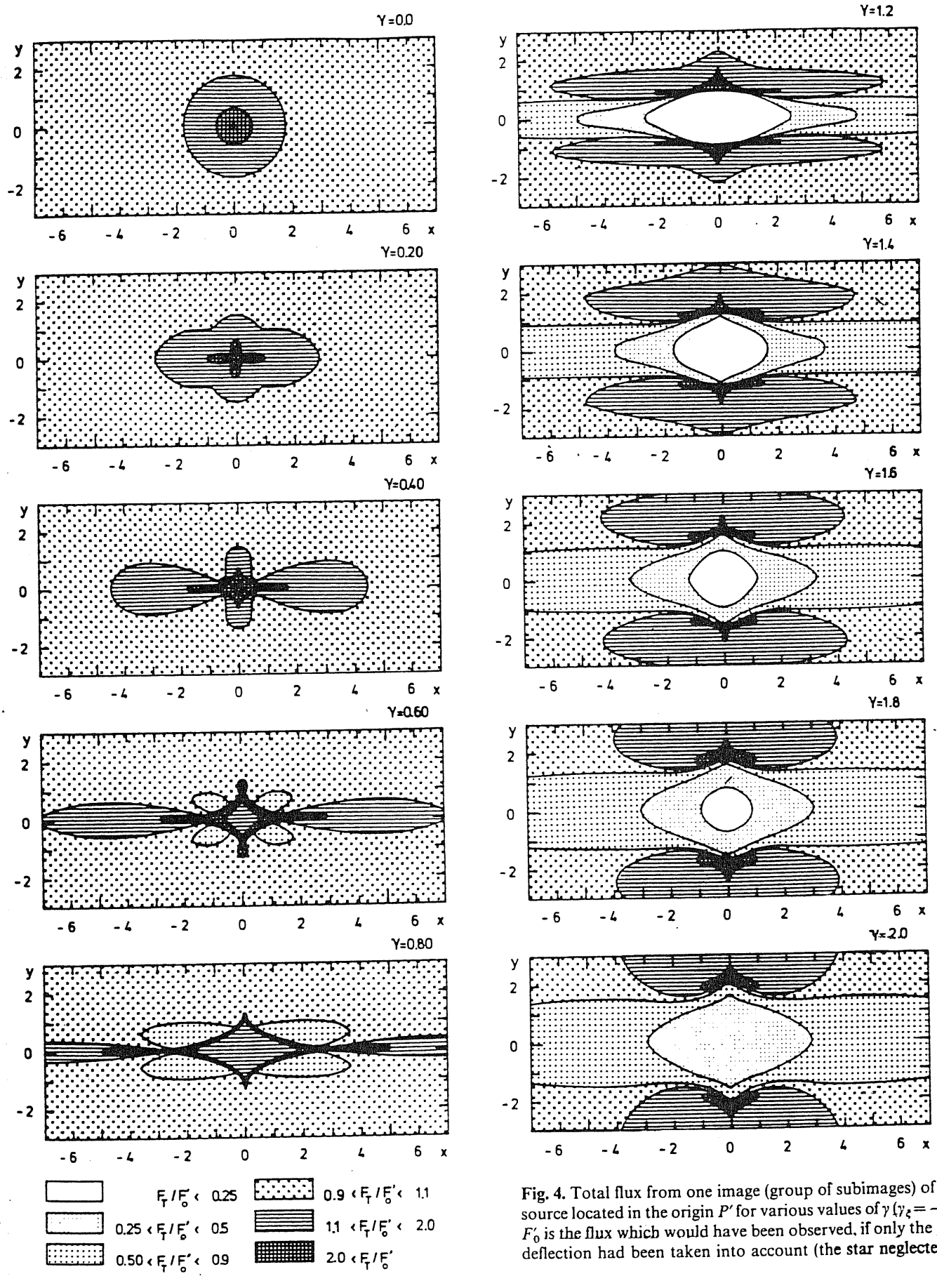

Fig. 4. Total flux from one image (group of subimages) of a point source located in the origin P' for various values of γ ($\gamma_\xi = -\gamma_\eta = \gamma$). F_0' is the flux which would have been observed, if only the galactic deflection had been taken into account (the star neglected)

Fig. 24.

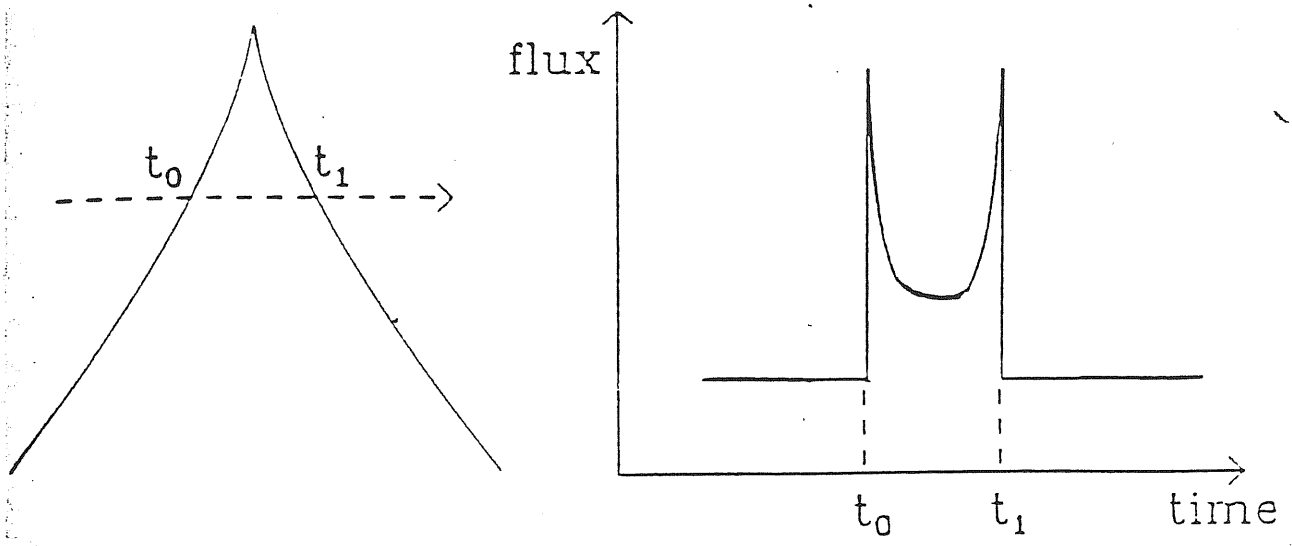

Amplification signature of microlensing event. After the source crosses the fold at t_0 (at which time the amplification is formally infinite), the observed flux decays as $|t - t_0|^{-1/2}$, and similarly the flux rises again as the source approaches the second caustic at time t_1.

Fig. 25.

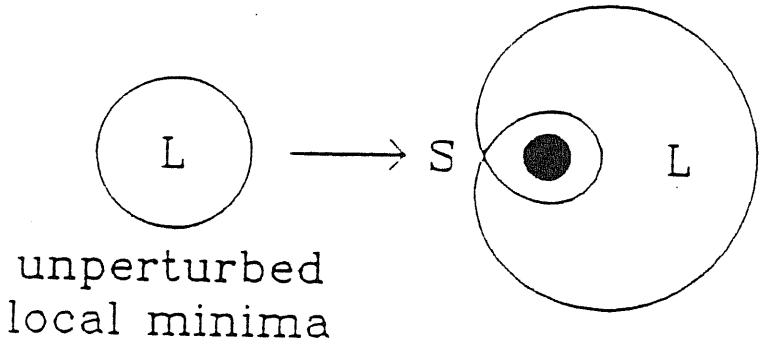

Crossing contours for microlensing at a minimum. The unperturbed minimum is distorted into a limaçon crossing contour. The black region covers the maximum, which is unobservable because it is inside the star.

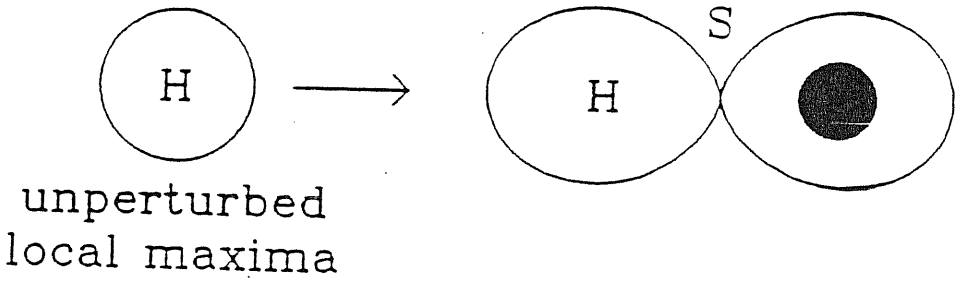

Crossing contours for microlensing at a maximum. The unperturbed maximum is distorted into a lemniscate crossing contour with two maxima and a saddle. The black region covers one of the maxima, which is unobservable because it is inside the star.

Fig. 26.

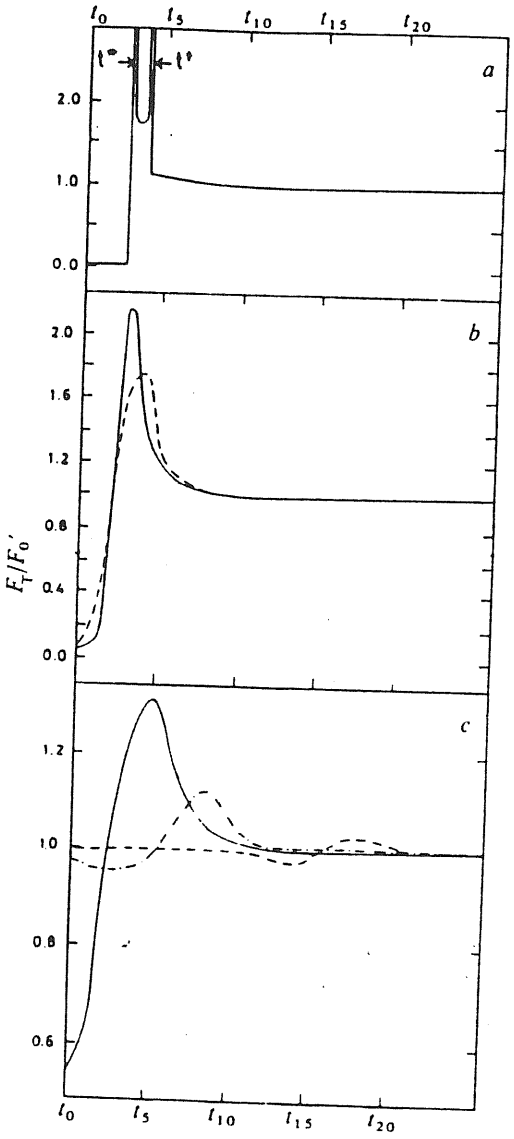

Fig. 27.

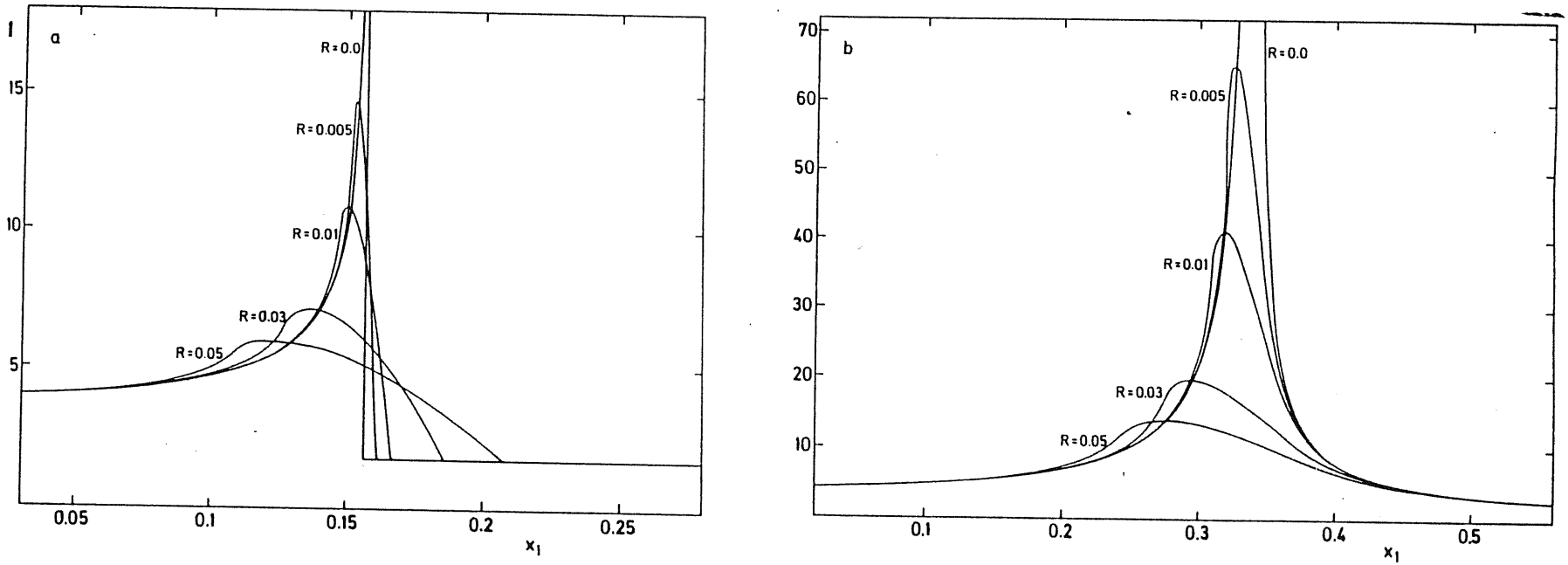
a
R=0.0
R=0.005
R=0.01
R=0.03
R=0.05
1
15
10
5
0.05
0.1
0.15
0.2
0.25
x1
b
R=0.0
R=0.005
R=0.01
R=0.03
R=0.05
70
60
50
40
30
20
10
0.1
0.2
0.3
0.4
0.5
x1

Fig. 28.

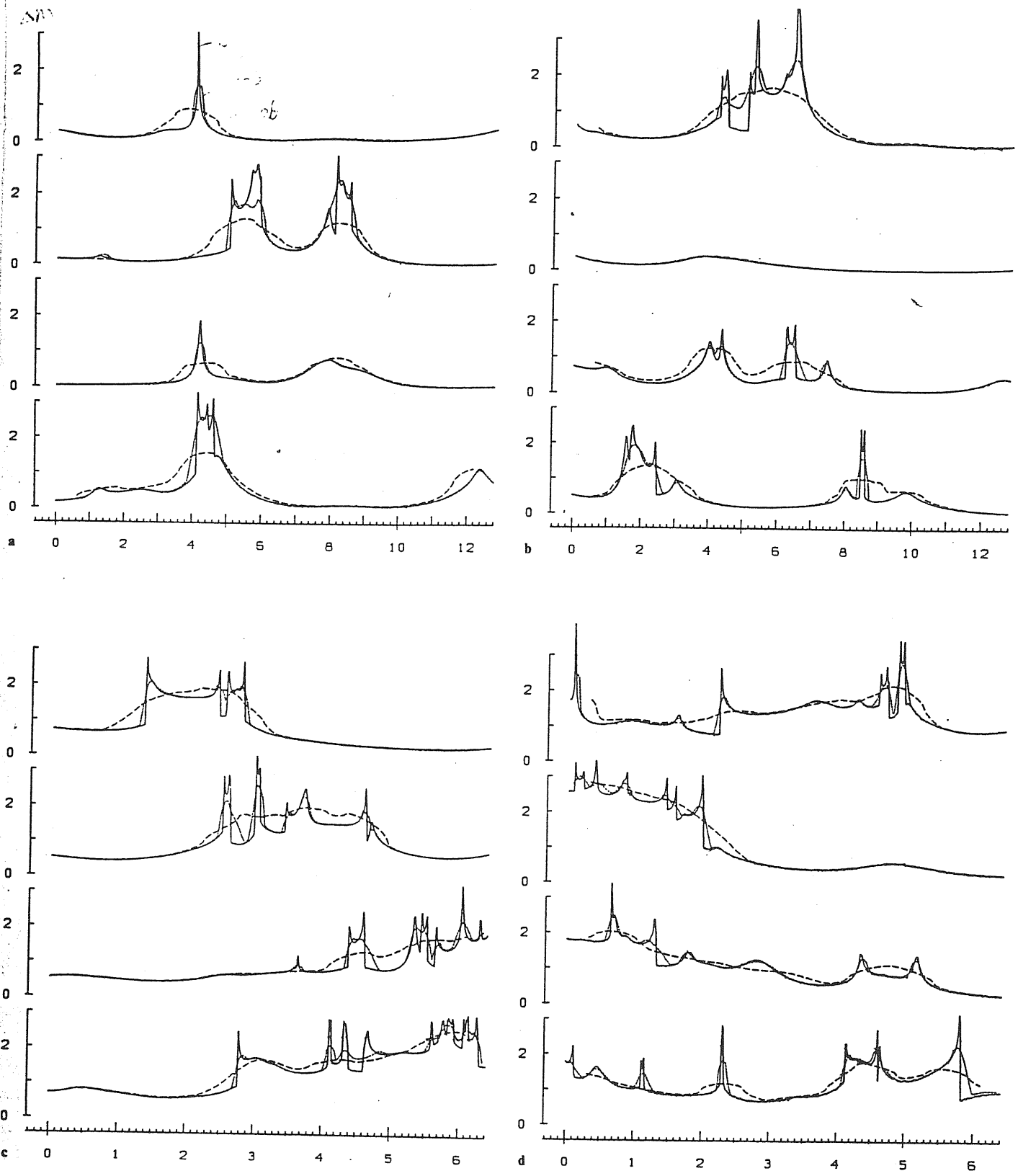

Fig. 29a-l.

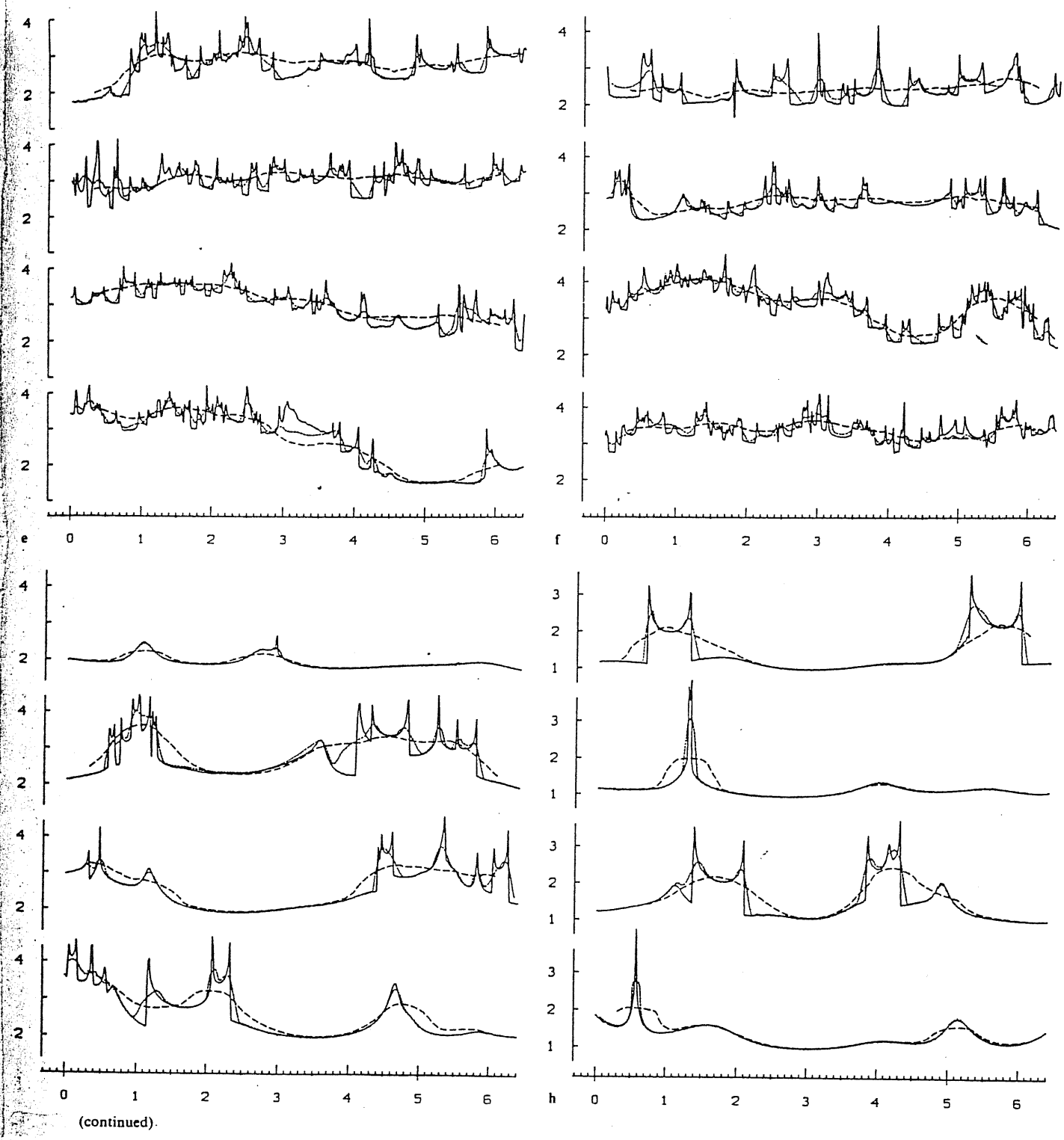

(continued).

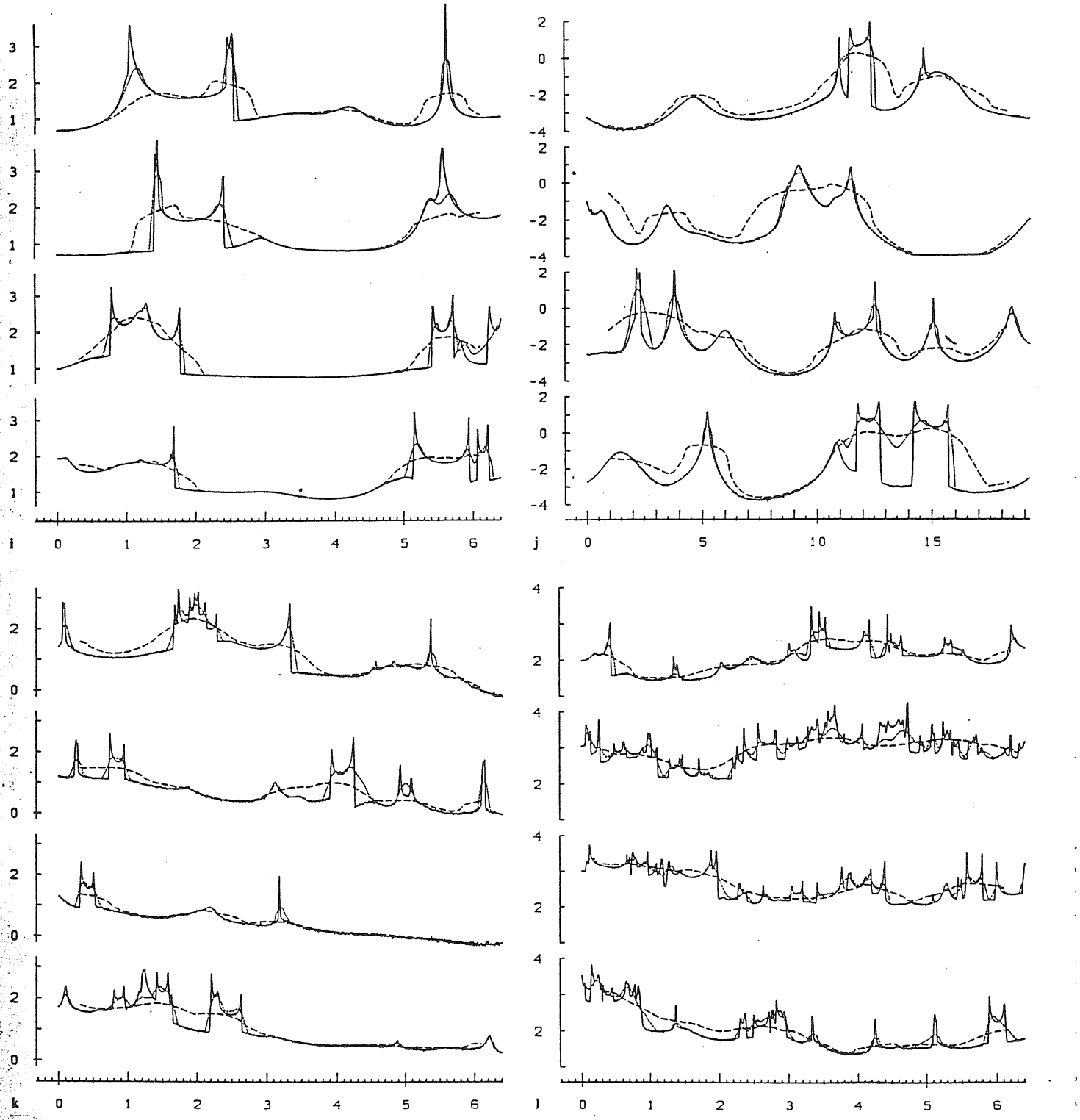

(continued)

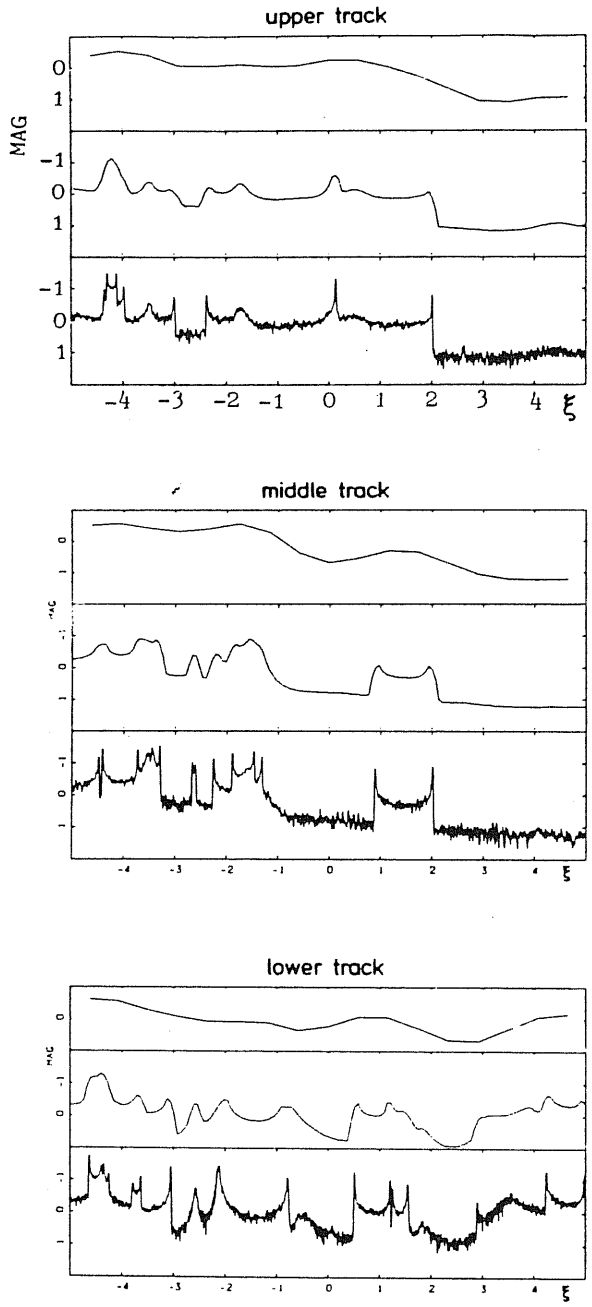

Figure 30 Representative changes in the total flux from all microimages (magnitudes) versus distance moved by an observer perpendicular to the line-of-sight (units are roughly a_o for typical parameters). "Track" refers to the choice of paths across the distribution of lensing masses. The three curves for each track are for source sizes of approximately 1, 0.1 and 0.01 a_o. Optical depth τ = 0.4 (from Kayser *et al.* 1986).

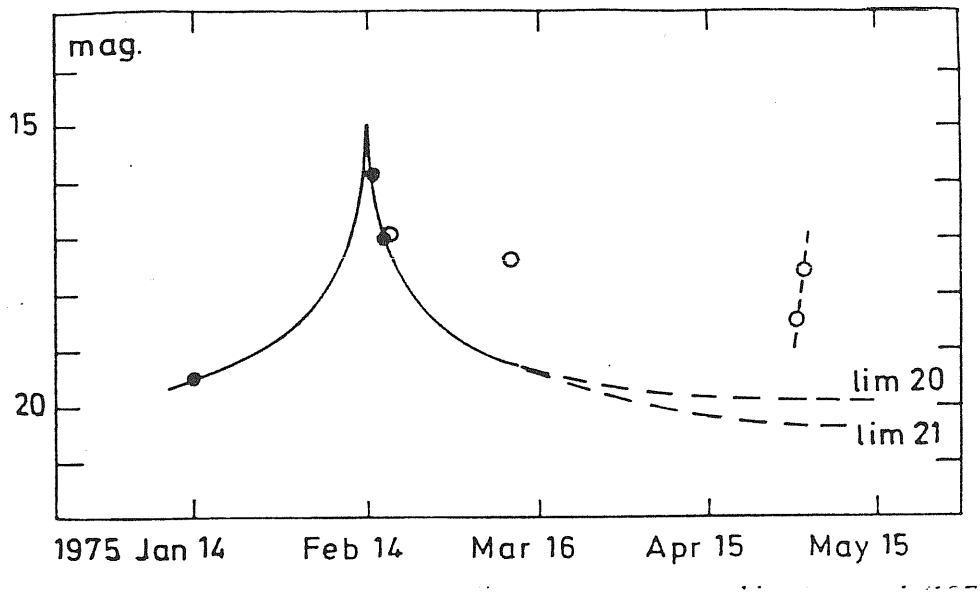

Fig. 31.